7-18-2022 10:00 AM

Motion and Crosslinked Polyethylene Wear in Reverse Total Shoulder Arthroplasty

Christopher Millward, *The University of Western Ontario*

Supervisor: Langohr, G Daniel G, *The University of Western Ontario*
Co-Supervisor: Medley, John B, *University of Waterloo*
A thesis submitted in partial fulfillment of the requirements for the Master of Engineering Science degree in Biomedical Engineering
© Christopher Millward 2022

Recommended Citation

Abstract

The reverse total shoulder arthroplasty (RTSA) has quickly grown to become the most commonly used shoulder arthroplasty design; however, reports have shown evidence of RTSA failures related to polyethylene wear and damage. Therefore, the present work investigated the wear of crosslinked polyethylene (XLPE) in environments similar to that of an *in vivo* RTSA. Additionally, a computational model was developed based on a previous study of the shoulder motions obtained from a selection of typical patients with RTSA. This model quantified the amount of glenohumeral motion that an RTSA may be subjected to *in vivo* and provided an approximate value for the number of cycles that the RTSA-bearing shoulder may see annually. The *in vitro* RTSA wear simulation detected a significant decrease in polyethylene wear for XLPE in humeral cup liners compared with an earlier very similar study using non-XLPE. The computational model based on *in vivo* data suggested that smaller neck shaft angles of te implant might reduce polyethylene damage and also suggested that 1.25 million cycles in our joint wear simulator provided a good representation of 1 year *in vivo*. It is likely that the use of XLPE in the RTSA may reduce the number of failures related to wear.

Keywords

Reverse total shoulder arthroplasty, crosslinked polyethylene, wear simulation, tribology, neck-shaft angle, scapular notching.

Summary for Lay Audience

The reverse total shoulder arthroplasty (RTSA) has become the most popular shoulder replacement design used today. RTSA is used to treat a variety of conditions including, but not limited to, shoulder arthropathy, shoulder arthritis, shoulder fracture, and failure of previous shoulder implants. There have been reports showing evidence of RTSA failures related to wear of the humeral cup that warrants an investigation into the materials being used. In hip implants, a very wear resistant crosslinked polyethylene (XLPE) is widely used. However, in RTSA, a non-crosslinked polyethylene material is the most common material used to line the humeral cup. When wear-related implant failures were seen in total hip arthroplasty, they were essentially eliminated by using XLPE. This material has now been described as the gold standard liner material in total hip replacements (and is gaining popularity in the knee). It is logical to believe using XLPE in RTSA may yield similar benefits to its use in the hip. Therefore, the objective of the present work was to investigate XLPE wear in environments similar to that of an *in vivo* RTSA. Wear simulations were conducted to measure the total volume of XLPE wear that may occur in the RTSA. Additionally, a computer model was developed based on a previous *in vivo* study of shoulder motion in RTSA patients. This model predicted the amount of relative motion that the RTSA may see annually. The computer model also simulated 4 different RTSA designs to investigate the effects that changing specific design parameters has on relative motion and risk of scapular notching (another common RTSA complication). The results of the simulations suggested that XLPE was significantly more wear resistant than non-XLPE in the RTSA. The computer model predicted that roughly 1.25 million cycles in our shoulder wear simulator represented 1 year *in vivo*. The model indicated that the risk of scapular notching was reduced by using implants having the specific geometrical feature of a lower neck shaft angle. The results of this work will help influence RTSA testing protocol and design and will afford surgeons the ability to make more informed clinical predictions.

Co-Authorship Statement

Chapter 1   C Millward – wrote manuscript

GDG Langohr – reviewed manuscript

JB Medley – reviewed manuscript

Chapter 2   C Millward – data collection, statistical analysis, wrote manuscript

GDG Langohr – study design, reviewed manuscript

JB Medley – study design, reviewed manuscript

Chapter 3   C Millward – study design, sole software developer, wrote manuscript

GDG Langohr – study design, data collection, statistical analysis, reviewed manuscript

JB Medley – reviewed manuscript

Chapter 4   C Millward – data collection, statistical analysis, wrote manuscript

GDG Langohr – study design, development of wear simulation strategy, reviewed manuscript

JB Medley – study design, reviewed manuscript

Chapter 5   C Millward – wrote manuscript

GDG Langohr – reviewed manuscript

JB Medley – reviewed manuscript

Acknowledgements

First, I would like to acknowledge Dr. Daniel Langohr and Dr. James Johnson who, in the spring of 2019, saw a curious kid from Kinesiology and bet on him to succeed in the School of Biomedical Engineering. Your trust in me has opened many doors in my life, and I cannot thank you enough.

Next, I would like to thank both Dr. John Medley and Dr. Daniel Langohr for their mentorship. The volumes of knowledge that I have received from the two of you, although may be just factions of what you have to offer, will guide my endeavors far beyond the ends of this degree. Thank you for your leadership, and I hope I will pass along your teachings justly.

Of course, none of this would be possible if not for my trusted companions that helped me unwind through our many long hours logged at the wood. A compressed mind provides no room for growth, so a toast is in order for you all.

I would like to specifically *not* thank the academic advisor who told me in my undergrad that it was "unrealistic" for me to pursue graduate research in biomechanics because I "clearly struggle with the sciences". You know nothing about me.

And on a related topic, thank you to my mother who has relentlessly insisted, for well over two decades, that there is nobody capable of stopping me from reaching my goals, so long as I am willing to work hard enough to achieve them.

Finally, thank you to my beloved Darling, who supported me endlessly through these past three years. You constantly motivate me to better myself, and I couldn't imagine doing this without you by my side.

Table of Contents

List of Tables

List of Figures

List of Appendices

Chapter 1

Introduction

OVERVIEW: The current thesis examines kinematics and polyethylene wear related to the reverse total shoulder arthroplasty (RTSA). To provide background for these studies, this chapter presents some basic anatomy and biomechanics of the shoulder joint as well as some of its common pathologies. RTSA is then described as a treatment for many of these pathologies, highlighting some of its mechanical advantages. The current complications to the RTSA designs are presented and used to justify an investigation of crosslinked polyethylene wear. A review of the published literature on polyethylene wear in the reverse total shoulder arthroplasty is then presented and objectives and hypotheses are stated.

1.1   Shoulder Anatomy and Pathology

1.1.1   Anatomy

The shoulder is the body's connection of the upper limb to the axial skeleton. It is composed of three bones (i.e., humerus, scapula, and clavicle) and three joints (i.e., acromioclavicular, glenohumeral, and scapulothoracic) [1,2] (Figure 1-1). Iannotti et al. [3] studied the anatomy of 140 shoulders and found that the glenohumeral joint is a somewhat sloppy ellipsoid-in-ellipsoid joint. They found that in the frontal plane, the glenoid had a superior-inferior radius of curvature an average of 2.3 mm greater than that of the humeral head. This means that there is a small amount of translational motion that can occur in the glenohumeral joint, and it is not, as is commonly described, a ball-in-socket joint. Like most other joints, the glenohumeral joint (Figure 1-2) is lined with cartilage for smooth, lubricated movement [1,2]. The scapulothoracic joint can be modelled as a sesamoid bone (scapula) floating in a web of tension from its attached tendons [2,4]. The scapula has no fixed fulcrum against the thorax, but instead translates across its surface, rotating triaxially wherever it lies.
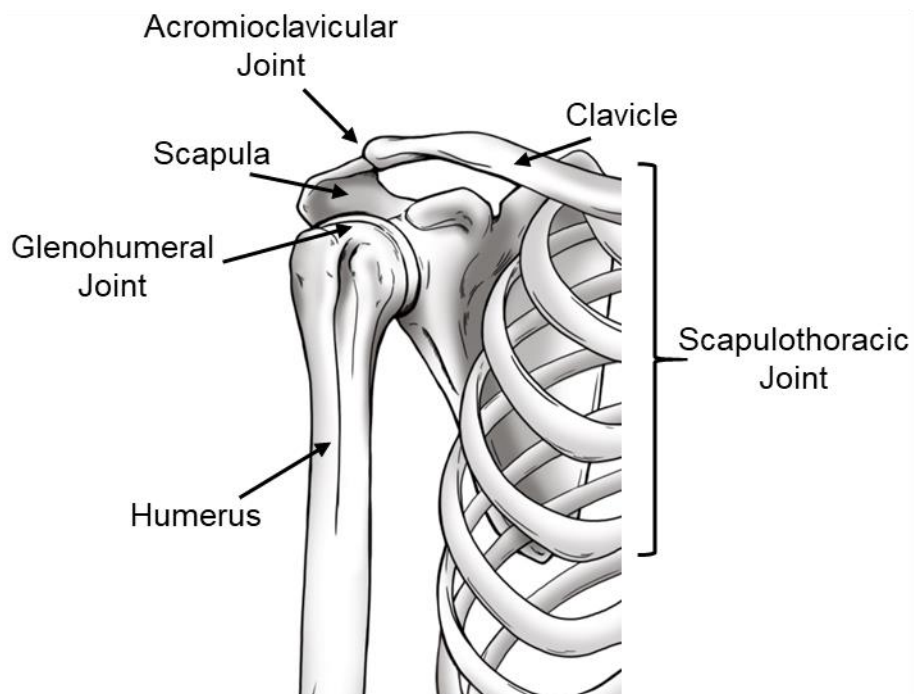
Figure 1-1: The bones and joints of the shoulder

Note that all figures not referenced are owned by our research group and have not yet been published in any academic journal.
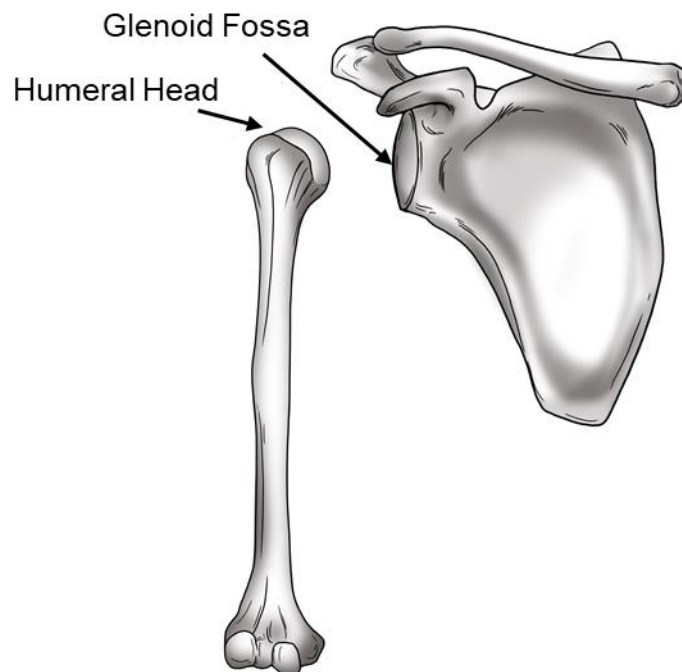
Figure 1-2: The glenohumeral joint components

There are twenty-two muscles that work in conjunction to coordinate glenohumeral motion [2]; however, only the deltoid and rotator cuff muscles need to be closely considered to understand the present work. The deltoid is a large muscle that lays most superficially on the shoulder and is typically broken up into three regions: anterior, middle, and posterior. All three regions insert distally onto the deltoid tuberosity of the humerus, but have varying proximal insertion points, altering the function of the muscle region: the anterior fibres insert proximally onto the clavicle and primarily flex and internally rotate the shoulder; the middle fibres insert proximally onto the acromion process of the scapula and contribute to shoulder abduction; and the posterior fibres insert proximally onto the spine of the scapula and contribute to extension and external rotation of the shoulder [2] (Figure 1-3). The rotator cuff is a group of four small muscles (supraspinatus, infraspinatus, teres minor, and subscapularis) that stabilize and rotate the shoulder. The supraspinatus inserts proximally onto the supraspinous fossa of the scapula and distally onto the greater tubercle of the humerus (Figure 1-3); it contributes to shoulder abduction [2]. The infraspinatus inserts proximally onto the infraspinous fossa of the scapula and distally onto the greater tubercle of the humerus (Figure 1-3), contributing to humeral external rotation [2]. The teres minor

inserts proximally onto the lateral border of the scapula and distally onto the greater tubercle of the humerus (Figure 1-3), causing some humeral external rotation [2]. The subscapularis inserts proximally onto the medial border of the scapula and distally onto the lesser tubercle of the humerus (Figure 1-3), creating humeral internal rotation [2]. In addition to their individual mobilizations of the shoulder, each of the rotator cuff muscles also contract to compress the glenohumeral joint, providing stability to the joint through all ranges of motion.
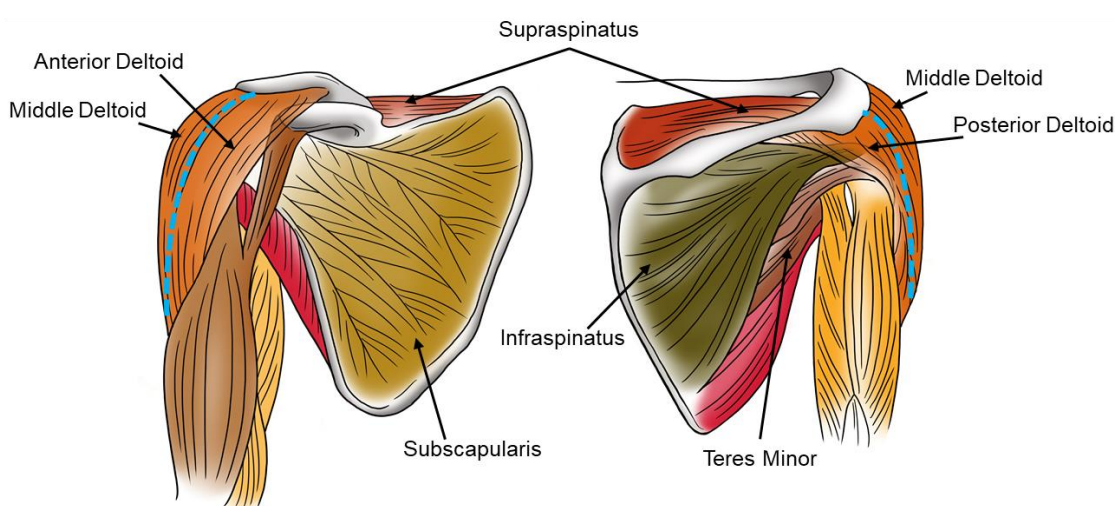
Figure 1-3: Anterior (left) and posterior (right) view of deltoid and rotator cuff

The glenohumeral joint rotates about three axes. Isolated, these rotations define humeral position as elevation, plane of elevation, and axial rotation (Figure 1-4) [5]. As previously mentioned, a small amount of translation occurs as a component of glenohumeral movement. This translation is not depicted in Figure 1-4 and is not discussed further in the present work. Abduction, characterized by elevation in the frontal plane (90° plane of elevation), is known to be mobilized primarily by the deltoid and supraspinatus, while the other muscles provide stability to the joint. Both the middle deltoid and the supraspinatus are activated prior to abduction movement [6]; however, at the early stages of abduction, the shoulder is in a position that does not afford the deltoid a significant abduction moment arm [7]. This suggests that while both muscles are active during initial abduction, the

deltoid mainly compresses the joint, providing stability while the supraspinatus mobilizes the shoulder into abduction. Only after about 15° of abduction does the deltoid have a long enough moment arm to become a fully effective abductor [1].

Elevation

POE
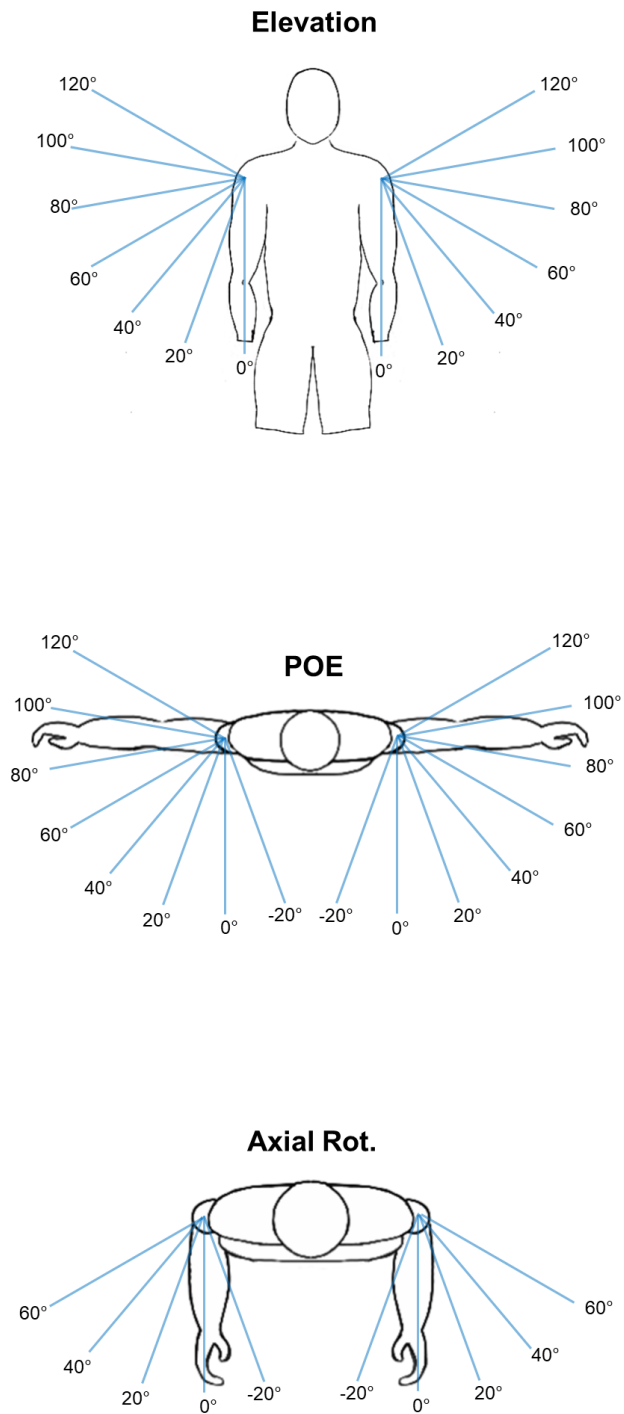
Axial Rot.

Figure 1-4: Rotations describing humeral position

Elevation (top), plane of elevation (middle), and axial rotation (bottom).

1.1.2   Common Pathologies

Rotator cuff pathologies have been identified in 38% of adults over the age of 60 [8]. This prevalence increases with age, affecting 62% of adults over the age of 80 [8]. Within this population, many tears are considered irreparable, meaning the degeneration is not reversible even with physical therapy and surgical intervention. When this occurs, individuals suffer the fate of living with impaired shoulder function indefinitely.

Articular cartilage degeneration, that is often classified as osteoarthritis (OA), presents in the shoulder in 16.1% - 17.4% of the adult population [9,10]. Individuals with OA typically experience pain when loading the joint, which may hinder their ability to perform daily activities. A typical treatment for late-stage OA is total joint arthroplasty, which includes replacing both the distal and proximal articulating surfaces of the joint with artificial components that allow a smooth, lubricated contact. The 2020 Australian Orthopaedic Association National Joint Replacement Registry (AOA NJRR) [11] noted that the number of total shoulder replacements performed had increased by 338% since 2008. Updating this value with the AOA NJRR's most recent count of total shoulder replacements performed [12] indicated an increase in 388% in total shoulder replacements from 2008 to 2020.

Rotator cuff arthropathy, a common condition in aging shoulders, presents with features of both glenohumeral articular cartilage degeneration and rotator cuff deficiency, but is further complicated by other degenerative changes including, but not limited to, superior migration of the humeral head [13]. The pathogenesis of rotator cuff arthropathy is not fully understood; however, it is believed to be a product of both intrinsic (within the tendon's physiology) and extrinsic (within the tendon's environment) factors that feed back into each other to accelerate the shoulder's degeneration [13]. Individuals with rotator cuff arthropathy are not usually eligible for an anatomic total shoulder replacement: since the rotator cuff cannot stabilize the joint even pre-surgery, it remains insufficient post-surgery, leading to limited progress in post-op rehabilitation and poor clinical outcomes. To overcome this problem, surgeons often replace the affected glenohumeral joint with an implant in a procedure that is described as a reverse total shoulder arthroplasty (RTSA).

1.2   The Reverse Total Shoulder Arthroplasty (RTSA)

1.2.1   General Description

The RTSA is a total shoulder arthroplasty system that both reverses the native anatomy of the joint as well as constrains the contact of the glenohumeral components. The native concave structure is moved from the glenoid to the humeral head, and the ellipsoidal component is removed from the humerus and replaced by a hemispherical component fixed into the glenoid space (Figure 1-5). The resulting design provides a smooth, lubricated, and constrained contact restoring pain-free motion while also presenting a more mechanically suitable orientation for the shoulder to function with a damaged rotator cuff [13–15].

Although the RTSA was originally designed to treat rotator cuff arthropathy, it is used to treat many more conditions including osteoarthritis without the presence of rotator cuff tear, humeral fracture, osteonecrosis, joint instability, and revision from failed anatomic or partial joint arthroplasty [16]. Since 2009, the RTSA has continued to increase in popularity, and the AOA NJRR noted that in 2020, over 80% of all total shoulder replacements performed were RTSAs [17]. A similar percentage may be revealed in Canada if the Canadian Joint Replacement Registry recorded shoulder surgeries.
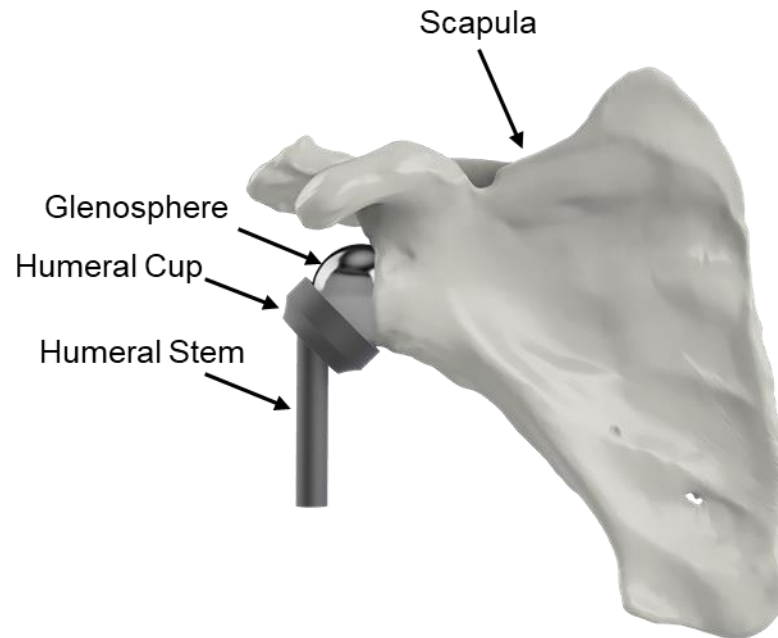
Figure 1-5: Reverse total shoulder arthroplasty

The most commonly used RTSA systems follow the metal-on-polymer design commonly used in the articulations of other total joint replacement implants, typically employing a cobalt-chromium glenosphere articulating against a non-cross linked ultra-high molecular weight polyethylene humeral cup liner [16].

1.2.2   Altered Biomechanics

In an RTSA, the centre of rotation is translated medially relative to the average position of the centre of rotation for the native anatomy (Figure 1-6), which not only increases the deltoid's abduction moment arm, but also recruits a greater proportion of muscle fibres during abduction [14]. This allows the deltoid to mobilize the joint through full range

(including initial abduction) and gives the shoulder the advantage of not having to rely on the (potentially) dysfunctional supraspinatus.

Trading the native mismatched ellipsoid-on-ellipsoid geometry of the joint for equal diameter hemisphere and cup components affords the glenohumeral joint very little room for articular translation, removing the reliance on the rotator cuff for stability.
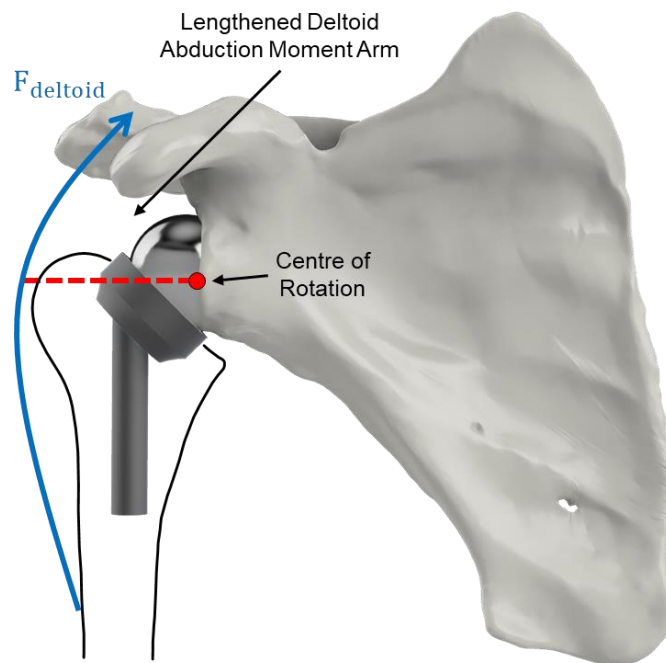
Figure 1-6: Deltoid abduction moment arm following RTSA

1.2.3   Complications

Like all other joint arthroplasties, the RTSA is subject to clinical complications. In the past 10 years, implant loosening was responsible for 16.6% of all RTSA revisions in Australia [18]. Two mechanisms that can contribute to implant loosening are wear particle-induced osteolysis and scapular notching damage to the humeral cup rim. Polyethylene damage is characterized by large, visible pieces of polyethylene getting severed away from the main body. This typically involves large contact stresses and high impacts. Polyethylene wear is a more gradual process that occurs when two surfaces undergo relative motion, and sometimes subsurface fatigue. Wear particles are often much smaller in diameter than

damage particles and possess a greater osteolytic potential [19]. If a substantial amount of wear particles from the arthroplasty are released within the joint space, a local immune response may be triggered, initiating wear particle-induced osteolysis. This immune response may result in bone resorption [20,21], which can lead to implant loosening, and ultimately, failure [21,22]. Polyethylene damage can accelerate wear, just as wear can accelerate damage. These two mechanisms may also occur simultaneously, producing some in-between deterioration mechanism with features similar to each. Polyethylene wear and damage have been found in 62.5% [23] to 100% [24–26] of RTSA retrievals, justifying the exploration of humeral cup deterioration in the RTSA [27–37].

Scapular notching is characterized by a "notch" receding from the lateral border of the scapula, just below the glenosphere base plate (Figure 1-7) [38]. Scapular notching is almost always accompanied by large amounts of polyethylene damage at the inferior border of the humeral cup liner [24,25,39], suggesting that repetitive contact of the lateral border of the scapula with the humeral cup may contribute to scapular notching. In severe cases, the recession of bone has been found to expose the glenosphere baseplate screws buried within the scapula, not only contributing to the loosening of the prosthesis, but also providing a sharp metallic surface with which the humeral liner may abrade against [24,25,39].
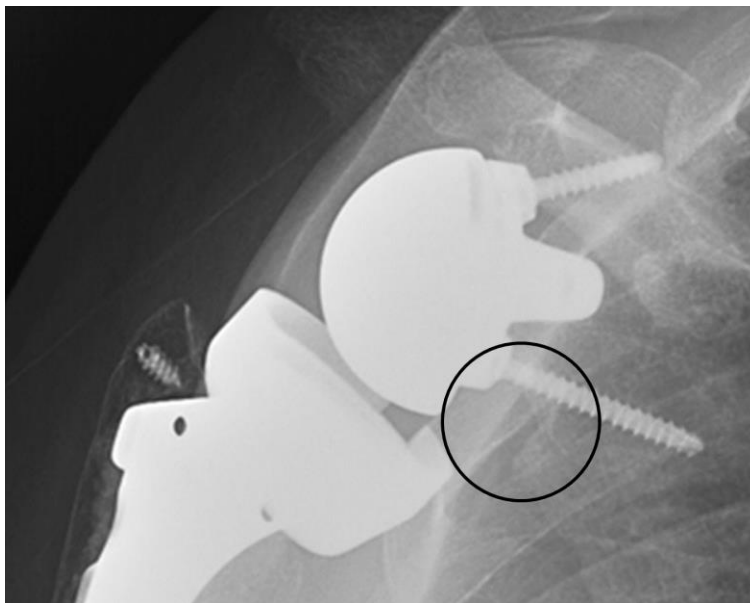
Figure 1-7: Scapular notching shown in radiograph. *Image courtesy of Dr. Ken Faber, Orthopaedic Surgeon at the Roth | McFarlane Hand and Upper Limb Centre, London, Ontario.*

1.2.4 Proposed Solutions to RTSA Wear

Wear particle-induced osteolysis was present in early hip arthroplasty designs, but was combatted by substituting the non-crosslinked polyethylene (non-XLPE) liners with a highly crosslinked polyethylene (XLPE) [40]. This XLPE is the same material as non-XLPE but exposed to at least 5 MRad (50 kGy) of irradiation, which causes scission (or cutting) of main polymeric chains within the material. Some processing must also be done to make sure that the free radicals created by chain scission combine to form crosslinks rather than just combine with oxygen which would weaken the material's resistance to wear. A common practice is the incorporation of vitamin E in the polyethylene, which acts as a strong antioxidant while preserving low wear rates [41]. The resulting XLPE has shown significant improvements in the wear resistance when paired with metal or ceramic surfaces, leading to reduced revision rates in both the hip and knee [42–46]. It is logical to hypothesize that the implementation of XLPE would have similar effects in the RTSA, aiding in the reduction of RTSA revision surgeries but the latest AOA NJRR Annual Report did not support this with their data [16]. When assessing the cumulative percent

revision of primary RTSAs in the last 10 years [47], the AOA NJRR found no difference in revision rate between non-XLPE and XLPE humeral cups. It may be the case that wear-related failures make up just a small proportion of failures within the first 10 years post-op, and a difference in wear rates may present later in the implant's lifetime. Furthermore, some of the RTSA implants that employ XLPE that are included in the AOA NJRR dataset include some more radial design options that include a 'reversing' of the articular material selections and lateralized glenospheres, which may have contributed to the lack of a difference in realized revision rates.

Other modifications to the RTSA design have been explored, most of which are based on geometric changes. Reducing the cup's neck-shaft angle (NSA) (Figure 1-8) has been shown to reduce the occurrence of scapular notching both experimentally [48–51] and clinically [52]. This lateral rotation of the humeral cup with respect to the humeral axis increases the distance between the inferior border of the cup and the lateral border of the scapula, reducing the risk of scapular impingement in adduction and at low abduction angles. Cup size has also been investigated as a potential for notch reduction [48–50,53]; however, this effect has yet to be clearly identified clinically [54].
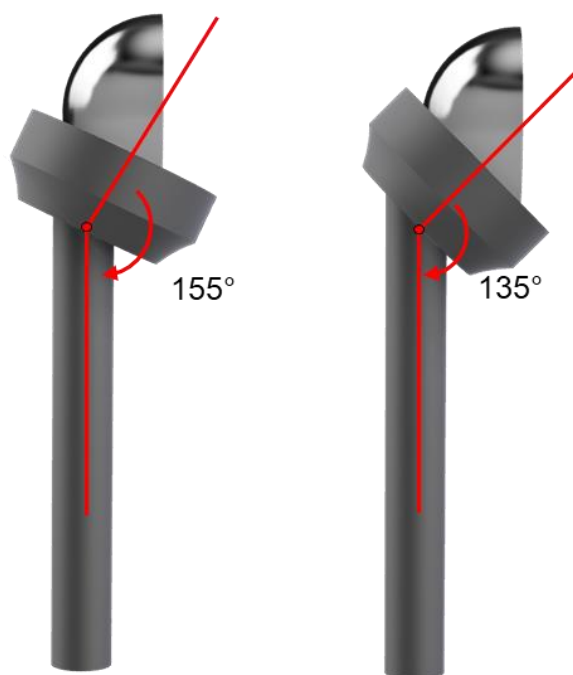
Figure 1-8: Neck-shaft angle examples

1.3   *In Vitro* Wear Simulation

In vitro wear simulations are performed in attempts to explore and predict ways to reduce *in vivo* surface wear. Pin-on-plate wear testing is a technique that has been used in early design stages when deciding whether or not a material is suitable for a specific task, or when attempting to screen the wear performance of a material subjected to identical test conditions. This process requires a pin-on-plate wear apparatus which introduces a prescribed relative motion between a pin and a plate, compressed by a specified load. The machine is programmed to run for a specific number of cycles, after which it stops, and the user is able to clean the specimens and assess wear. Results from the wear test can be directly compared to the results of other materials to help decide which material will produce the most favourable outcomes; however, this approach requires careful interpretation because wear is not a material property but rather a consequence of the whole bearing and its conditions. Thus, the low wear in a pin-on-plate test may not occur when the materials are paired in an actual implant and subject to clinically relevant loads and motions.

In vitro wear simulator testing is a more advanced method used to predict clinical wear of a full-scale joint replacement implant. This method involves installing clinically available total joint replacement implants into a joint wear simulator and running it for a specific number of cycles. The simulator applies a known load and relative motion to the arthroplasty each cycle suitable for the testing of the joint in question.

The current best practice for wear assessment during wear testing is the gravimetric method, during which the mass of each specimen is assessed before and after wear simulation to measure the total mass lost during testing. This can be converted to volumetric wear using the material density. Wear can also be presented as mass loss per million cycles (Mc) of the test motion investigated. The inclusion of load soak control specimens for polymeric specimens increases the accuracy of this process by considering the change in mass due to fluid adsorption that would occur without relative motion. Equations 4-1 and 4-2 detail this process thoroughly.

1.3.1 Current results for pin-on-plate wear of XLPE

Previous pin-on-plate wear studies have reported wear rates ranging from 0.28 mm^3/Mc to 6.43 mm^3/Mc in XLPE vs cobalt-chromium (CoCr), a common bearing surface in metal-on-plastic arthroplasty designs [55–59]. Although these studies are technically sound for materials science investigations, their limited translatability to clinical wear predictions is hindered by the mistaken notion that wear is a material property rather than a phenomenon governed by the entire contact and the imposed conditions. Even when just considering pin-on-plate configurations, different results can occur for the same material. One example is the use of XLPE pins and CoCr plates (or discs) [55–61]; this configuration holds the XLPE under constant load rather than cyclically loading it, as it is *in vivo*. It is likely that this lack of cyclic loading of the polymeric component results in varied wear rates of XLPE compared with *in vivo* wear. Having CoCr pins articulate against XLPE plates might more accurately represent XLPE loading mechanics *in vivo* but it would still not be the same as *in vivo* in terms of frequency, path over the surface, or frictional heating. Another example of test variance includes the choice of testing lubricant. Many studies have used a serum diluted with DI water [55,57–60,62], which has been shown to produce polyethylene wear that was dissimilar to that found clinically [63,64]. The use of a non-iron alpha calf serum diluted with phosphate-buffered solution to a total protein concentration of 30 g/L supplemented with sodium hyaluronate (1.5 g/L) and antimycotic antibiotic (10 mL/L) is recommended to produce a clinically-relevant lubricant [63–65] and perhaps a more clinically relevant wear rate [66].

Although investigations of contact pressure on XLPE wear have been conducted, these studies held nominal load constant while altering the contact area of the pin [57,60]. The results of these studies show an inverse relationship between contact pressure and wear rate, which is likely confounded by the effect of having a lower contact area. The relationship between nominal load and XLPE wear against CoCr is still unknown and is the primary focus of Chapter 2.

1.3.2   Current results of *in vitro* wear of XLPE in RTSA

In vitro wear simulations of non-XLPE in the RTSA have been conducted many times before, but comprehensive wear testing of XLPE in the RTSA has only been published in the full-length literature once, by Peers et al. [27] (Table 1-1). When comparing this group's XLPE (5 MRad) wear results to those of non-XLPE wear studies using the same protocol and out of the same institution [28,30,31], XLPE appeared to be much more resistant to wear. That being said, their wear rate of XLPE remained higher than the non-XLPE wear rates from other lab groups [29,32,34–37] (Figure 1-9). This was likely a consequence of varying simulation protocols amongst research groups.

Table 1-1: Summary of in-vivo RTSA wear simulations

				RTSA Simulation Studies				
Authors	Group	Material	Lubricant	Load (N)	Range of Motion	Control	Wear Rate (mm^3 / Mc)	Comments
Carpenter et al. [30]	Beaumont	non-XLPE	Bovine calf serum (21 g/L) + DI water	20 - 617.8 / 20 - 926.7	46° flex/ext / 46° add/abd	Load / Soaked	88.1	Tested pure abduction and then pure flexion afterwards.
Haggart et al. [28]	Beaumont	non-XLPE	Bovine calf serum (21 g/L) + DI water	20 - 617.8 / 20 - 926.7	46° flex/ext / 46° add/abd	Load / Soaked	68.0	Tested pure abduction and then pure flexion afterwards.
Peers et al. [27]	Beaumont	XLPE (5 Mrad)	Bovine calf serum (21 g/L) + DI water	20 - 617.8 / 20 - 926.7	46° flex/ext / 46° add/abd	Load / Soaked	36.5	Tested pure abduction and then pure flexion afterwards.
Vaupel et al. [31]	Beaumont	non-XLPE	Bovine calf serum (21 g/L) + DI water	20 - 617.8 / 20 - 926.7	46° flex/ext / 46° add/abd	Load / Soaked	125.5	Tested pure abduction and then pure flexion afterwards.
Mattei et al. [34]	Newcastle	non-XLPE	Newborn calf serum (26 g/L)	180 - 250	28° flex/ext / 13° add/abd / 59° IR/ER	Load / Soaked	13.3	
Smith et al. [35]	Newcastle	non-XLPE	Newborn calf serum (26 g/L)	180 - 250	28° flex/ext / 13° add/abd / 25° IR/ER	Load / Soaked	14.3	
Smith et al. [36]	Newcastle	non-XLPE	Newborn calf serum (26 g/L)	150 - 450	44° flex/ext / 48° add/abd / 43° IR/ER	Load / Soaked	14.2	Pilot study (n=1)
Griffiths et al. [32]	HULC	non-XLPE	Alpla calf serum (30 g/L) + posphate buffered solution	813 - 914	45° flex/ext / 45° add/abd	Load / Soaked	29.7	
Langohr et al. [33]	HULC	non-XLPE	Alpla calf serum (30 g/L) + posphate buffered solution	813 - 914	45° flex/ext / 45° add/abd	Load / Soaked	42.0	Pilot study (n=1)
Kohut et al. [37]	Hopital Cantonal, Switzerland	non-XLPE	Bovine calf serum (30 g/L)	250 - 1000	43° flex/ext / 11° add/abd / 13° IR/ER	Soaked	17.4	Inversed Bearing
Dieckmann et al. [29]	Munster University, Germany	non-XLPE	Alpla calf serum (30 g/L) + phosphate buffered solution	100 - 500	20° flex/ext / 70° add/abd	Soaked	29.7	Pilot study (n=1) Did not use CoCr glenosphere
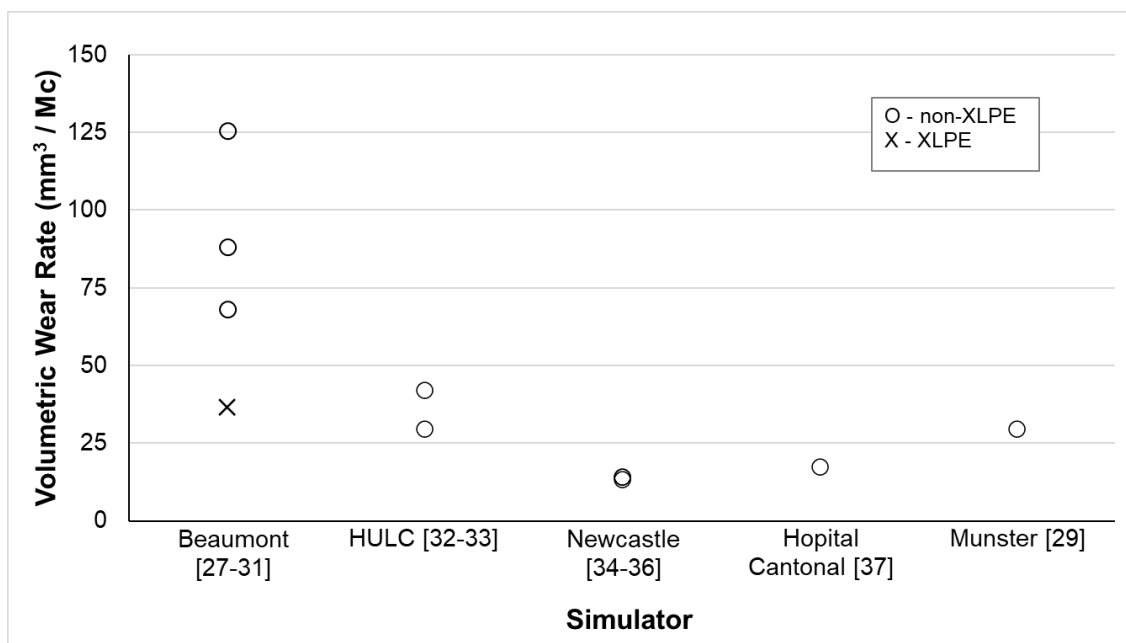
Figure 1-9: Volumetric wear rates of *in vitro* RTSA simulations

Even though XLPE has been described as the gold standard liner material in hip implants due to its wear resistance [40], at present there remains hesitation to accept it as the best-practice material for the RTSA. The clinical data from the 2021 AOA NJRR suggests there is no reduction in revision rate when using XLPE instead of non-XLPE in the RTSA [16], but it may be the case that confounding variables are hiding the benefits of using XLPE in such designs. Since XLPE liners have improved clinical outcomes in the hip and knee [42–46], as well as having shown a promising reduction of wear in an RTSA wear simulation [27], further research must be conducted to identify clear benefits and detriments to using XLPE as a humeral cup liner material.

Another shortcoming within the current literature involves the differences between the published simulation strategies and their associated reported wear rates (Table 1-1), which makes it difficult to compare wear rates across research groups. This includes the relative motion and loads applied, the lubricant composition, and the implant designs themselves used during the wear simulation testing. Although the Peers et al. provided very strong evidence to suggest XLPE was more wear resistant in RTSA designs [27], other groups must also repeat their methodologies using XLPE in order to directly compare the two

materials' wear rates and build a stronger body of evidence to help guide arthroplasty design. In 2016, Langohr et al. developed a shoulder wear simulation protocol [33] that introduced loads and motions different to those used by Peers et al. [27]. This protocol has already been used to investigate the wear of non-XLPE humeral cups [28], so by using the same protocol to investigate XLPE wear, a greater understanding of the two materials' performance in the RTSA can be provided.

In the lower limb, the number of gait cycles that occur annually has been estimated to be 2 Mc/year [67], which not only justifies simulation lengths, but also provides an approximate clinical translation of the wear simulator results. Having a similar annual estimation of the shoulder joint would allow researchers to tailor their simulator's kinematic profiles to represent a given time (in years) and allow clinicians to make an estimate of how much wear can be expected for a given period *in vivo*.

1.4   Objectives & Hypotheses

Therefore, the purpose of the present work was to investigate the wear of XLPE in the context of finding a suitable replacement for non-XLPE in RTSA. Additionally, a duty cycle was assumed and a link between the number of cycles in the simulator and encountered *in vivo* was sought.

1.4.1   Objectives

1. To investigate the wear of XLPE against CoCr in pin-on-plate testing and its response to increased contact load.

2. To quantify an average daily, *in vivo* glenohumeral sliding distance at various points on the humeral cup and extrapolate to estimate an average yearly number of cycles for RTSA implants.

3. To determine the proportion of time that the inferior border of the cup overlapped the medial border of the glenosphere, which is a position with a high risk of scapular notching.

4. To investigate the effect that NSA and cup size had on daily sliding distance and medial overlapping.

5. To investigate XLPE wear in an RTSA implant and compare it with the wear of non-XLPE under identical test conditions using a shoulder joint wear simulator.

1.4.2   Hypotheses

1. An increase in load will increase XLPE wear against CoCr in pin-on-plate wear testing.

2. The yearly number of cycles experienced in the shoulder will be similar to that of the lower limb (roughly 2 Mc/year).

3. The inferior point on the cup will spend over 50% of the time in medial overlap.

4. A decrease in NSA will increase sliding distance at the inferior point but have no effect on the remaining points. The decreased NSA will also decrease the proportion of time the inferior point spent in medial overlap. An increase in cup size will increase sliding distance at all points but have no influence on medial overlap.

5. XLPE wear will be less than non-XLPE wear in *in vitro* RTSA wear simulations.

1.5   Thesis Overview

Chapter 2 describes the investigation of XLPE wear in pin-on-plate wear testing under two different loads. The simulation environment was chosen to best represent *in vivo* conditions.

Chapter 3 describes the development of a software model to determine the daily glenohumeral sliding distances in fully recovered individuals with an RTSA. These values were extrapolated to estimate an annual total number of cycles for the RTSA. Additionally, the proportion of time the inferior aspect of the cup spent overlapped with the medial border of the glenosphere was calculated. The influence of NSA and implant size on the former two measures was also assessed.

Chapter 4 describes the simulator wear testing of an RTSA design with methodologies identical to a previous study investigating non-XLPE wear in RTSA to allow a direct comparison of the two liner materials.

Chapter 5 presents a brief summary of chapters 2-4 and gives conclusions for the entire thesis research.

1.6 References

[1]   K. L., Moore;A. F., Dalley; A. M. R. A. Moore Clinically Oriented Anatomy. 7th
ed. Baltimore, MD: Lippincott Williams & Wilkins; 2014.
https://doi.org/10.1017/CBO9781107415324.004.

[2]   Tortora GJ, Nielsen MT. Principles of Human Anatomy. 13th ed. Hobogen, NJ,
USA: John Wiley & Sons; 2014.

[3]   Iannotti JP, Gabriel J, Schneck S, Evans B. The Normal Glenohumeral
Relationships. J Bone Jt Surgery, Am Vol 1992;74:491–500.

[4]   Levin SM. The scapula is a sesamoid bone. J Biomech 2005;38:1733–4.
https://doi.org/10.1016/j.jbiomech.2004.12.001.

[5]   Wu G, Van Der Helm FCT, Veeger HEJ, Makhsous M, Van Roy P, Anglin C, et
al. ISB recommendation on definitions of joint coordinate systems of various joints
for the reporting of human joint motion - Part II: Shoulder, elbow, wrist and hand.
J Biomech 2005;38:981–92. https://doi.org/10.1016/j.jbiomech.2004.05.042.

[6]   Wickham J, Pizzari T, Stansfeld K, Burnside A, Watson L. Quantifying "normal"
shoulder muscle activity during abduction. J Electromyogr Kinesiol 2010;20:212–
22. https://doi.org/10.1016/j.jelekin.2009.06.004.

[7]   Ackland DC, Pak P, Richardson M, Pandy MG. Moment arms of the muscles
crossing the anatomical shoulder. J Anat 2008;213:383–90.
https://doi.org/10.1111/j.1469-7580.2008.00965.x.

[8]   Teunis T, Lubberts B, Reilly BT, Ring D. A systematic review and pooled analysis
of the prevalence of rotator cuff disease with increasing age. J Shoulder Elb Surg
2014;23:1913–21. https://doi.org/10.1016/j.jse.2014.08.001.

[9]   Oh JH, Chung SW, Oh CH, Kim SH, Park SJ, Kim KW, et al. The prevalence of
shoulder osteoarthritis in the elderly Korean population: Association with risk
factors and function. J Shoulder Elb Surg 2011;20:756–63.

https://doi.org/10.1016/j.jse.2011.01.021.

[10]   Kobayashi T, Takagishi K, Shitara H, Ichinose T, Shimoyama D, Yamamoto A, et al. Prevalence of and risk factors for shoulder osteoarthritis in Japanese middle-aged and elderly populations. J Shoulder Elb Surg 2014;23:613–9. https://doi.org/10.1016/j.jse.2013.11.031.

[11]   Australian Orthopaedic Association National Joint Replacement Registry. Australian Orthopaedic Association National Joint Replacement Registry (AOANJRR). Hip Knee & Shoulder Arthroplasty: 2020 Annual Report 2020:328.

[12]   Australian Orthopaedic Association National Joint Replacement Registry. Australian Orthopaedic Association National Joint Replacement Registry (AOANJRR). Hip Knee & Shoulder Arthroplasty: 2021 Annual Report 2021:283.

[13]   Eckland KJ, Lee TQ, Tibone J, Gupta R. Rotator Cuff Tear Arthropathy. J Am Acad Orthop Surg 2007;15:340–9.

[14]   Ackland DC, Roshan-Zamir S, Richardson M, Pandy MG. Moment arms of the shoulder musculature after reverse total shoulder arthroplasty. J Bone Jt Surg - Ser A 2010;92:1221–30. https://doi.org/10.2106/JBJS.I.00001.

[15]   Grammont PM, Baulot E. Delta shoulder prosthesis for rotator cuff rupture. Orthopedics 1993;16:65–8. https://doi.org/10.3928/0147-7447-19930101-11.

[16]   Australian Orthopaedic Association National Joint Replacement Registry. Australian Orthopaedic Association National Joint Replacement Registry (AOANJRR). Hip Knee & Shoulder Arthroplasty: 2021 Annual Report 2021.

[17]   Australian Orthopaedic Association National Joint Replacement Registry. Australian Orthopaedic Association National Joint Replacement Registry (AOANJRR). Hip Knee & Shoulder Arthroplasty: 2020 Annual Report 2020:281.

[18]   Australian Orthopaedic Association National Joint Replacement Registry. Australian Orthopaedic Association National Joint Replacement Registry

(AOANJRR). Hip Knee & Shoulder Arthroplasty: 2021 Annual Report 2021:319.

[19]   Green TR, Fisher J, Bridget Matthews J, Stone MH, Ingham E. Effect of size and dose on bone resorption activity of macrophages by in vitro clinically relevant ultra high molecular weight polyethylene particles. J Biomed Mater Res 2000;53:490–7. https://doi.org/10.1002/1097-4636(200009)53:5<490::AID-JBM7>3.0.CO;2-7.

[20]   Revell PA, Weightman B, Freeman MAR, Roberts BV. The production and biology of polyethylene wear debris. Arch Orthop Trauma Surg 1978;91:167–81. https://doi.org/10.1007/BF00379748.

[21]   Ingham E, Fisher J. Biological reactions to wear debris in total joint replacement. Proc Inst Mech Eng Part H J Eng Med 2000;214:21–37. https://doi.org/10.1243/0954411001535219.

[22]   Wirth MA, Mauli Agrawal C, Mabrey JD, Dean DD, Blanchard CR, Miller MA, et al. Isolation and characterization of polyethylene wear debris associated with osteolysis following total shoulder arthroplasty. J Bone Jt Surg - Ser A 1999;81:29–37. https://doi.org/10.2106/00004623-199901000-00005.

[23]   Kurdziel MD, Newton MD, Hartner S, Baker KC, Wiater JM. Quantitative evaluation of retrieved reverse total shoulder arthroplasty liner surface deviation and volumetric wear. J Orthop Res 2018;36:2007–14. https://doi.org/10.1002/jor.23849.

[24]   Day JS, MacDonald DW, Olsen M, Getz C, Williams GR, Kurtz SM. Polyethylene wear in retrieved reverse total shoulder components. J Shoulder Elb Surg 2012;21:667–74. https://doi.org/10.1016/j.jse.2011.03.012.

[25]   Nam D, Kepler CK, Nho SJ, Craig E V., Warren RF, Wright TM. Observations on retrieved humeral polyethylene components from reverse total shoulder arthroplasty. J Shoulder Elb Surg 2010;19:1003–12. https://doi.org/10.1016/j.jse.2010.05.014.

[26] Wiater BP, Baker EA, Salisbury MR, Koueiter DM, Baker KC, Nolan BM, et al. Elucidating trends in revision reverse total shoulder arthroplasty procedures: A retrieval study evaluating clinical, radiographic, and functional outcomes data. J Shoulder Elb Surg 2015;24:1915–25. https://doi.org/10.1016/j.jse.2015.06.004.

[27] Peers S, Moravek JE, Budge MD, Newton MD, Kurdziel MD, Baker KC, et al. Wear rates of highly cross-linked polyethylene humeral liners subjected to alternating cycles of glenohumeral flexion and abduction. J Shoulder Elb Surg 2015;24:143–9. https://doi.org/10.1016/j.jse.2014.05.001.

[28] Haggart J, Newton MD, Hartner S, Ho A, Baker KC, Kurdziel MD, et al. Neer Award 2017: wear rates of 32-mm and 40-mm glenospheres in a reverse total shoulder arthroplasty wear simulation model. J Shoulder Elb Surg 2017;26:2029–37. https://doi.org/10.1016/j.jse.2017.06.036.

[29] Dieckmann R, Liem D, Gosheger G, Henrichs MP, Höll S, Hardes J, et al. Evaluation of a reconstruction reverse shoulder for tumour surgery and tribological comparision with an anatomical shoulder arthroplasty. Int Orthop 2013;37:451–6. https://doi.org/10.1007/s00264-012-1771-7.

[30] Carpenter S, Pinkas D, Newton MD, Kurdziel MD, Baker KC, Wiater JM. Wear rates of retentive versus nonretentive reverse total shoulder arthroplasty liners in an in vitro wear simulation. J Shoulder Elb Surg 2015;24:1372–9. https://doi.org/10.1016/j.jse.2015.02.016.

[31] Vaupel ZM, Baker KC, Kurdziel MD, Wiater JM. Wear simulation of reverse total shoulder arthroplasty systems: Effect of glenosphere design. J Shoulder Elb Surg 2012;21:1422–9. https://doi.org/10.1016/j.jse.2011.10.024.

[32] Griffiths MW, Athwal GS, Medley JB, Johnson JA, Langohr GDG. Wear of humeral polyethylene cups in reverse total shoulder arthroplasty with simulated rim damage from scapular notching. Biotribology 2020;22:1–8. https://doi.org/10.1016/j.biotri.2020.100123.

[33] Langohr GDG, Athwal GS, Johnson JA, Medley JB. Wear simulation strategies for reverse shoulder arthroplasty implants. Proc Inst Mech Eng Part H J Eng Med 2016;230:458–69. https://doi.org/10.1177/0954411916642801.

[34] Mattei L, Di Puccio F, Joyce TJ, Ciulli E. Numerical and experimental investigations for the evaluation of the wear coefficient of reverse total shoulder prostheses. J Mech Behav Biomed Mater 2016;55:53–66. https://doi.org/10.1016/j.jmbbm.2015.10.007.

[35] Smith SL, Li BL, Buniya A, Ho Lin S, Scholes SC, Johnson G, et al. In vitro wear testing of a contemporary design of reverse shoulder prosthesis. J Biomech 2015;48:3072–9. https://doi.org/10.1016/j.jbiomech.2015.07.022.

[36] Smith SL, Li L, Joyce TJ. Engineering of a multi-station shoulder simulator. Proc Inst Mech Eng Part H J Eng Med 2016;230:470–80. https://doi.org/10.1177/0954411915611161.

[37] Kohut G, Dallmann F, Irlenbusch U. Wear-induced loss of mass in reversed total shoulder arthroplasty with conventional and inverted bearing materials. J Biomech 2012;45:469–73. https://doi.org/10.1016/j.jbiomech.2011.11.055.

[38] Lévigne C, Garret J, Boileau P, Alami G, Favard L, Walch G. Scapular notching in reverse shoulder arthroplasty: Is it important to avoid it and how? Clin Orthop Relat Res 2011;469:2512–20. https://doi.org/10.1007/s11999-010-1695-8.

[39] Mueller U, Harzi A, Loescher R, Buelhoff M, Eckert JA, Kretzer JP. Wear and damage in retrieved humeral inlays of reverse total shoulder arthroplasty—where, how much, and why? J Shoulder Elb Surg 2021;30:e517–30. https://doi.org/10.1016/j.jse.2020.10.015.

[40] Medley JB. Highly cross-linked polyethylene is the new 'gold standard' bearing material for total hip arthroplasty. Biosurface and Biotribology 2021:1–7. https://doi.org/10.1049/bsb2.12007.

[41] Lambert B, Neut D, van der Veen HC, Bulstra SK. Effects of vitamin E

incorporation in polyethylene on oxidative degradation, wear rates, immune response, and infections in total joint arthroplasty: a review of the current literature. Int Orthop 2019;43:1549–57. https://doi.org/10.1007/s00264-018-4237-8.

[42]   Baxter RM, MacDonald DW, Kurtz SM, Steinbeck MJ. Characteristics of highly cross-linked polyethylene wear debris in vivo. J Biomed Mater Res - Part B Appl Biomater 2013;101 B:467–75. https://doi.org/10.1002/jbm.b.32902.

[43]   Civinini R, Carulli C, Matassi F, Cozzi Lepri A, Sirleo L, Innocenti M. The Survival of Total Knee Arthroplasty: Current Data from Registries on Tribology: Review Article. HSS J 2017;13:28–31. https://doi.org/10.1007/s11420-016-9513-9.

[44]   De Steiger R, Lorimer M, Graves SE. Cross-linked polyethylene for total hip arthroplasty markedly reduces revision surgery at 16 years. J Bone Jt Surg - Am Vol 2018;100:1281–8. https://doi.org/10.2106/JBJS.17.01221.

[45]   Khoshbin A, Wu J, Ward S, Melo LT, Schemitsch EH, Waddell JP, et al. Wear Rates of XLPE Nearly 50% Lower Than Previously Thought After Adjusting for Initial Creep. JBJS Open Access 2020;5:e0066–e0066. https://doi.org/10.2106/jbjs.oa.19.00066.

[46]   Pritchett JW. Very large diameter polymer acetabular liners show promising wear simulator results. J Long Term Eff Med Implants 2016;26:311–9. https://doi.org/10.1615/JLongTermEffMedImplants.2017019182.

[47]   Australian Orthopaedic Association National Joint Replacement Registry. Australian Orthopaedic Association National Joint Replacement Registry (AOANJRR). Hip Knee & Shoulder Arthroplasty: 2021 Annual Report 2021:329–66.

[48]   Gutiérrez S, Comiskey IV CA, Luo ZP, Pupello DR, Frankle MA. Range of impingement-free abduction and adduction deficit after reverse shoulder

arthroplasty. Hierarchy of surgical and implant-design-related factors. J Bone Jt Surg - Ser A 2008;90:2606–15. https://doi.org/10.2106/JBJS.H.00012.

[49]   Gutiérrez S, Levy JC, Frankle MA, Cuff D, Keller TS, Pupello DR, et al. Evaluation of abduction range of motion and avoidance of inferior scapular impingement in a reverse shoulder model. J Shoulder Elb Surg 2008;17:608–15. https://doi.org/10.1016/j.jse.2007.11.010.

[50]   Roche C, Flurin PH, Wright T, Crosby LA, Mauldin M, Zuckerman JD. An evaluation of the relationships between reverse shoulder design parameters and range of motion, impingement, and stability. J Shoulder Elb Surg 2009;18:734–41. https://doi.org/10.1016/j.jse.2008.12.008.

[51]   De Wilde LF, Poncet D, Middernacht B, Ekelund A. Prosthetic overhang is the most effective way to prevent scapular conflict in a reverse total shoulder prosthesis. Acta Orthop 2010;81:719–26. https://doi.org/10.3109/17453674.2010.538354.

[52]   Kempton LB, Balasubramaniam M, Ankerson E, Wiater JM. A radiographic analysis of the effects of prosthesis design on scapular notching following reverse total shoulder arthroplasty. J Shoulder Elb Surg 2011;20:571–6. https://doi.org/10.1016/j.jse.2010.08.024.

[53]   Langohr GDG, Giles JW, Athwal GS, Johnson JA. The effect of glenosphere diameter in reverse shoulder arthroplasty on muscle force, joint load, and range of motion. J Shoulder Elb Surg 2015;24:972–9. https://doi.org/10.1016/j.jse.2014.10.018.

[54]   Mollon B, Mahure SA, Roche CP, Zuckerman JD. Impact of glenosphere size on clinical outcomes after reverse total shoulder arthroplasty: An analysis of 297 shoulders. J Shoulder Elb Surg 2016;25:763–71. https://doi.org/10.1016/j.jse.2015.10.027.

[55]   Brandt JM, Vecherya A, Guenther LE, Koval SF, Petrak MJ, Bohm ER, et al.

Wear testing of crosslinked polyethylene: Wear rate variability and microbial contamination. J Mech Behav Biomed Mater 2014;34:208–16. https://doi.org/10.1016/j.jmbbm.2014.02.016.

[56]   Fu J, Doshi BN, Oral E, Muratoglu OK. High temperature melted, radiation cross-linked, vitamin e stabilized oxidation resistant UHMWPE with low wear and high impact strength. Polymer (Guildf) 2013;54:199–209. https://doi.org/10.1016/j.polymer.2012.11.017.

[57]   Kandemir G, Smith S, Joyce TJ. The influence of contact stress on the wear of cross-linked polyethylene. Proc Inst Mech Eng Part H J Eng Med 2018;232:1008–16. https://doi.org/10.1177/0954411918796047.

[58]   Laraia K, Leone N, MacDolanald R, Blanchet TA. Effect of water and serum absorption on wear of unirradiated and crosslinked UHMWPE orthopedic bearing materials. Tribol Trans 2006;49:338–46. https://doi.org/10.1080/05698190600678663.

[59]   Harsha AP, Joyce TJ. Comparative wear tests of ultra-high molecular weight polyethylene and cross-linked polyethylene. Proc Inst Mech Eng Part H J Eng Med 2013;227:600–8. https://doi.org/10.1177/0954411913479528.

[60]   Abdelgaied A, Brockett CL, Liu F, Jennings LM, Fisher J, Jin Z. Quantification of the effect of cross-shear and applied nominal contact pressure on the wear of moderately cross-linked polyethylene. Proc Inst Mech Eng Part H J Eng Med 2012;227:18–26. https://doi.org/10.1177/0954411912459423.

[61]   Saikko V. Effect of serum dilution fluids on the wear of unirradiated and high dose gamma-irradiated, vitamin E stabilized UHMWPE. Wear 2019;430–431:76–80. https://doi.org/10.1016/j.wear.2019.04.022.

[62]   Saikko V. Effect of type of contact, counterface surface roughness, and contact area on the wear and friction of extensively cross-linked, vitamin E stabilized UHMWPE. J Biomed Mater Res - Part B Appl Biomater 2020;108:1985–92.

https://doi.org/10.1002/jbm.b.34539.

[63]   Brandt JM, Brière LK, Marr J, MacDonald SJ, Bourne RB, Medley JB. Biochemical comparisons of osteoarthritic human synovial fluid with calf sera used in knee simulator wear testing. J Biomed Mater Res - Part A 2010;94:961–71. https://doi.org/10.1002/jbm.a.32728.

[64]   Brandt JM, Charron K, Zhao L, MacDonald SJ, Medley JB. Calf serum constituent fractions influence polyethylene wear and microbial growth in knee simulator testing. Proc Inst Mech Eng Part H J Eng Med 2012;226:427–40. https://doi.org/10.1177/0954411912444248.

[65]   Brandt JM, Mahmoud KK, Koval SF, MacDonald SJ, Medley JB. Antimicrobial agents and low-molecular weight polypeptides affect polyethylene wear in knee simulator testing. Tribol Int 2013;65:97–104. https://doi.org/10.1016/j.triboint.2013.02.019.

[66]   Brandt JM, Charron KD, Zhao L, MacDonald SJ, Medley JB. Lubricant Biochemistry Affects Polyethylene Wear in Knee Simulator Testing. Biotribology 2021;27:100185. https://doi.org/10.1016/j.biotri.2021.100185.

[67]   Silva M, Shepherd EF, Jackson WO, Dorey FJ, Schmalzried TP. Average patient walking activity approaches 2 million cycles per year: Pedometers under-record walking activity. J Arthroplasty 2002;17:693–7. https://doi.org/10.1054/arth.2002.32699.

Chapter 2

Investigation of Vitamin E-Stabilized Crosslinked Polyethylene Wear Under Various Loads in Pin-on-Plate Wear Simulation

OVERVIEW: Crosslinked polyethylene (XLPE), often with vitamin E infused to act as an antioxidant (VEXLPE), has become the typically used material for hip implant liners due to its high resistance to wear. The use of VEXLPE in knee and shoulder joint replacement implants is currently increasing in prevalence. Although revision rates have decreased significantly for hip implants since VEXLPE's implementation, its mechanical behaviour is still not fully understood, and some wear is still occurring. As joint load is subject to vary throughout any given activity, the effect of contact loading on VEXLPE wear is important to consider when designing joint implants (such as those used in reverse total shoulder arthroplasty). The purpose of this study was to investigate the effect of increased load on VEXLPE wear in a pin-on-plate simulator.

2.1   Introduction

Metal-on-polyethylene is a common configuration in total joint arthroplasty designs. These designs typically consist of a cobalt-chromium (CoCr) head articulating against a polyethylene liner. The current "gold standard" liner material in hip arthroplasties (and rapidly gaining popularity in the knee and shoulder) is a highly crosslinked polyethylene (XLPE) [1,2]. Many XLPE variants include the addition of vitamin E in attempts to reduce oxidation and increase wear resistance [3–8]. Although XLPE has shown substantial improvements to implant longevity compared to its non-crosslinked predecessor [1,9–12], wear-related failure mechanisms are still causes for revision surgery in some total joint replacements [1,12]. Consequently, understanding the wear of vitamin E stabilized XLPE (hereon referred to as VEXLPE) against CoCr is an important task in the orthopaedic engineering community.

Pin-on-plate testing is a common method used to explore the wear materials used in joint replacement implants in an indirect manner. The wear mechanisms involved at VEXLPE surfaces are still not fully understood and this limits the ability of wear simulators to predict clinical wear. As joint load magnitudes are subject to variations, it is necessary to understand how VEXLPE wears under different loads. Therefore, the purpose of this study was to investigate VEXLPE wear against CoCr and its response to increased contact load. The contact conditions (lubricant, temperature, etc.) were chosen to best represent intracapsular joint conditions.

2.2   Materials and Methods

2.2.1   Wear Simulation Strategy and Protocols

A six-station pin-on-plate wear machine [13] (OrthoPOD, AMTI, Watertown, Massachusetts, USA; Figure 2-1) was used to load and introduce motion (both reciprocating translation and axial rotation) to the CoCr-VEXLPE articulation. The six pins were machined from Carpenter Biodur CCM Alloy 1 (Carpenter Technology Corporation, Reading, Pennsylvania, USA) by University Machining Services (UMS) (Western

University, London, Ontario, CA). Each pin was 19 mm in length, 9.5 mm in diameter, with a 100 mm radius spherical tip (Figure 2-2). A spherical tip having a large diameter was used to prevent large contact stresses forming at the pin edges that might cut into, tear, or plastically deform the polyethylene during simulation. The articulating surface of the pins were polished to a mirror finish and were thoroughly cleaned in an ultrasonicator to prevent residual polishing compound from introducing 3rd body wear to the wear test.
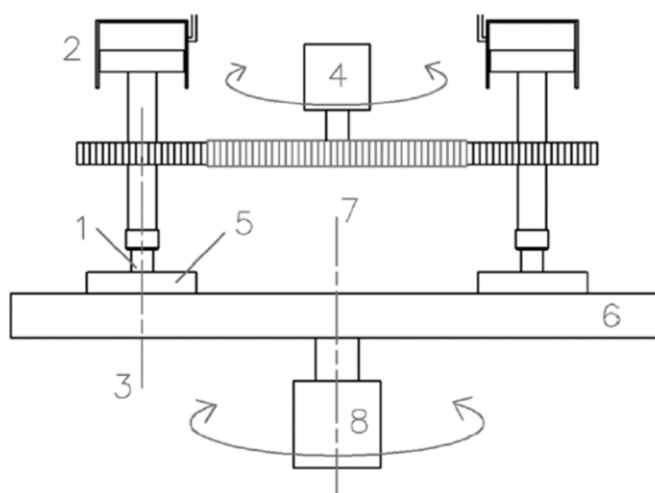
Figure 2-1: Cross-section schematic drawing of the six-station OrthoPOD wear machine from [13] **(1: pin, 2: pin load cylinder, 3: centre of rotation of pin, 4: pin drive, 5: plate, 6: lower disc, 7: centre of rotation of lower disc, 8: lower disc drive)**

Six plates were machined from vitamin E-stabilized GUR-1020 UHMWPE (Orthoplastics Ltd., Grove Mill, Bacup, England) bar stock that had been irradiated at 90 – 110 kGy. The VEXLPE was believed to have a density of 0.937 mg/mm^3 from the density stated in Hunt and Joyce (2016) for GUR-1020. Vitamin E infusion and crosslinking was assumed to have no significant influence the overall density. Using polyethylene plates allows the VEXLPE to be loaded cyclically, which is representative of the natural loading observed in orthopaedic implants [15,16], as opposed to if the pins were polymeric which would result

in them being consistently subjected to loading in a pin-on-plate configuration. Each plate was 32 mm in diameter with a thickness of 6.5 mm (Figure 2-2).

Prior to the start of the wear test, both the pins and plates were successively marked with numbers 1 – 6 to ensure consistent positioning and pairing between the two (e.g., pin 1 was always paired with plate 1, and both were always positioned in the same orientation in the wear simulator).
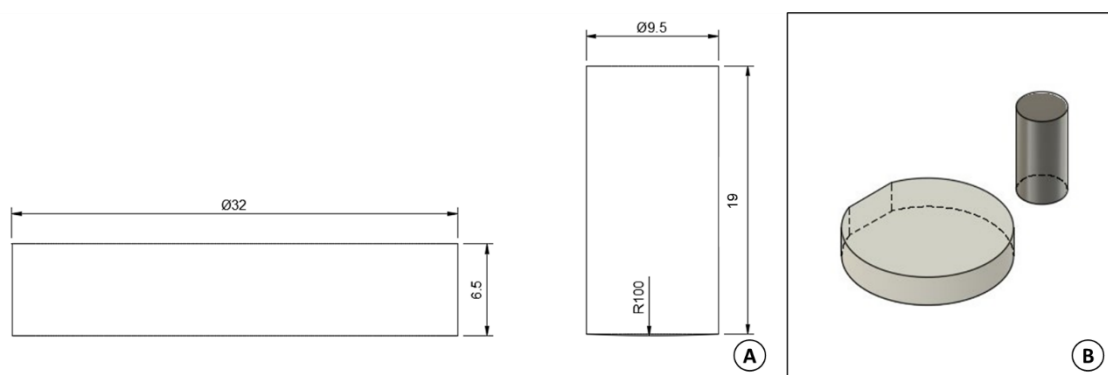
Figure 2-2: A) Pin and plate dimensions (mm) in profile view; B) 3D Pin and plate isometric view

The lubricant for wear testing was made by diluting non-iron alpha calf fraction serum (HyClone; GE Healthcare Life Sciences, South Logan, UT, USA) to a total protein concentration of 30 g/L using a phosphate buffered solution (VWR International, Mississauga, Ontario, CA). Both sodium hyaluronate and antimycotic antibiotic were added to the lubricant at concentrations of 1.5 g/L and 10 mL/L, respectively. This lubricant had been used in simulator testing that gave wear levels that could be related to clinical wear levels [17–20].

The specimen pairs were organized into two testing groups (3 in each), with the two groups alternating acting as the soak control and experimental wear test groups for each testing condition, as described in Table 2-1. As there were 6 wear stations and 6 specimen pairs, each specimen pair inhabited only its corresponding wear station (e.g., pin 1 and plate 1 were installed only into station 1). If a station was to be a soak control, the pin was lifted

such that no contact between the pin and plate would occur, exposing the control specimens to all the same elements in the simulations except for the loaded articular relative motion.

Each specimen was subjected to 1 million cycles (Mc) of wear in each trial (under both 80 N and 160 N of load). One Mc in the present wear machine was representative of about 17 km of relative motion. Each VEXLPE plate was pre-soaked in de-ionized (DI) water to minimize the amount of fluid absorbed during the simulation. Each trial was then conducted using the protocol outlined in Table 2-2.

Table 2-1: Testing plan

Trial #	Round #	Load	Duration	Experimental Specimens	Control Specimens
1	1	80 N	0.5 Mc	4, 5, 6	1, 2, 3
	2	80 N	0.5 Mc	4, 5, 6	1, 2, 3
	3	80 N	0.5 Mc	1, 2, 3	4, 5, 6
	4	80 N	0.5 Mc	1, 2, 3	4, 5, 6
2	5	160 N	0.5 Mc	4, 5, 6	1, 2, 3
	6	160 N	0.5 Mc	4, 5, 6	1, 2, 3
	7	160 N	0.5 Mc	1, 2, 3	4, 5, 6
	8	160 N	0.5 Mc	1, 2, 3	4, 5, 6

Table 2-2: Testing protocol

Step	Description
1	Specimens (pins and plates) were cleaned in an ultrasonic cleaner in baths of 2% Liqui-NOX® solution (Alconox Inc., White Plains, NY, USA) for 10 minutes.
2	Specimens were remove from Liqui-NOX® solution and rinsed with DI water.
3	Specimens were cleaned in an ultrasonic cleaner in baths of DI water for 5 minutes.
4	Specimens were removed from water bath and soaked in isopropyl alcohol for 5 minutes (to remove any water on the surface).
5	Specimens were removed from isopropyl alcohol and dried using a stream of nitrogen gas.
6	Plates were set down and allowed to acclimatize next to the analytical balance for 10 minutes.
7	The analytical balance was calibrated using the automatic calibration feature, and then tared.
8	The two standard masses (20 g and 100 g) were weighed.
9	Each plate's mass was weighed.
10	Repeat step 9 two more times to obtain three measurements for each plate.
11	The average of the three measurements was taken for each plate. If the average was not within 0.2 mg of each of the three readings, steps 7-11 were repeated.
12	Step 8 was repeated to ensure the measurements were within 0.2 mg of the previous reading.
13	Specimens were installed into the wear machine and lubricant was added.
14	The wear machine ran for 0.5 Mc.
15	Specimens were removed from the simulator.
16	Specimens were scrubbed with a soft brush and rinsed with DI water to remove any adhered contaminants.
17	Steps 1-12 were repeated.
18	All lubricant was removed, and the wear machine was thoroughly cleaned using DI water, a soft brush, and isopropyl alcohol.
19	Steps 13-18 were repeated thrice, swapping experimental and control groups each time, exposing each specimen to a cumulative 1 Mc under experimental conditions.

2.2.2   Wear Assessment

Volumetric wear was assessed gravimetrically using a Mettler Toledo X205 Analytical Balance (Columbus, OH, USA) with a precision of 0.01 mg. Real mass loss (Δm) was calculated by adding the mass of fluid absorbed by the controls (Δm_c) to the apparent mass loss due to wear (Δm_w) (Equation 2-1).

$$\Delta m = \Delta m_w + \Delta m_c \qquad\qquad (2\text{-}1)$$

The real mass loss was then divided by the density of XLPE (0.937 mg/mm^3) to produce total volumetric wear (w) (Equation 2-2).

$$w = \frac{\Delta m}{0.937} \qquad\qquad (2\text{-}2)$$

2.2.3   Statistics

A two-tailed paired t-test was performed in Microsoft Excel (Version 2111 Build 16.0.14701.20254, 64-bit) to assess statistical significance of wear between the two loads investigated. A paired t-test was used to compare the wear of each specimen under the higher load directly to the wear of that same specimen under the lesser load. Alpha level was set to $\alpha = 0.05$.

2.3   Results

All wear measurements were negative, which indicated that mass gain due to fluid absorption overshadowed the actual mass loss due to wear (Figure 2-3), and since soak controls were used, this meant that the wear specimens absorbed more fluid than the controls. After 1 Mc, the VEXLPE plates exhibited an average mass gain ± STD of 0.4 mg ± 0.02 mg and 0.26 mg ± 0.08 mg (p<0.02) for the 80 N and 160 N trials, respectively.

Despite detecting overall mass gain, the VEXLPE still exhibited visual evidence of surface changes indicated by polishing along the contact's motion path (Figure 2-4).
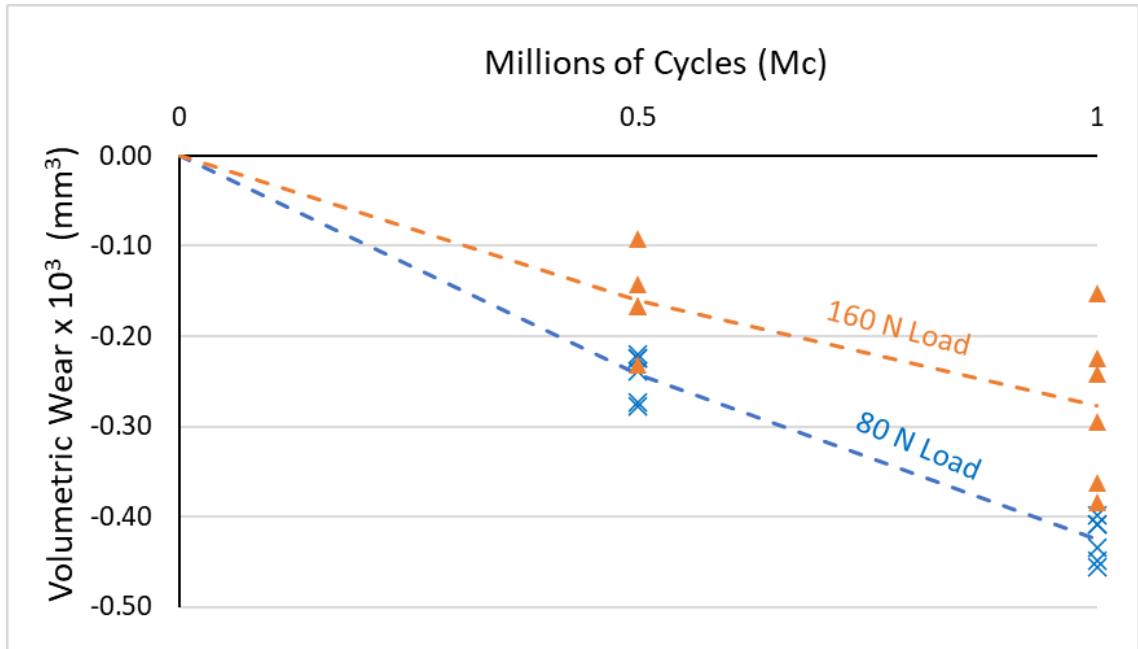
Figure 2-3: VEXLPE wear

Figure 2-4: Wear scar on VEXLPE plate

2.4 Discussion

Although the gravimetric assessment indicated a net mass gain, the VEXLPE still presented with a wear scar, suggesting that polyethylene wear could have been present, but masked by the magnitude of fluid absorption into the material. Surprisingly, while we did use soak controls to accommodate the fluid uptake during testing, clearly the addition of loading affected the fluid uptake of the VEXLPE. This could have been due to the reciprocating motion causing a 'pumping' effect on the surface or the backside of the plate, resulting in fluid being driven into the specimen. The addition of loading to the soak controls might have alleviated this problem, however these load-soak controls would also lack the reciprocating motion, and the current wear simulator used in the present study did not permit loading without relative motion. This issue combined with the very low wear rate of VEXLPE is hypothesized to be the main reason why negative wear was measured.

Saikko [21] investigated non-crosslinked UHMWPE wear under varying loads and showed that as nominal contact pressure increased, gravimetric wear increased until a critical pressure, after which wear rates diverged and the observed wear mechanisms differed from those seen clinically. In the case of the present study, the higher load likely fell into the range before this 'critical pressure' where wear rate increased with contact pressure. For the current study, this meant that the VEXLPE wear increased, and the higher degree of fluid absorption of the wear test specimens either stayed the same or increased at a lesser rate than the change in wear, resulting in a 'less negative' wear result.

Another possible contributor to the less negative wear with increased load may be an increased contact area as the spherical tip of the pin was pressed further into the VEXLPE, similar to that observed in the total knee simulation [22]. This relationship between contact area and XLPE wear has been previously reported in pin-on-plate studies [23,24]. Both of these pin-on-plate studies used an XLPE pin vs CoCr plate configuration, which introduced constant load and relative motion to the polyethylene and was likely a contributing factor to their wear detection. Kandemir et al. [23] also ran their experiment for 2.5 Mc, introducing about 87 km of relative motion to the polyethylene. This was over 5x more relative motion than what was simulated in the present study. As a result of using a XLPE pin, the polymeric surface area would have been significantly less than the present work,

and if fluid absorption is proportional to the available surface over which fluid uptake can occur, this may have also contributed to the present studies finding of negative wear.

The result of this study questions whether the gravimetric approach to wear measurement is sensitive enough to detect the very low XLPE wear in pin-on-plate studies. Another study has shown an overall gain in mass when investigating XLPE wear [25], which suggests it is not an uncommon finding. Other groups have employed micro-CT scans to measure volumetric wear [26,27], but this method has limited sensitivity and cannot distinguish between surface creep and lost volume. It is very likely that differences in fluid uptake between the wear test and soak specimens in the present study resulted in the negative wear rates observed. In this case, the wear test specimens are hypothesized to have absorbed more fluid than their soak specimen counterparts. Reducing the ratio of XLPE specimen surface area to articular area may reduce this effect, as less available surface area for fluid absorption may reduce the magnitude of mass change due to this phenomenon. This could be accomplished with either smaller plates or reversing the configuration and using XLPE pins, although the latter forfeits the ability to cyclically load the XLPE. Ultimately, the lack of sensible wear results encouraged the move to wear simulator testing in which the wear amounts would be higher and the contact would be much closer to clinical reality.

It seems that almost all of the published studies that have detected XLPE wear in pin-on-plate testing have used XLPE pins against CoCr plates [6,21,24,28–33]. Perhaps this configuration is, although not as accurate a representation of *in vivo* loading mechanics, necessary to elucidate detectible wear volumes in the highly wear resistant VEXLPE.

Limitations of this study include the omission of load-soaked controls, although this is technically difficult as to fully simulate the applied loading scenario, a roller style device might do this, but it would need to apply a reciprocating load to the load-soak specimens, adding additional complexity and potential error to the wear simulation. Accounting for fluid uptake under loaded conditions may allow a closer assessment of real polyethylene wear.

The strengths of this study include the partial replication of clinical conditions in the wear simulation by using clinically relevant surfaces, lubricants, and lubricant temperature. Also, the use of CoCr pins and XLPE plates allows the polyethylene to be loaded cyclically, as it does *in vivo,* and the use of spherical tips rather than flat ended pins negates the possibility of edge effects producing wear that might not occur in clinical application.

2.5 Conclusion

Although this was not a successful study for measuring wear and the influence of load on wear, some observations can be made. Crosslinked polyethylene wear showed a significantly different response to the 80 N load than the 160 N load, suggesting that XLPE wear may be load-dependent for the loads applied in the present study. Although volumetric wear was measured to be negative, the results still highlight the resistance of XLPE to wear against CoCr and points out the potential for issues arising from the uneven fluid uptake of wear and soak specimens for such a low-wearing material pairing.

2.6 References

[1]   Australian Orthopaedic Association National Joint Replacement Registry.
        Australian Orthopaedic Association National Joint Replacement Registry
        (AOANJRR). Hip Knee & Shoulder Arthroplasty: 2020 Annual Report 2020.

[2]   Medley JB. Highly cross-linked polyethylene is the new 'gold standard' bearing
        material for total hip arthroplasty. Biosurface and Biotribology 2021:1–7.
        https://doi.org/10.1049/bsb2.12007.

[3]   Alexander JJ, Bell SN, Coghlan J, Lerf R, Dallmann F. The effect of vitamin E–
        enhanced cross-linked polyethylene on wear in shoulder arthroplasty—a wear
        simulator study. J Shoulder Elb Surg 2019;28:1771–8.
        https://doi.org/10.1016/j.jse.2019.01.014.

[4]   Ansari F, Ries MD, Pruitt L. Effect of processing, sterilization and crosslinking on
        UHMWPE fatigue fracture and fatigue wear mechanisms in joint arthroplasty. J
        Mech Behav Biomed Mater 2016;53:329–40.
        https://doi.org/10.1016/j.jmbbm.2015.08.026.

[5]   Ftaita S, Vanden Berghe A, Thienpont E. Vitamin E-enriched polyethylene
        bearings are not inferior to Arcom bearings in primary total knee arthroplasty at
        medium-term follow-up. Arch Orthop Trauma Surg 2021;141:1027–33.
        https://doi.org/10.1007/s00402-020-03727-6.

[6]   Fu J, Doshi BN, Oral E, Muratoglu OK. High temperature melted, radiation cross-
        linked, vitamin e stabilized oxidation resistant UHMWPE with low wear and high
        impact strength. Polymer (Guildf) 2013;54:199–209.
        https://doi.org/10.1016/j.polymer.2012.11.017.

[7]   Mathis DT, Schmidli J, Hirschmann MT, Amsler F, Henckel J, Hothi H, et al.
        Comparative retrieval analysis of antioxidant polyethylene: bonding of vitamin-E
        does not reduce in-vivo surface damage. BMC Musculoskelet Disord 2021;22:1–
        11. https://doi.org/10.1186/s12891-021-04898-y.

[8]   Nebergall AK, Greene ME, Laursen MB, Nielsen PT, Malchau H, Troelsen A. Vitamin E diffused highly cross-linked polyethylene in total hip arthroplasty at five years. Bone Jt J 2017;99B:577–84. https://doi.org/10.1302/0301-620X.99B5.37521.

[9]   De Steiger R, Lorimer M, Graves SE. Cross-linked polyethylene for total hip arthroplasty markedly reduces revision surgery at 16 years. J Bone Jt Surg - Am Vol 2018;100:1281–8. https://doi.org/10.2106/JBJS.17.01221.

[10]   Devane PA, Horne JG, Ashmore A, Ortho F, Mutimer J, Ortho F, et al. Revision Rates in Total Hip Arthroplasty 2017:1703–14.

[11]   Khoshbin A, Wu J, Ward S, Melo LT, Schemitsch EH, Waddell JP, et al. Wear Rates of XLPE Nearly 50% Lower Than Previously Thought After Adjusting for Initial Creep. JBJS Open Access 2020;5:e0066–e0066. https://doi.org/10.2106/jbjs.oa.19.00066.

[12]   Civinini R, Carulli C, Matassi F, Cozzi Lepri A, Sirleo L, Innocenti M. The Survival of Total Knee Arthroplasty: Current Data from Registries on Tribology: Review Article. HSS J 2017;13:28–31. https://doi.org/10.1007/s11420-016-9513-9.

[13]   Langohr GDG, Gawel HA, Medley JB. Wear performance of all-polymer PEEK articulations for a cervical total level arthroplasty system. Proc Inst Mech Eng Part J J Eng Tribol 2011;225:499–513. https://doi.org/10.1177/2041305X10395062.

[14]   Hunt BJ, Joyce TJ. A tribological assessment of Ultra High Molecular Weight Polyethylene types GUR 1020 and GUR 1050 for orthopedic applications. Lubricants 2016;4. https://doi.org/10.3390/lubricants4030025.

[15]   Langohr GDG, Giles JW, Athwal GS, Johnson JA. The effect of glenosphere diameter in reverse shoulder arthroplasty on muscle force, joint load, and range of motion. J Shoulder Elb Surg 2015;24:972–9. https://doi.org/10.1016/j.jse.2014.10.018.

[16] Varadarajan KM, Moynihan AL, D'Lima D, Colwell CW, Li G. In vivo contact kinematics and contact forces of the knee after total knee arthroplasty during dynamic weight-bearing activities. J Biomech 2008;41:2159–68. https://doi.org/10.1016/j.jbiomech.2008.04.021.

[17] Brandt JM, Brière LK, Marr J, MacDonald SJ, Bourne RB, Medley JB. Biochemical comparisons of osteoarthritic human synovial fluid with calf sera used in knee simulator wear testing. J Biomed Mater Res - Part A 2010;94:961–71. https://doi.org/10.1002/jbm.a.32728.

[18] Brandt JM, Charron K, Zhao L, MacDonald SJ, Medley JB. Calf serum constituent fractions influence polyethylene wear and microbial growth in knee simulator testing. Proc Inst Mech Eng Part H J Eng Med 2012;226:427–40. https://doi.org/10.1177/0954411912444248.

[19] Brandt JM, Mahmoud KK, Koval SF, MacDonald SJ, Medley JB. Antimicrobial agents and low-molecular weight polypeptides affect polyethylene wear in knee simulator testing. Tribol Int 2013;65:97–104. https://doi.org/10.1016/j.triboint.2013.02.019.

[20] Brandt JM, Charron KD, Zhao L, MacDonald SJ, Medley JB. Lubricant Biochemistry Affects Polyethylene Wear in Knee Simulator Testing. Biotribology 2021;27:100185. https://doi.org/10.1016/j.biotri.2021.100185.

[21] Saikko V. Effect of contact pressure on wear and friction of ultra-high molecular weight polyethylene in multidirectional sliding. Proc Inst Mech Eng Part H J Eng Med 2006;220:723–31. https://doi.org/10.1243/09544119JEIM146.

[22] O'Brien ST, Luo Y, Brandt JM. In-vitro and in-silico investigations on the influence of contact pressure on cross-linked polyethylene wear in total knee replacements. Wear 2015;332–333:687–93. https://doi.org/10.1016/j.wear.2015.02.048.

[23] Kandemir G, Smith S, Joyce TJ. The influence of contact stress on the wear of

cross-linked polyethylene. Proc Inst Mech Eng Part H J Eng Med 2018;232:1008–16. https://doi.org/10.1177/0954411918796047.

[24] Abdelgaied A, Brockett CL, Liu F, Jennings LM, Fisher J, Jin Z. Quantification of the effect of cross-shear and applied nominal contact pressure on the wear of moderately cross-linked polyethylene. Proc Inst Mech Eng Part H J Eng Med 2012;227:18–26. https://doi.org/10.1177/0954411912459423.

[25] Estok DM, Burroughs BR, Muratoglu OK, Harris WH. Comparison of Hip Simulator Wear of 2 Different Highly Cross-linked Ultra High Molecular Weight Polyethylene Acetabular Components Using Both 32- and 38-mm Femoral Heads. J Arthroplasty 2007;22:581–9. https://doi.org/10.1016/j.arth.2006.07.009.

[26] Day JS, MacDonald DW, Olsen M, Getz C, Williams GR, Kurtz SM. Polyethylene wear in retrieved reverse total shoulder components. J Shoulder Elb Surg 2012;21:667–74. https://doi.org/10.1016/j.jse.2011.03.012.

[27] Van de Kleut ML, Athwal GS, Faber KJ, Teeter MG. In vivo volumetric and linear wear measurement of reverse shoulder arthroplasty at minimum 5-year follow-up. J Shoulder Elb Surg 2020;29:1695–702. https://doi.org/10.1016/j.jse.2019.11.031.

[28] Brandt JM, Vecherya A, Guenther LE, Koval SF, Petrak MJ, Bohm ER, et al. Wear testing of crosslinked polyethylene: Wear rate variability and microbial contamination. J Mech Behav Biomed Mater 2014;34:208–16. https://doi.org/10.1016/j.jmbbm.2014.02.016.

[29] Harsha AP, Joyce TJ. Comparative wear tests of ultra-high molecular weight polyethylene and cross-linked polyethylene. Proc Inst Mech Eng Part H J Eng Med 2013;227:600–8. https://doi.org/10.1177/0954411913479528.

[30] Laraia K, Leone N, MacDolanald R, Blanchet TA. Effect of water and serum absorption on wear of unirradiated and crosslinked UHMWPE orthopedic bearing materials. Tribol Trans 2006;49:338–46. https://doi.org/10.1080/05698190600678663.

[31]   Saikko V. Effect of serum dilution fluids on the wear of unirradiated and high dose gamma-irradiated, vitamin E stabilized UHMWPE. Wear 2019;430–431:76–80. https://doi.org/10.1016/j.wear.2019.04.022.

[32]   Yao JQ, Blanchet TA, Murphy DJ, Laurent MP. Effect of fluid absorption on the wear resistance of UHMWPE orthopedic bearing surfaces. Wear 2003;255:1113–20. https://doi.org/10.1016/S0043-1648(03)00167-4.

[33]   Galvin A, Kang L, Tipper J, Stone M, Ingham E, Jin Z, et al. Wear of crosslinked polyethylene under different tribological conditions. J Mater Sci Mater Med 2006;17:235–43. https://doi.org/10.1007/s10856-006-7309-z.

Chapter 3

In Vivo Assessment of Reverse Total Shoulder Arthroplasty Articular Sliding Distances

OVERVIEW: The reverse total shoulder arthroplasty (RTSA) is an increasingly used treatment for many shoulder conditions. In vitro wear simulation studies have been conducted to investigate the wear performance of RTSA implants with non-crosslinked polyethylene humeral cups, but there has been variance in the duration of these simulations, and an estimated yearly number of cycles experienced by these devices has not been offered. The purpose of the present study was to quantify the daily glenohumeral articular sliding distance (relative motion) in fully recovered patients following RTSA shoulder reconstruction. Additionally, we sought to determine the proportion of time the inferior aspect of the cup overlapped the back side of the glenosphere medially, which is a position with a high risk of scapular notching.

3.1 Introduction

The reverse total shoulder arthroplasty (RTSA) is currently the most common total shoulder replacement, making up over 80% of all total shoulder arthroplasty surgeries, and being used to treat a wide variety of conditions including, but not limited to, rotator cuff arthropathy, osteoarthritis, humeral fracture, osteonecrosis, joint instability, and failed anatomic total shoulder arthroplasty [1]. The procedure reverses the native geometry of the glenohumeral joint, instrumenting a hemisphere onto the glenoid cavity and a cup onto the humeral head. Although this treatment has shown promising clinical outcomes, it is still experiencing some wear-related complications [2–4]. Additionally, a common complication known as *scapular notching* [5] (Figure 3-1) may develop, which occurs when the inferior aspect of the humeral cup repeatedly contacts the lateral border of the scapula and results in the removal of bone along the lateral edge of the scapula as well as damage to the rim of the polyethylene humeral cup (Figure 3-1). Scapular notching and the related humeral cup rim damage have been observed in upwards of 68% of RTSA primaries [6], and 76% of RTSA revisions [7].
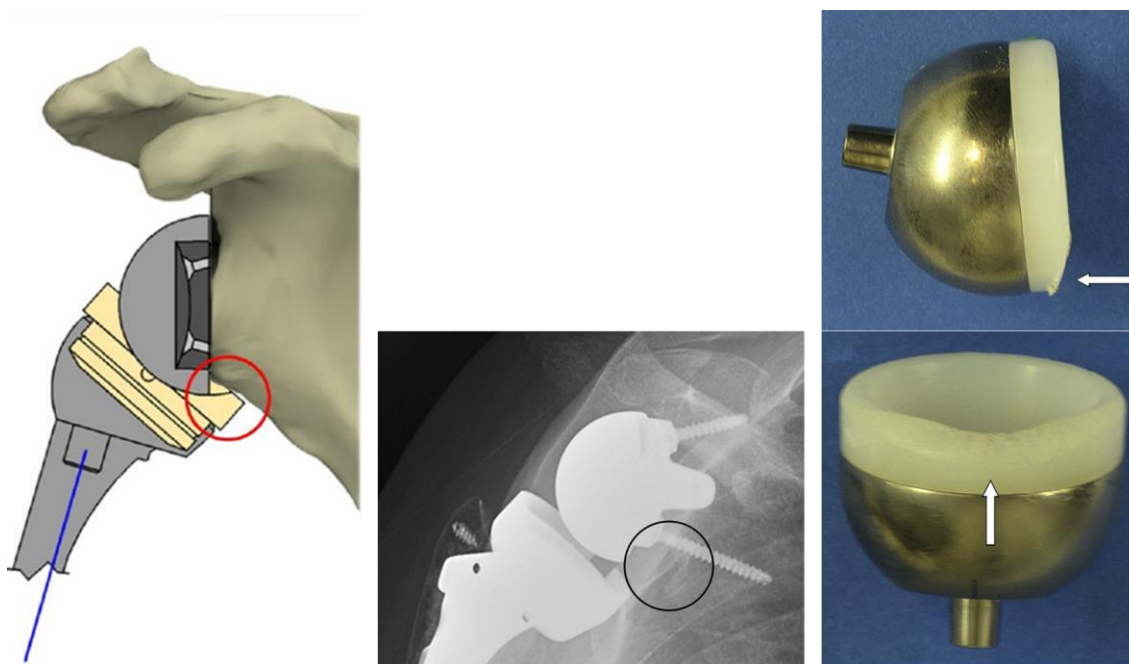
Figure 3-3: Contact between the inferior aspect of the humeral cup and the lateral border of the scapula resulting in scapular impingement (left), a radiograph of its clinical progression showing scapular notching (centre), and the resulting inferior rim damage of the non-crosslinked (non-XLPE) polyethylene humeral cup (right) from Nam et al. (2010) [8]

While several research groups have investigated the *in vitro* simulator wear of RTSA implants, there has been significant variation in both motion profile and testing duration. Some previously published works have subjected implants to as little as 0.5 million cycles (Mc) [9] while others test up to 5 Mc [10], often with no justification provided for their selections, nor any indication for how many cycles represents one year *in vivo*. In other joints, such as the hip and knee, there is a clearly defined amount of gait cycles that occur yearly [11], which influences simulation lengths and provides an approximate clinical translation of the results. Currently, the annual number of cycles for the RTSA is not defined, creating a gap between *in vitro* testing protocol and clinical relevance of the results.

Multiple simulations of varying designs (i.e. experiments with cadavers, sawbones in place of natural bone, and with computational models) have suggested RTSAs with lower neck-

shaft angles (NSAs) (less than or equal to 145°) produced a lower incidence of inferior scapular impingement relative to 155° designs [12–15]. Alterations to the NSA affect the relative position of the humeral cup with respect to the humerus, with lower angles resulting in the humeral cup being rotated in the direction of abduction relative to the humeral shaft axis, thus moving the medial edge of the cup further away from the lateral border of the scapula, resulting in a reduced risk of scapular impingement. This effect has been observed clinically, with lower neck-shaft angles reducing the reported incidence of scapular notching down from the previously stated 68% [6] to between 9.8% [16] and 16.2% [17]. Glenosphere size has also been shown to influence the incidence of scapular notching in sawbones and computational models [12–14,18], but this effect has not been clearly confirmed in clinical studies [16].

While some work has been done to investigate the *in vitro* wear of RTSA implants [9,10,19–27], and there is a significant volume of work in the literature investigating the effects of altering neck-shaft angle and glenosphere diameter on shoulder biomechanics and range of motion [12–15,18,28–30], there is little information regarding the relative motions at the articular surface – hereon described as articular sliding distances – observed on the face of the humeral cup. Additionally, no one has investigated how changes in RTSA implant parameters affect these sliding distances.

Therefore, the purpose of the present study was to quantify the daily glenohumeral articular sliding distance for varying RTSA implant configurations at 5 locations on the humeral cup using motion data obtained from fully recovered patients following primary RTSA surgery. Although the patients had been reconstructed with an RTSA implant with a specific configuration, their shoulder motions were extended analytically to predict glenohumeral articular sliding distances for implants with different neck-shaft angles and glenosphere diameters. Using a computational model, we also sought to determine the amount of time the inferior aspect of the cup overlapped the back side of the glenosphere medially (Figure 3-2), which is a position with a high risk of scapular notching. This was done for four common RTSA implant geometrical configurations: a combination of 155° and 135° NSAs with each 38 mm and 42 mm diameter glenospheres.
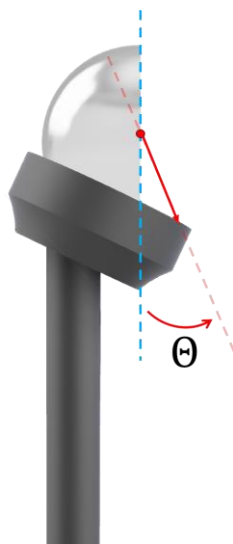
Figure 3-4: Medial overlap angle

3.2   Materials and Methods

3.2.1   Custom Instrumented Motion Shirt

This chapter serves as a secondary analysis on previously-captured data. Sections 3.2.1 and 3.2.2 were performed by Dr. G Daniel G Langohr, a co-author on this chapter, using the following protocol. A previously used and validated [31–33] custom, instrumented motion capture (MOCAP) shirt (Figure 3-3) was used to allow the recording of upper-limb kinematics during activities of daily living. The MOCAP shirt utilized a stretchable compression shirt (Nike Inc., Beaverton, OR, USA) that housed 3 inertial measurement units (IMUs; YEI Technology, Portsmouth, OH, USA) which were capable of tracking their orientation in 3D space. One IMU was inserted into a pocket and sewn onto the anterior surface of the shirt, directly over the sternum. The remaining 2 IMUs were similarly affixed, one on each sleeve, to the lateral aspect of the mid-humerus. Together, the IMUs allowed the recording of bilateral 3D humerothoracic motion.

Figure 3-3: Custom motion capture (MOCAP) shirt with pockets shown for the sternal and humeral inertial measurement units (IMUs)

Each IMU included an onboard triaxial accelerometer, gyroscope, and magnetometer. The accelerometer was used to measure acceleration in all 3 directions and the gyroscope was used to measure rotation about all 3 axes. The magnetometer measured the magnetic field around the IMU and, by detecting the earth's magnetic field, was able to help augment the determination of the orientation of the IMU. Alone, each of these three sensor types does not provide full orientation and position information, but in conjunction, they provide quite accurate and consistent data. All three signals were fused using an on onboard, real-time Kalman filter to produce the measured IMU orientation. This algorithm has been reported by the manufacturer to have an accuracy of $\pm 1°$ in all orientations.

An accuracy study compared joint angles reported by the MOCAP shirt and a passive reflective marker-based motion capture system; the MOCAP shirt had a difference of $4° \pm$

3º (average ± standard deviation) from the marker-based system [31]. These differences were likely caused by the inherent errors in each of the tracking systems including skin movement between the sensor attachment sites for both the shirt and the reflective marker system which served to distort the actual motion of the humerus with respect to the thorax. However, this difference between the measurement techniques was considered to be small enough to support the use of the MOCAP shirt for full-day patient monitoring when compared to the commonly used in-lab marker-based motion capture systems.

Each IMU stored its orientation at a frequency of 10 Hz on an accompanying micro-secure digital (SD) card. A study of shoulder movements in healthy elderly individuals during activities of daily living reported average and peak angular velocities during humeral elevation to be 44 °/s and 51 °/s, respectively [34]. If the humerus moves at this maximum velocity of 51 °/s, the IMU's 10 Hz sampling frequency would be able to detect a minimum change of 5.1° in humeral orientation per sample, which was deemed satisfactory for this study. All sensors were time-synchronized immediately before the shirt was donned and were confirmed to still be time-synchronized upon data retrieval. An external battery pack was fastened to a belt and wired to each IMU to provide continuous power using low-voltage, low-gauge wires. The wiring was done in such a way to ensure minimal discomfort or constriction to the wearer, allowing for natural, full-range upper extremity motion. The resulting motion-tracking system was low profile enough to be worn beneath normal clothing and still permitted the subject to perform most daily activities, barring those that included submersion of the torso in water (such as bathing or swimming).

3.2.2   Research Participants and Study Protocol

Seventeen human subjects (6 males, 11 females) aged 75 ± 6.5 years (average ± standard deviation) ranging from 56 to 84 years who had previously undergone RTSA reconstruction (5 left, 12 right; 13 dominant, 4 non-dominant; all unilateral) were recruited to participate in the study. All participants were greater than one-year postoperative status at the time of inclusion in the study, had undergone primary arthroplasties, lived independently, were fully ambulatory without aids, and were generally well-functioning.

Exclusion criteria included revision cases, institutionalization, and contralateral shoulder disease.

At the start of each testing day, the participants performed their normal daily morning bathing and grooming activities at their own home prior to travelling to the clinic. Once at the clinic, a research associate assisted the participant in donning the MOCAP shirt. This 'fitting' appointment was scheduled as early as feasible based on the participant's daily schedule. To calibrate the sensors, the subject was then asked to assume a 'tin soldier' position, which was defined as standing erect with 0° of humerothoracic elevation (or as close to 0° as possible), 0° of humerothoracic rotation in the plane of elevation, 0° of elbow flexion, and 0° of humeral internal rotation, following which, the sensors were activated. The patient was then asked to perform a series of movements through maximum range of motion to visually confirm that there were no physical constraints from the sensors or their power distribution system.

Each participant was then dismissed to continue their normal daily routine and instructed to briefly log activities for the rest of the day on a log sheet provided to allow the investigation of any potential motion anomalies (ex. a long period of non-movement could be identified as a nap rather than sensor malfunction) – none of which were noted for the present study population. At the end of the test day, just before the participants retired to bed, they were asked to remove the shirt and to cease the recording of motion. The motion-tracking garment was later returned to the clinic, and the data was downloaded and analyzed.

3.2.3   Kinematic Model Development

3.2.3.1   Motion Data Preparation

The data file from each IMU was inspected to ensure no data was collected following the removal of the MOCAP shirt. If the sensor system was not powered off upon doffing (indicated by a prolonged period of non-movement at the end of the data file), the data was trimmed from the end, backward, until the last instance of purposeful movement.

The files were then individually assessed to identify any overly noisy data that may disqualify the participant's data from further analysis. A humerothoracic plane of elevation angle of -76.8° (where 0° was arm in front, increasing negative as arm moved medially) was used to represent the limit of "humanly possible" movement in this plane, as determined by calculating the third standard deviation (99.7% of the sample) of the reported average active cross-body adduction in pre-op RTSA patients [35]. Since the authors detected no statistically significant differences between pre-op and post-op cross-body adduction, the reported pre-op values [35] were considered representative of a fully-recovered RTSA population. In the present study, if the motion data reported the wearer of the motion shirt had their humerus in a humerothoracic plane of elevation less than -76.8° for more than 5% of the day, the patient was excluded from further analysis. This resulted in the exclusion of two patient files. Furthermore, an interquartile analysis was performed to identify any outliers. One participant was identified as an outlier, largely attributed to their physically demanding occupation that required a great deal of upper limb movement. This participant was also removed from further analysis, resulting in the total of 17 participants included in the present study.

3.2.3.2 Kinematic Model

A custom program was developed using Python (64-bit, version 3.9.2, Python Software Foundation) to analyze the glenohumeral motion of each participant in their operated shoulder and simulated four various implant designs using each participant's motion data. The calculations in this program utilized NumPy (version 1.20.1).

The details of this program are provided in Appendix A. Briefly, the quaternions from the sensors embedded in the MOCAP shirt were converted to rotation matrices, which were then input into the model described by the flowchart in Figure 3-4. The algorithm identified five points on the face of the humeral cup (superior, inferior, anterior, posterior, and centre; Figure 3-5) and tracked the relative motion between each of these five points and the articulating surface of the glenosphere. Scapulothoracic rotation values were extracted from published literature [36] and used to account for scapulothoracic motion during humeral elevation, providing a more accurate approximation of glenohumeral motion. The model also tracked any event during which the inferior point of the humeral cup overlapped

the backside of the glenosphere medially, indicating periods when no relative sliding occurred for that point as well as for which there was an increased risk of contact between the humeral cup and the lateral border of the scapula. Both the total sliding distances at each of the five points on the cup and the percentage of time the inferior point spent overlapped were output from the model and used for analysis. The model was run using each combination of NSA (135° and 155°) and glenosphere diameter (38 mm and 42 mm) for each participant file.

Start

Initialize

Humeral Cup Point Generation

Calculate the position of all 5 humeral cup points of interest (Figura A-4) with respect to the humerus for:
a) Two neck-shaft angles (Figure A-1)
b) Two cup sizes

Scapular Kinematics Calculation

Load data relating 3D scapular rotation to humerothorcic abduction

Fit linear equations to the data, producing equations for scapular rotation as a function of humerothoracic abduction (Figure A-7)

for each time step

Kinematic Analysis

Extract 3D position of humerus with respect to the torso (from MOCAP shirt)

Next time step

no

Is this last time step?

yes

Exit loop

Assign a 0 magnitude to the relative motion between the glenosphere and point

Calculate the magnitude of relative motion between the glenosphere and point

no

yes

Is the point in contact with the glenosphere?

for each point

Calculate the location of the 5 humeral cup points relative to the glenosphere

Calculate humerothoracic abduction angles shown in Figure A-6

Input humerothoracic abduction angle into scapular rotation equations to determine 3D scapular (glenosphere) rotation

Rotate the glenosphere based on these values

Sum relative motion for each humeral cup point

Figure 3-4: Flowchart of glenohumeral kinematics algorithm
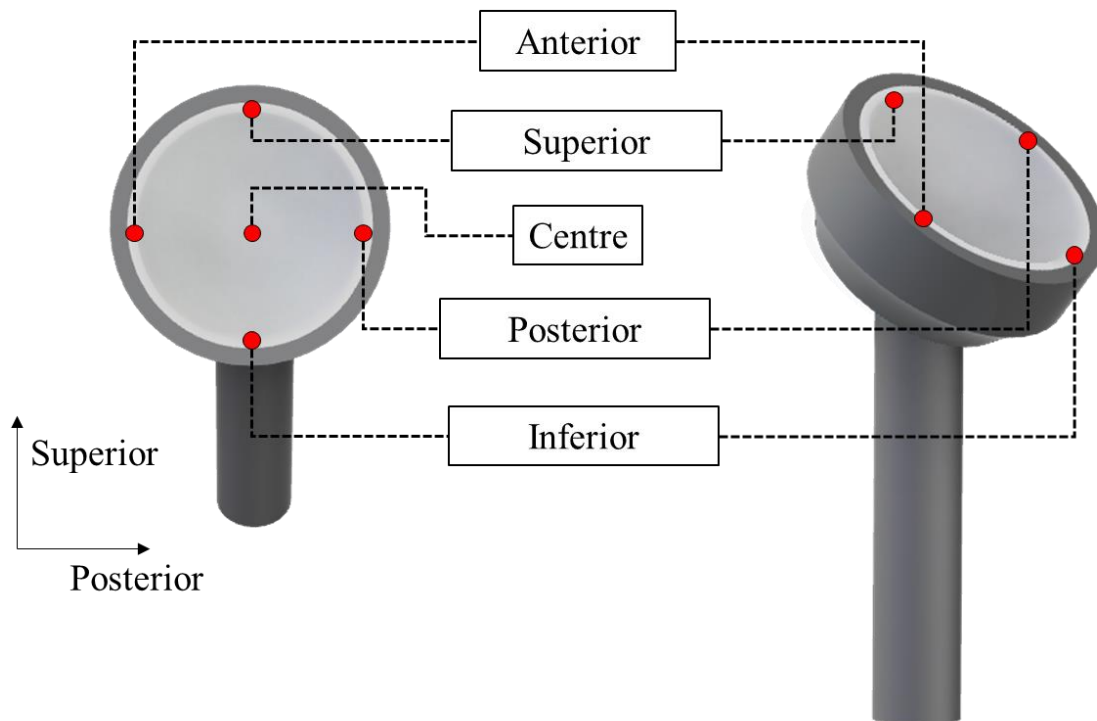
Figure 3-5: Five tracked points on the face of the humeral cup

3.2.4 Articular Sliding Distance Determination of In vitro RTSA Wear Simulator

In order to provide a link between *in vivo* sliding distances and *in vitro* simulation durations, the sliding distances introduced during shoulder simulation must be determined. The motion profile of our previously developed custom RTSA wear simulator [27] was input into custom code (Python, 64-bit, version 3.9.2, Python Software Foundation) that sampled the motion at 100 Hz and used the instantaneous glenohumeral rotation angles as Euler angles to produce rotation matrices. This series of rotation matrices represented the simulator's motion over 1 Mc, sampled at 100 Hz. The file containing these rotation matrices was then input into the above model with the scapulothoracic rhythm algorithm turned off (the simulator's kinematic data already represented the true glenohumeral motion) to obtain sliding distances.

3.2.5   Statistical Analysis

A repeated measures analysis of variance (RM-ANOVA) was conducted to identify statistically significant differences in sliding distance between the various points on the cup. The same tests were also used to determine the significance of the NSA's and glenosphere diameter's influence on sliding distance and the proportion of time the inferior point on the cup spent in medial overlap. Tests were performed using SPSS (version 27; IBM Inc., Armonk, NY, USA). Alpha levels were set to $\alpha = 0.05$.

3.3   Results

3.3.1   Articular Sliding Distance

Average daily articular sliding distances varied amongst humeral cup points (Table 3-1). Significant differences were detected between the average sliding distances for all humeral cup points except for the anterior and centre points for all combinations of NSA and cup size (p<0.05 for all). Increasing NSA increased the sliding distance at the superior point (p=0.002), and decreased sliding distance at inferior (p<0.001), posterior (p=0.035), and centre (p=0.014) points for all glenosphere diameters (Figure 3-6). No significant difference was detected at the anterior point when increasing NSA (p=0.09). Increasing the glenosphere diameter significantly increased sliding distance at all points for both NSAs tested (p<0.01 for all; Figure 3-6).

Table 3-1: Average daily sliding distance (m) at each humeral cup point tracked for each implant configuration investigated

NSA	Cup Size	Location				
		Superior	Inferior	Anterior	Posterior	Centre
135°	38 mm	126.3 ± 59.5	93.8 ± 33.8	149.8 ± 59.1	51.5 ± 33.1	137.4 ± 57.2
	42 mm	139.5 ± 65.8	103.5 ± 37.3	165.5 ± 65.3	56.6 ± 36.4	151.9 ± 63.3
155°	38 mm	134.7 ± 60.0	75.4 ± 30.4	148.2 ± 57.9	46.1 ± 29.9	128.1 ± 51.0
	42 mm	148.8 ± 66.3	83.1 ± 33.6	163.8 ± 64.0	50.6 ± 32.9	141.6 ± 56.3
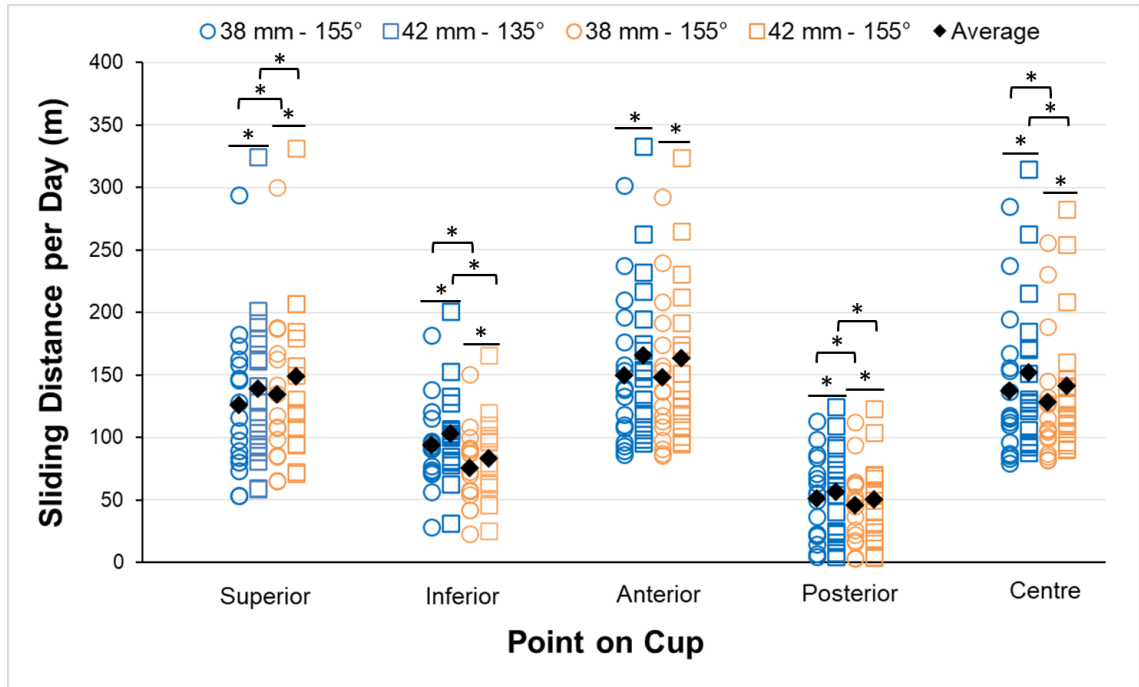
Figure 3-6: Sliding distance per day (m) for each implant configuration for all patients measured

3.3.2 Inferior Glenosphere Overlap

The average proportion of time the inferior point spent in medial overlap was expressed as a percentage (Figure 3-7). Increasing glenosphere diameter did result in a statistically significant increase in the average percent overlap ($p<0.01$), but this increase was so small (0.2% ± 0.2% for 135° NSA, 0.1% ± 0.1% for 155° NSA) that a clinical effect was considered to be negligible. Decreasing the NSA from 155° to 135° significantly decreased overlap time for both glenosphere diameters ($p<0.01$ for both). The 38 mm glenosphere experienced a 12.3% ± 11.7% decrease and the 42 mm glenosphere experienced a 12.3% ± 11.6% decrease. Implants with a 135° NSA had an average overlap percentage of 38.5% ± 21.7% and 38.7% ± 21.7% with a 38 mm and a 42 mm implant diameter, respectively. Implants with a 155° NSA had an average overlap time of 50.8% ± 23.8% and 51.0 ± 23.8% with a 38 mm and a 42 mm implant diameter, respectively.
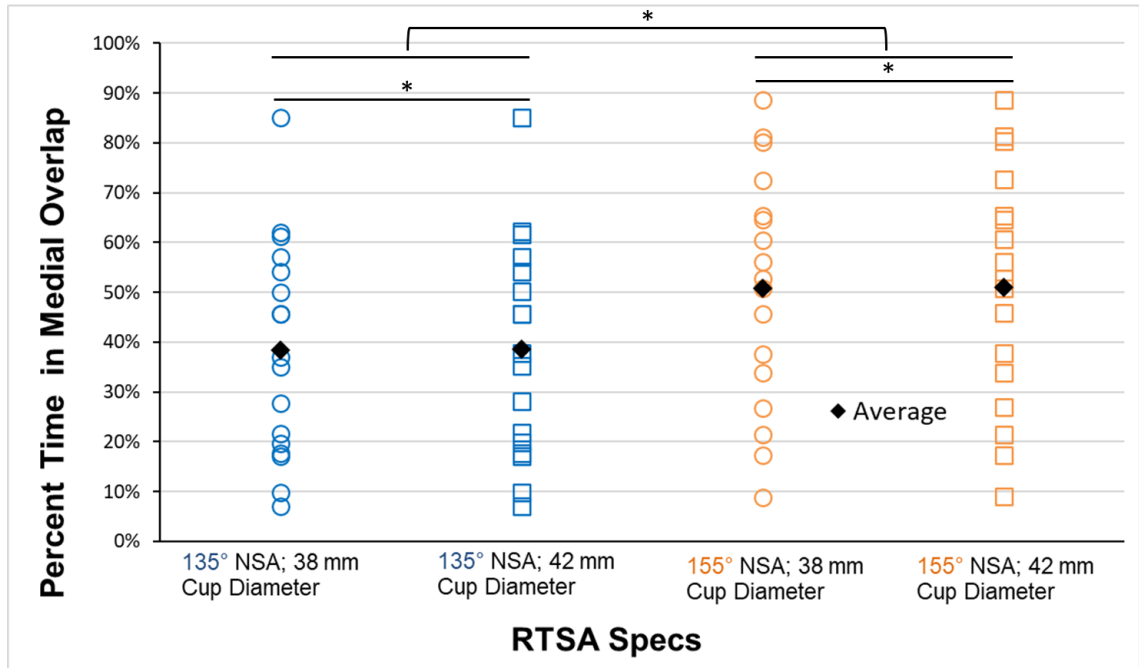
Figure 3-7: Percentage of time the inferior point spent in medial overlap

3.3.3   Articular Sliding Distance of In vitro RTSA Wear Simulator

The results from the analysis of the simulator motion profile revealed sliding distances ranging from 28.3 km to 49.9 km over a duration of 1 Mc, depending on the humeral cup point location and implant configuration (Table 3-2). When deciding which points are most relevant for comparison of wear simulator and *in vivo* data, it is important to consider the loading of the implant. The general loading of the humeral cup is likely to be centered in the inferior aspect owing to the musculature lines of action driving most shoulder motion [27,30]. As a result, since the superior point is seldomly loaded during shoulder motion, the relative sliding observed at this location is likely less contributory to overall humeral cup wear, and moreover, the longevity of the RTSA. Furthermore, simulator and retrieval studies consistently show the most polyethylene wear occurring at the inferior pole of the cup, with moderate wear at the centre and very little at the superior pole [2,3,26,37]. For these reasons, the sliding distances at the inferior and centre points of the cup during simulation and in the *in vivo* data should take priority when determining the annual number of cycles of the RTSA. When extrapolating the *in vivo* data to represent one year and

comparing it to the simulator's motion profile, approximately 1.25 Mc of motion in the simulator is expected to be representative of 1 year *in vivo* (Figure 3-8).

Table 3-2: Sliding distances introduced to various points on the humeral cup during *in vitro* simulation for each implant configuration

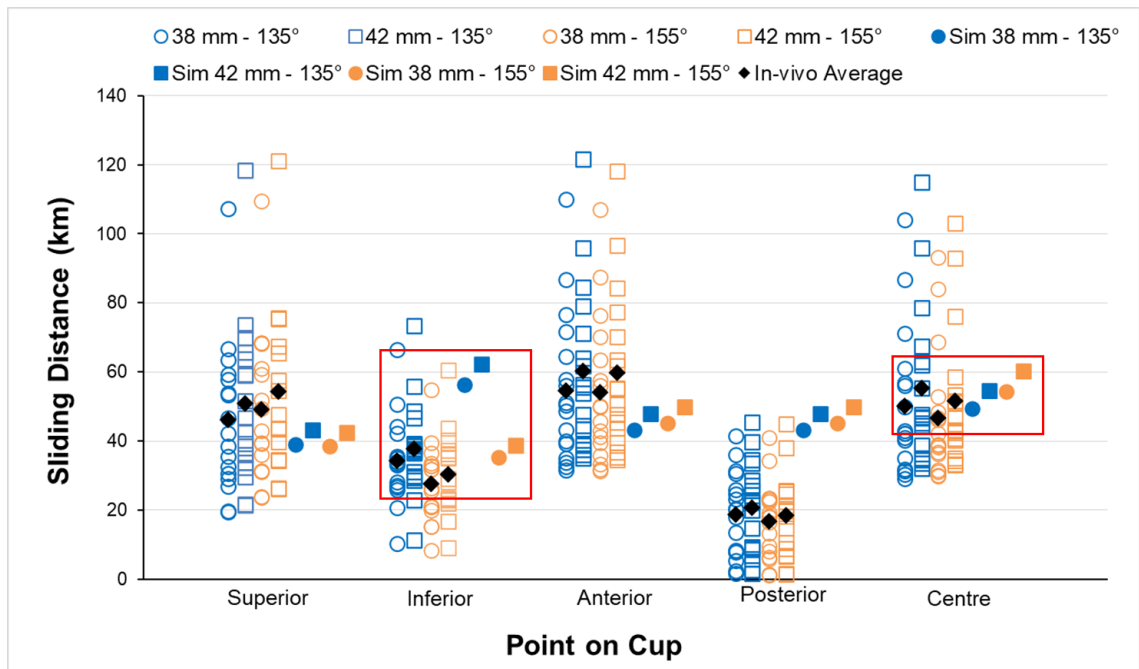| NSA	Diameter	Superior	Inferior	Anterior	Posterior	Centre
135	38	31.2	45.1	34.6	34.6	39.5
155	38	30.8	28.3	36.2	36.2	43.6
135	42	34.5	49.9	38.3	38.3	43.7
155	42	34.0	31.1	40.0	40.0	48.1

Figure 3-8: Extrapolated sliding distance representing 1 year *in vivo* compared to 1.25 Mc in simulator

3.4 Discussion

The inferior aspect of the humeral cup has been repeatedly identified as the site which experiences the most polyethylene wear and damage in retrieved RTSA implants (Figure

3-9) [2,3]. This location was found to experience comparatively small amount of relative motion against the glenosphere, and large amounts of medial overlapping, suggesting that a primary mechanism for XLPE damage/wear at the inferior aspect of the humeral cup may be repetitive contact with the scapular border. Although small overlap angles may not result in contact, this is the result of glenosphere placement and the true angle at which the contact occurs would vary patient to patient. Nonetheless, the repetitive overlapping provides an opportunity for surgical complication, mainly by means of scapular notching. A smaller NSA was associated with a reduced incidence of inferior cup overlap (Figure 3-7), suggesting a lesser risk of damage to the implant. This effect of a smaller NSA agreed with published modelling studies [12–15] as well as clinical observations [17,38]; notably, Mollon et al. [38] who showed a presence of scapular notching in just 10% of RTSAs employing a 145° NSA, down from the reported 68% [6] and 76% [7], after assessing 476 reconstructed shoulders. Reducing NSA may be an important factor in reducing the risk of scapular notching and its associated damage to the polyethylene cup.

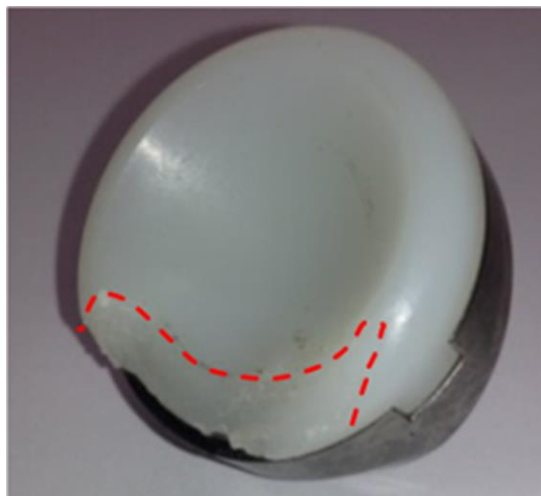**Figure 3-9: Polyethylene damage to inferior aspect of the humeral cup.**

It has been suggested by modelling and computational studies that larger glenosphere diameters can increase adduction range of motion, and decrease the risk of scapular impingement by moving the articular surface of the humeral cup farther from the center of rotation [12–14,18], although clinical evidence has suggested that going from a 38 mm

glenosphere diameter to a 42 mm glenosphere diameter may not influence the severity of medial overlapping [16].

While the current findings did show a statistically significant increase in medial overlapping with the larger cup size, the changes in overlap time (0.1% - 0.2% of the sample duration) are likely to be clinically inconsequential. The detection of an increased overlap time was a result of only measuring when the inferior humeral cup point passed beneath the medial backside plane of the glenosphere. This is a simple geometric relationship, and a larger humeral cup diameter will not affect the degree of adduction where this occurs (unless the cup depth is different). What may be occurring clinically, however, is the lateral scapular border may be located further in the medial direction at the humeral cup inferior point location of the larger cup, meaning that more adduction range of motion is afforded by the larger size before contact with the scapula. Thus, the larger diameter implants would sustain less scapular notching damage.

In the present study, increasing the implant diameter did, however, result in approximately a 10% increase in average articular sliding distance for all cup locations investigated. If wear is considered to be proportional to relative motion through a contact, a 10% increase in sliding may produce significantly more polyethylene wear and introduce more wear debris into the joint. An increase in glenosphere diameter has also been found to increase the contact area of the RTSA [30], which is also likely to produce more wear [26].

Loading is important to consider, as it has been suggested that the inferior aspect of the cup experiences the most contact and largest contact stresses [30,39]. Although medial overlapping decreased with a smaller NSA, average maximum contact stress at the inferior cup has been found to increase by 286% when moving from a 155° NSA to a 135° NSA [30]. For a clinician installing an RTSA system with a highly wear-resistant humeral cup liner material, this increase in contact stress may not provoke significant arthroplasty wear, in which case the implant may benefit from the reduced risk of scapular contact inherit with the smaller NSA. For an implant system using a conventional humeral liner material, a reduction in NSA may cause significantly greater implant wear due to the high contact stress. An increase in glenosphere diameter from 38

mm to 42 mm has also been shown to increase average joint load by 5% in RTSA implants [18], which, in conjunction with an increased sliding distance, may increase arthroplasty wear in RTSAs employing a conventional humeral cup liner material.

The present model assumed that the humeral cup had the exact same diameter as the glenosphere and did not experience any deformation due to loading, which is not accurate of true RTSA loading characteristics. A computational finite element study reported that the superior 1/3 of the humeral cup does not experience significant contact with the glenosphere during simulated abduction motion using joint reaction forces measured during *in vitro* cadaveric testing [30]. It was also reported that the humeral cup centre point was in contact for only some abduction angles for an RTSA having a NSA of 135°. The same study showed constant contact at the centre point in an RTSA implant with a 155° NSA [30]. Therefore, it is suggested that only the inferior and centre points on the cup should be taken into consideration when evaluating sliding distances in the present study, weighing emphasis on the centre point values only in the 155° NSA configurations. On these considerations, the results of the current study show that 1.25 Mc in our shoulder wear simulator is a good representation of 1 year *in vivo*.

Our simulator also mimicked just one motion (circumduction). Simulating other motions is expected to produce differing sliding distances. Due to the variety of kinematic profiles used in RTSA simulations, it is suggested that future RTSA wear studies relate their testing durations to the *in vivo* sliding distances produced by the present computational model. This would allow some comparison between simulator wear studies and *in vivo* wear.

Strengths of this study include the large sample size and the long durations of motion capture of RTSA recipients, which has a clear advantage over recording the shoulder kinematics for only a few activities in a controlled laboratory setting. It was very important that the MOCAP garment was found to be comfortable and unrestrictive to the participants and allowed the recording of the large variety of movements that occur during the participants' normal daily routines.

Limitations of this study include the potential error associated with the assumptions that were required to accommodate and estimate the scapulohumeral rhythm. This is exacerbated by the general lack of published literature on glenohumeral kinematics and scapulothoracic rotations in reconstructed RTSA shoulders. Although the motion curves taken from Matsuki et al. [36] were of high methodological integrity, the captured movements occurred only in the scapular plane, limiting our understanding of scapular kinematics in other ranges of plane of elevation. Nevertheless, the magnitude of scapulothoracic rotation as a contribution to humerothoracic motion meant that some accounting for scapulothoracic rotation was necessary to prevent greatly overestimating sliding distances. Participants were also unable to wear the MOCAP apparatus during personal bathing and any night-time (post-doffing) activities, causing an omission of a reoccurring series of motions. The model also does not account for load-dependant changes to implant geometry and assumes a conforming fit of components. The model assumes that implant geometry would not affect motion and thus the same patient motion can be used to predict overlap and sliding for different implant geometries.

3.5   Conclusions

This work addresses the current understanding of the risk of scapular notching for RTSA implants by linking it kinematically to the large proportion of time the inferior aspect of the cup spent medial to the glenosphere border. A lesser NSA reduced the amount of medial overlapping that occurred at the inferior aspect of the humeral cup, which may give a greater longevity to the implant. Extrapolation of the *in vivo* RTSA motion data to represent one year of motion resulted in a range from 35.4 km to 62.3 km of relative sliding distance at the inferior point for all implant configurations tested. When comparing this distance to the motion profile of our shoulder simulator, 1.25 Mc was representative of approximately 1 year *in vivo*. An increased implant diameter resulted in more sliding at all cup points but did not considerably influence the amount of time the inferior point spent in medial overlap.

Appendix A – Kinematic Model Development

A.1 Data Formatting

A custom program was developed using Python (64-bit, version 3.9.2, Python Software Foundation) to analyze the glenohumeral motion of each participant in their operated shoulder and simulated four various implant designs using each participant's motion data. The calculations in this program utilized NumPy (version 1.20.1).

The IMUs embedded in the MOCAP shirt stored quaternions representing the angular position of each sensor at 0.1 s intervals (10 Hz) on the micro-SD cards (a quaternion is a mathematical way to represent the three-dimensional orientation and rotation of an object using complex numbers). These quaternions were extracted from the micro-SD card and converted to rotation matrices using Equation A-1 implemented with custom code (LabVIEW 2018, National Instruments). This custom code also applied alignment corrections to make the y axis of the humeral and sternal sensor values coaxial at baseline to represent the starting 'tin solder' starting position and to account for any variations in body geometry. The resulting rotation matrices represented each humeral sensor's orientation with respect to (wrt) the sternal sensor. The result was a 10 Hz data set of the participant's humerothoracic motion for the entire time the shirt was worn.

$$R(Q) = \begin{bmatrix} 2(q_0^2 + q_1^2) - 1 & 2(q_1 q_2 - q_0 q_3) & 2(q_1 q_3 + q_0 q_2) \\ 2(q_1 q_2 + q_0 q_3) & 2(q_0^2 + q_2^2) - 1 & 2(q_2 q_3 - q_0 q_1) \\ 2(q_1 q_3 - q_0 q_2) & 2(q_2 q_3 + q_0 q_1) & 2(q_0^2 + q_3^2) - 1 \end{bmatrix} \qquad (A\text{-}1)$$

where

Q= the quaternion for a given humeral orientation ($Q = q_0, q_1, q_2, q_3$)

A.2 RTSA Implant Geometric Assumptions

Two NSAs of 155° and 135° were modeled (Figure A-1). Additionally, two glenosphere diameters of 38 mm and 42 mm were modeled. Based on the geometry of common commercially available implants, the articulating surface of the glenosphere was assumed to be a perfect hemisphere, and the 38 mm implants had a cup depth of 8.38 mm, and the 42 mm implants had a cup depth of 9.33 mm. The implants were modelled with 0° of humeral retroversion.
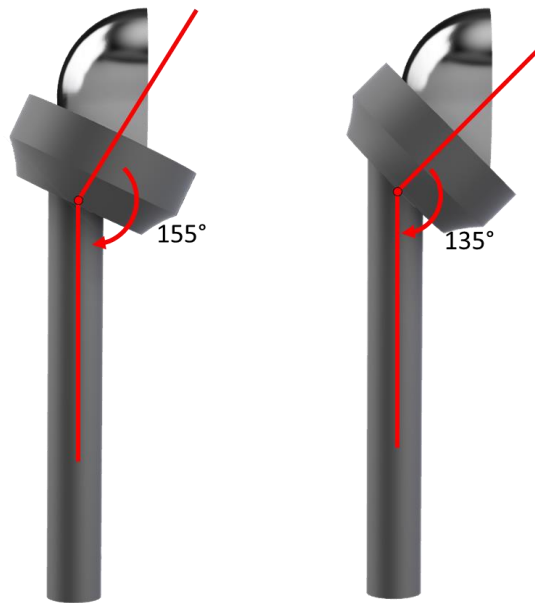
Figure A-1: RTSA implant with 155° (left) and 135° (right) neck-shaft angles investigated

A.3 RTSA Humeral Component Positioning

The glenohumeral coordinate system (GCS) was defined as per the International Society of Biomechanics [40] with the centre of rotation located at the centre of the glenosphere (Figure A-2). The long axis of the humerus, prior to any rotations, was represented as a unit vector $(\overrightarrow{h_0})$ coaxial to the system's y axis (Figure A-3). With the humerus still in this position, 5 points were identified on the surface of the humeral cup (one at the centre and four more on the cup rim at the most inferior, superior, anterior, and posterior locations) and represented as unit vectors originating from the cup's centre of rotation directed

towards each location (Figure A-4). These points were determined mathematically, producing the polar-most vectors in each direction from the centre of rotation to the cup rim, based on the implant geometry.
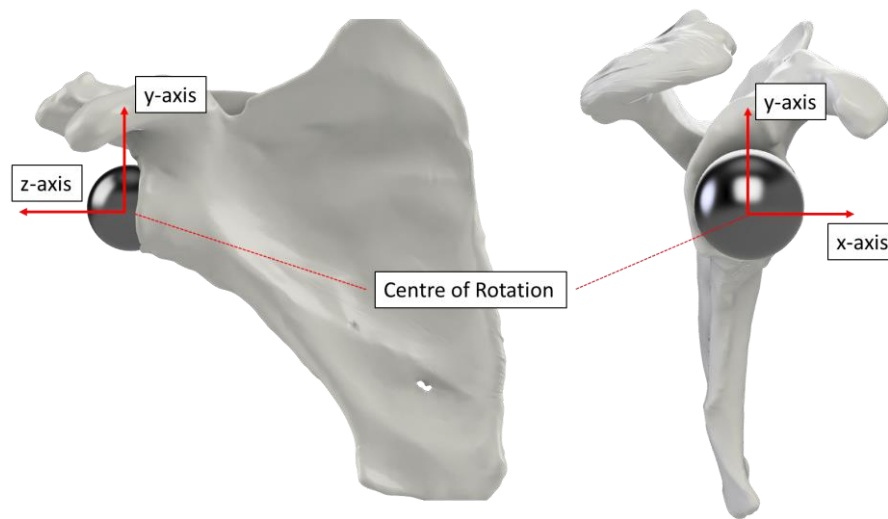
Figure A-2: Coordinate system shown on a right scapula from the anterior view (left) and lateral view (right)
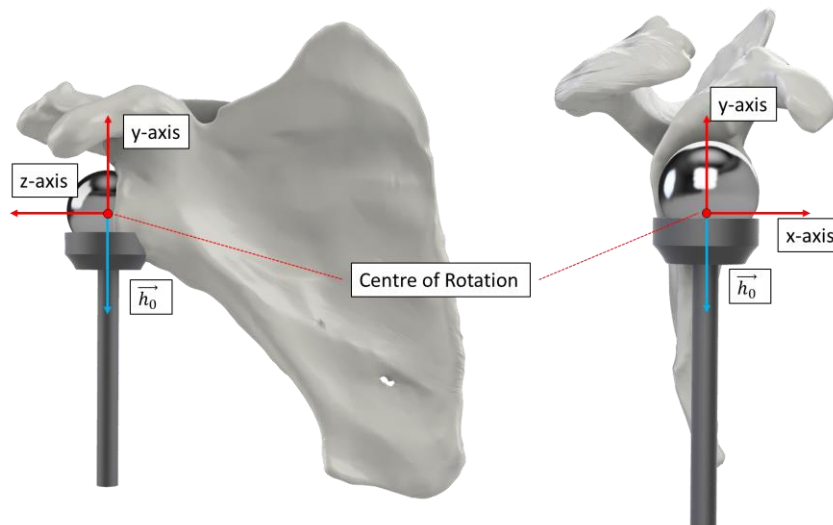
Figure A-3: Long axis of the humerus shown coaxial with the y axis of the glenohumeral coordinate system

Figure A-4: The five points on the humeral cup that were investigated, with the glenohumeral coordinate system shown for the humerus in the initial position
Note that 180° NSA is shown as this represents an intermediate step in the algorithm prior to NSA correction.

To account for the NSA of the RTSA implant, the vectors representing all five points on the humeral cup were then rotated about the system's *x* axis using the *Rodrigues rotation formula* (Figure A-5). The resulting vectors represented the points on the cup for all NSAs investigated. For example, the unit vector representing the superior point on the cup with a given NSA ($\overrightarrow{p_{sup'}}$) was calculated as:

$$\overrightarrow{p_{sup'}} = \overrightarrow{p_{sup_0}} \cos\theta + \left(\hat{\imath} \times \overrightarrow{p_{sup_0}}\right) \sin\theta + \hat{\imath} \cdot p_{sup_0} (1 - \cos\theta) \qquad (A\text{-}2)$$

where

$\overrightarrow{p_{sup_0}}$ = The unit vector representing the location of the superior point on the cup prior to humeral rotation and NSA correction

$$\theta = 180° - \text{the NSAngle}$$

$$\hat{\imath} = [1, 0, 0]$$
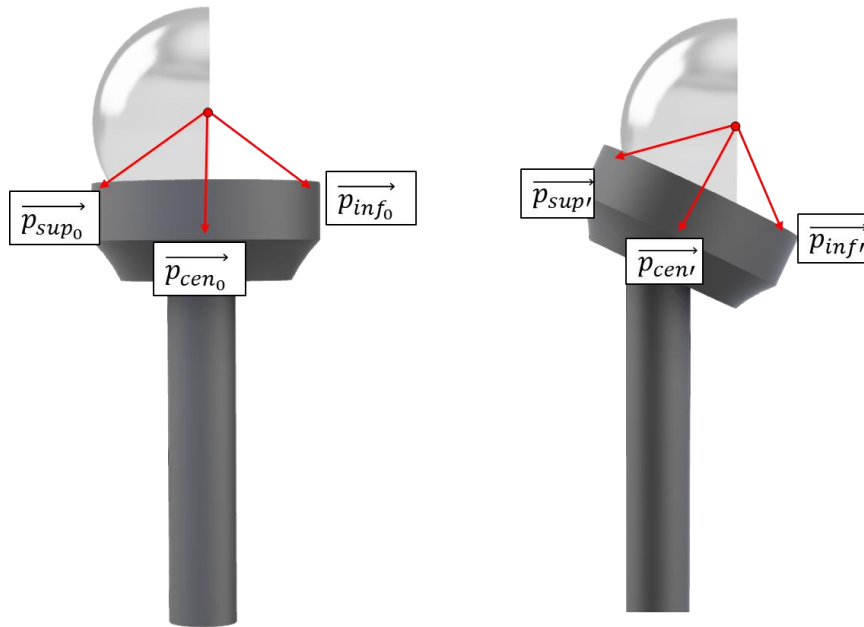
Figure A-5: Rotation of humeral cup point unit vectors according to NSA shown for a 155° NSA

A.4 Glenohumeral Motion Determination with Estimated Scapular Rotation

At the time of the MOCAP shirt initiation, with the patient in the tin solder position, the orientation of the glenosphere was assumed to be identical to that of the sternum, save for a 90° external rotation about its y axis. This meant that after the 90° axial rotation correction, the rotation matrices describing humeral position wrt the sternum would also represent humeral position wrt the GCS ($^{GCS}R_{hum}$). Therefore, the second rows of the $^{GCS}R_{hum}$ matrices (y values) represented the long axis of the humerus wrt the GCS at each time point.

Because the scapular rotation curves were formed as a function of shoulder abduction (Figure A-7), the two-dimensional frontal plane elevation angles were required rather than the three-dimensional angles. Humerothoracic abduction angles (θ_{abd}) were determined by calculating the angle between the humeral shaft ($\vec{h}$) and the -y axis of the GCS ($-\hat{j}$) in the frontal (Y-Z) plane (Equation A-3; Figure A-6).

$$\theta_{abd} = cos^{-1}(\vec{h} \cdot -\hat{j}) \qquad\qquad (A\text{-}3)$$

where

$\vec{h}$ = The two-dimensional [y, z] unit vector representing the position of the long axis of the humerus in the frontal plane following humeral rotation

$\hat{j}$ = The two-dimensional [y, z] unit vector representing the y axis of the GCS in the frontal plane = [1, 0]
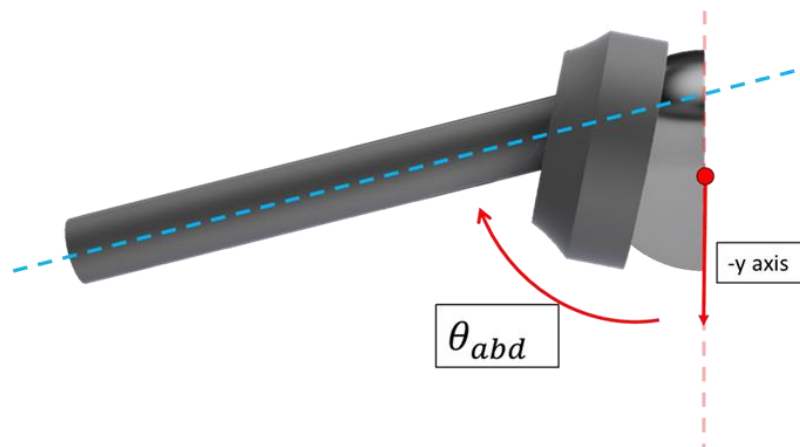
Figure A-6: Humeral abduction angle shown with respect to the negative y axis of the glenohumeral coordinate system

The resulting humerothoracic abduction was a summation of both glenohumeral and scapulothoracic rotation. Since discrete scapulothoracic motion was not measured with the MOCAP apparatus, it was necessary to account for it analytically in order to allow the glenohumeral rotation to be estimated. This was achieved by examining the results from previously published research that had elucidated the scapulothoracic rhythms from varying shoulder motions in fully recovered RTSAs reported by Matsuki et al. [36].

The data representing the average glenosphere rotations about each axis at one year post-op were digitized from Matsuki et al. [36] and linear equations were fit to each rotation profile. These equations modelled scapulothoracic (i.e., glenosphere) rotation about each axis as a function of humerothoracic abduction (Figure A-7). The measured humerothoracic abduction angles (from Equation A-3) were input into these three functions to determine the angles by which to rotate the glenosphere about each axis (ϕ_x, ϕ_y, ϕ_z).
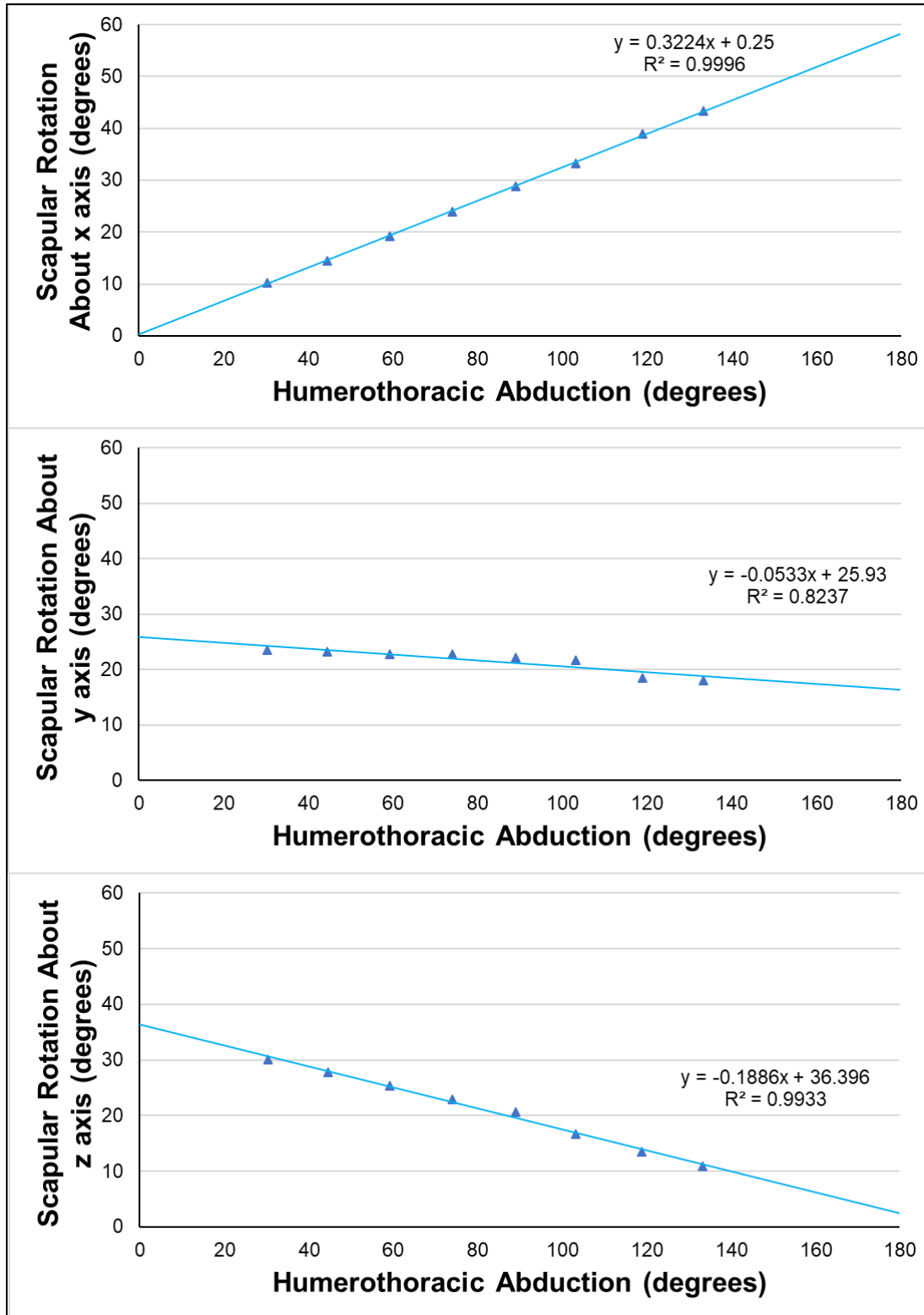
Figure A-7: Scapulothoracic rotation curves about all three axes obtained from Matsuki et al. [36]

Rotation matrices were then created to describe the orientation of the glenosphere wrt the GCS following humeral rotation at each recorded time point ($^{GCS}R_{glen}$) using the angles output from the Matsuki curves (Equation A-4).

$$^{GCS}R_{glen} = R_y R_x R_z \tag{A-4}$$

where

$$R_y = \begin{bmatrix} cos\phi_y & 0 & sin\phi_y \\ 0 & 1 & 0 \\ -sin\phi_y & 0 & cos\phi_y \end{bmatrix}$$

$$R_x = \begin{bmatrix} 1 & 0 & 0 \\ 0 & cos\phi_x & -sin\phi_x \\ 0 & sin\phi_x & cos\phi_x \end{bmatrix}$$

$$R_z = \begin{bmatrix} cos\phi_z & -sin\phi_z & 0 \\ sin\phi_z & cos\phi_z & 0 \\ 0 & 0 & 1 \end{bmatrix}$$

Rotation matrices representing the humerus wrt the glenosphere at each time point ($^{glen}R_{hum}$) were then created by multiplying the inverse of the rotation matrix representing the glenosphere wrt the GCS (from Equation A-4) by the rotation matrix representing the humerus wrt the GCS (Equation A-5).

$$^{glen}R_{hum} = \, ^{GCS}R_{glen}^{-1} \, ^{GCS}R_{hum} \tag{A-5}$$

All five vectors representing the points on the cup after NSA adjustment (following Equation A-2) were then multiplied by the rotation matrices from Equation A-5 to produce the position of each point on the cup relative to the glenosphere for each time point. For example, the cup's superior point ($\overrightarrow{p_{sup}}$) was calculated as:

$$\overrightarrow{p_{sup}} = \, ^{glen}R_{hum} \, \overrightarrow{p_{sup'}} \tag{A-6}$$

A.5 RTSA Implant Articular Sliding Distance Determination

The relative motions between the glenosphere and each of the five points on the cup were determined by calculating the magnitude of the vector representing the distance travelled by each point between each time sample. For example, the motion between the superior point at the first sample and the second sample (Δp_{sup}) was calculated as:

$$\Delta p_{sup} = \left| \overrightarrow{p_{sup_{t2}}} - \overrightarrow{p_{sup_{t1}}} \right|$$

(A-7)

where

$\overrightarrow{p_{sup_{t2}}}$ =The position of $\overrightarrow{p_{sup}}$ at the second time sample

$\overrightarrow{p_{sup_{t1}}}$ =The position of $\overrightarrow{p_{sup}}$ at the first time sample

The backside of the glenosphere (non-articulating surface) was on a plane formed by the x and y axes of the GCS (Figure A-8). If any point on the cup possessed a negative z value following Equation A-6, it meant that the point had crossed this plane, indicating a period during which that point was not in contact with the glenosphere. During these periods, glenohumeral relative motion was not tracked and sliding distances were not accumulated for the corresponding points.
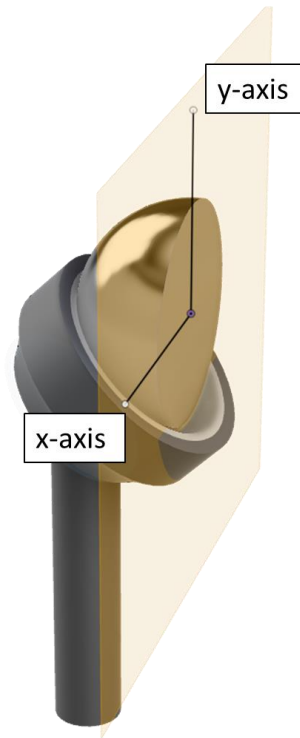
Figure A-8: Plane of glenosphere backside defined as the plane formed by the x and y axes of the glenohumeral coordinate system

The relative motions at each tracked point were then summed and scaled to the corresponding glenosphere diameter to produce a single value of total sliding distance. For example, the total sliding distance at the superior point on the cup (d_{sup}) was calculated as:

$$d_{sup} = r \sum \Delta p_{sup}$$

$(A\text{-}8)$

where
   r = radius of the glenosphere

A.6   Inferior Glenosphere Overlap Assessment

The proportion of time that the inferior point spent in medial overlap (negative z value) was calculated by dividing the total number of instances during which the inferior point had a negative z value by the total number of samples.

Appendix B - List of Nomenclature

Variable	Definition
$R(Q)$	The rotation matrix formed from the specific quaternion, Q
Q	The quaternion $(Q = q_0, q_1, q_2, q_3)$
q_0	The first term in the quaternion
q_1	The second term in the quaternion
q_2	The third term in the quaternion
q_3	The fourth term in the quaternion
$\overrightarrow{h_0}$	The unit vector representing the long axis of the humerus prior to humeral rotation
$\overrightarrow{p_{sup_0}}$	The unit vector representing the location of the superior point on the cup prior to humeral rotation and NSA correction
$\overrightarrow{p_{inf_0}}$	The unit vector representing the location of the inferior point on the cup prior to humeral rotation and NSA correction
$\overrightarrow{p_{ant_0}}$	The unit vector representing the location of the anterior point on the cup prior to humeral rotation and NSA correction
$\overrightarrow{p_{post_0}}$	The unit vector representing the location of the posterior point on the cup prior to humeral rotation and NSA correction

$\overrightarrow{p_{cen_0}}$	The unit vector representing the location of the centre point on the cup prior to humeral rotation and NSA correction
θ	The angle by which the humeral cup is to be rotated about the x axis of the GCS. Determined by subtracting the value of the NSA from $180°$
$\hat{\imath}$	The x axis of the GCS = [1, 0, 0]
$\overrightarrow{p_{sup'}}$	The unit vector representing the location of the superior point on the cup following NSA correction and prior to humeral rotation
$\overrightarrow{p_{inf'}}$	The unit vector representing the location of the inferior point on the cup following NSA correction and prior to humeral rotation
$\overrightarrow{p_{ant'}}$	The unit vector representing the location of the anterior point on the cup following NSA correction and prior to humeral rotation
$\overrightarrow{p_{post'}}$	The unit vector representing the location of the posterior point on the cup following NSA correction and prior to humeral rotation
$\overrightarrow{p_{cen'}}$	The unit vector representing the location of the centre point on the cup following NSA correction and prior to humeral rotation
$^{GCS}R_{hum}$	The rotation matrix representing the orientation of the humerus with respect to the GCS
θ_{abd}	The two-dimensional angle representing humerothoracic elevation in the frontal (Y-Z) plane

$\vec{h}$	The two-dimensional unit vector representing the position of the long axis of the humerus in the frontal plane following humeral rotation
$\hat{j}$	The two-dimensional unit vector representing the y axis of the GCS in the frontal plane = [1, 0]
ϕ_x	The angle by which the scapula is to be rotated about its x axis
ϕ_y	The angle by which the scapula is to be rotated about its y axis
ϕ_z	The angle by which the scapula is to be rotated about its z axis
$^{GCS}R_{glen}$	The rotation matrix representing the orientation of the glenosphere with respect to the GCS following humeral rotation
R_y	The rotation matrix representing the rotation of the glenosphere about the y axis of the GCS = $\begin{bmatrix} cos\phi_y & 0 & sin\phi_y \\ 0 & 1 & 0 \\ -sin\phi_y & 0 & cos\phi_y \end{bmatrix}$
R_x	The rotation matrix representing the rotation of the glenosphere about the x axis of the GCS = $\begin{bmatrix} 1 & 0 & 0 \\ 0 & cos\phi_x & -sin\phi_x \\ 0 & sin\phi_x & cos\phi_x \end{bmatrix}$

R_z	The rotation matrix representing the rotation of the glenosphere about the z axis of the GCS = $\begin{bmatrix} cos\ \phi_z & -sin\phi_z & 0 \\ sin\phi_z & cos\phi_z & 0 \\ 0 & 0 & 1 \end{bmatrix}$
$^{glen}R_{hum}$	The rotation matrix representing the orientation of the humerus with respect to the glenosphere following humerus and glenosphere rotation
$\overrightarrow{p_{sup}}$	The unit vector representing the position of the superior point on the humeral cup relative to the glenosphere following NSA correction, humeral rotation, and glenosphere rotation
$\overrightarrow{p_{inf}}$	The unit vector representing the position of the inferior point on the humeral cup relative to the glenosphere following NSA correction, humeral rotation, and glenosphere rotation
$\overrightarrow{p_{ant}}$	The unit vector representing the position of the anterior point on the humeral cup relative to the glenosphere following NSA correction, humeral rotation, and glenosphere rotation
$\overrightarrow{p_{post}}$	The unit vector representing the position of the posterior point on the humeral cup relative to the glenosphere following NSA correction, humeral rotation, and glenosphere rotation
$\overrightarrow{p_{cen}}$	The unit vector representing the position of the centre point on the humeral cup relative to the glenosphere following NSA correction, humeral rotation, and glenosphere rotation

Δp_{sup}	The scalar value representing the superior point's change in position between two adjacent time points
Δp_{inf}	The scalar value representing the inferior point's change in position between two adjacent time points
Δp_{ant}	The scalar value representing the anterior point's change in position between two adjacent time points
Δp_{post}	The scalar value representing the posterior point's change in position between two adjacent time points
Δp_{cen}	The scalar value representing the centre point's change in position between two adjacent time points
$\overrightarrow{p_{sup_{t2}}}$	The unit vector representing the position of $\overrightarrow{p_{sup}}$ at the second time sample
$\overrightarrow{p_{sup_{t1}}}$	The unit vector representing the position of $\overrightarrow{p_{sup}}$ at the first time sample
d_{sup}	The scalar value representing the linear distance travelled by the superior point during the entire day
d_{inf}	The scalar value representing the linear distance travelled by the inferior point during the entire day
d_{ant}	The scalar value representing the linear distance travelled by the anterior point during the entire day
d_{post}	The scalar value representing the linear distance travelled by the superior point during the entire day

d_{cen}	The scalar value representing the linear distance travelled by the centre point during the entire day
r	The radius of the glenosphere

3.6 References

[1]   Australian Orthopaedic Association National Joint Replacement Registry.
        Australian Orthopaedic Association National Joint Replacement Registry
        (AOANJRR). Hip Knee & Shoulder Arthroplasty: 2021 Annual Report 2021.

[2]   Day JS, MacDonald DW, Olsen M, Getz C, Williams GR, Kurtz SM. Polyethylene
        wear in retrieved reverse total shoulder components. J Shoulder Elb Surg
        2012;21:667–74. https://doi.org/10.1016/j.jse.2011.03.012.

[3]   Kurdziel MD, Newton MD, Hartner S, Baker KC, Wiater JM. Quantitative
        evaluation of retrieved reverse total shoulder arthroplasty liner surface deviation
        and volumetric wear. J Orthop Res 2018;36:2007–14.
        https://doi.org/10.1002/jor.23849.

[4]   Wiater BP, Baker EA, Salisbury MR, Koueiter DM, Baker KC, Nolan BM, et al.
        Elucidating trends in revision reverse total shoulder arthroplasty procedures: A
        retrieval study evaluating clinical, radiographic, and functional outcomes data. J
        Shoulder Elb Surg 2015;24:1915–25. https://doi.org/10.1016/j.jse.2015.06.004.

[5]   Farshad M, Gerber C. Reverse total shoulder arthroplasty-from the most to the
        least common complication. Int Orthop 2010;34:1075–82.
        https://doi.org/10.1007/s00264-010-1125-2.

[6]   Lévigne C, Garret J, Boileau P, Alami G, Favard L, Walch G. Scapular notching in
        reverse shoulder arthroplasty: Is it important to avoid it and how? Clin Orthop
        Relat Res 2011;469:2512–20. https://doi.org/10.1007/s11999-010-1695-8.

[7]   Mueller U, Harzi A, Loescher R, Buelhoff M, Eckert JA, Kretzer JP. Wear and
        damage in retrieved humeral inlays of reverse total shoulder arthroplasty—where,
        how much, and why? J Shoulder Elb Surg 2021;30:e517–30.
        https://doi.org/10.1016/j.jse.2020.10.015.

[8]   Nam D, Kepler CK, Nho SJ, Craig E V., Warren RF, Wright TM. Observations on
        retrieved humeral polyethylene components from reverse total shoulder

arthroplasty. J Shoulder Elb Surg 2010;19:1003–12. https://doi.org/10.1016/j.jse.2010.05.014.

[9]   Haggart J, Newton MD, Hartner S, Ho A, Baker KC, Kurdziel MD, et al. Neer Award 2017: wear rates of 32-mm and 40-mm glenospheres in a reverse total shoulder arthroplasty wear simulation model. J Shoulder Elb Surg 2017;26:2029–37. https://doi.org/10.1016/j.jse.2017.06.036.

[10]   Kohut G, Dallmann F, Irlenbusch U. Wear-induced loss of mass in reversed total shoulder arthroplasty with conventional and inverted bearing materials. J Biomech 2012;45:469–73. https://doi.org/10.1016/j.jbiomech.2011.11.055.

[11]   Silva M, Shepherd EF, Jackson WO, Dorey FJ, Schmalzried TP. Average patient walking activity approaches 2 million cycles per year: Pedometers under-record walking activity. J Arthroplasty 2002;17:693–7. https://doi.org/10.1054/arth.2002.32699.

[12]   Gutiérrez S, Levy JC, Frankle MA, Cuff D, Keller TS, Pupello DR, et al. Evaluation of abduction range of motion and avoidance of inferior scapular impingement in a reverse shoulder model. J Shoulder Elb Surg 2008;17:608–15. https://doi.org/10.1016/j.jse.2007.11.010.

[13]   Gutiérrez S, Comiskey IV CA, Luo ZP, Pupello DR, Frankle MA. Range of impingement-free abduction and adduction deficit after reverse shoulder arthroplasty. Hierarchy of surgical and implant-design-related factors. J Bone Jt Surg - Ser A 2008;90:2606–15. https://doi.org/10.2106/JBJS.H.00012.

[14]   Roche C, Flurin PH, Wright T, Crosby LA, Mauldin M, Zuckerman JD. An evaluation of the relationships between reverse shoulder design parameters and range of motion, impingement, and stability. J Shoulder Elb Surg 2009;18:734–41. https://doi.org/10.1016/j.jse.2008.12.008.

[15]   De Wilde LF, Poncet D, Middernacht B, Ekelund A. Prosthetic overhang is the most effective way to prevent scapular conflict in a reverse total shoulder

prosthesis. Acta Orthop 2010;81:719–26.
https://doi.org/10.3109/17453674.2010.538354.

[16]   Mollon B, Mahure SA, Roche CP, Zuckerman JD. Impact of glenosphere size on clinical outcomes after reverse total shoulder arthroplasty: An analysis of 297 shoulders. J Shoulder Elb Surg 2016;25:763–71. https://doi.org/10.1016/j.jse.2015.10.027.

[17]   Kempton LB, Balasubramaniam M, Ankerson E, Wiater JM. A radiographic analysis of the effects of prosthesis design on scapular notching following reverse total shoulder arthroplasty. J Shoulder Elb Surg 2011;20:571–6. https://doi.org/10.1016/j.jse.2010.08.024.

[18]   Langohr GDG, Giles JW, Athwal GS, Johnson JA. The effect of glenosphere diameter in reverse shoulder arthroplasty on muscle force, joint load, and range of motion. J Shoulder Elb Surg 2015;24:972–9. https://doi.org/10.1016/j.jse.2014.10.018.

[19]   Dieckmann R, Liem D, Gosheger G, Henrichs MP, Höll S, Hardes J, et al. Evaluation of a reconstruction reverse shoulder for tumour surgery and tribological comparision with an anatomical shoulder arthroplasty. Int Orthop 2013;37:451–6. https://doi.org/10.1007/s00264-012-1771-7.

[20]   Carpenter S, Pinkas D, Newton MD, Kurdziel MD, Baker KC, Wiater JM. Wear rates of retentive versus nonretentive reverse total shoulder arthroplasty liners in an in vitro wear simulation. J Shoulder Elb Surg 2015;24:1372–9. https://doi.org/10.1016/j.jse.2015.02.016.

[21]   Peers S, Moravek JE, Budge MD, Newton MD, Kurdziel MD, Baker KC, et al. Wear rates of highly cross-linked polyethylene humeral liners subjected to alternating cycles of glenohumeral flexion and abduction. J Shoulder Elb Surg 2015;24:143–9. https://doi.org/10.1016/j.jse.2014.05.001.

[22]   Vaupel ZM, Baker KC, Kurdziel MD, Wiater JM. Wear simulation of reverse total

shoulder arthroplasty systems: Effect of glenosphere design. J Shoulder Elb Surg 2012;21:1422–9. https://doi.org/10.1016/j.jse.2011.10.024.

[23]   Mattei L, Di Puccio F, Joyce TJ, Ciulli E. Numerical and experimental investigations for the evaluation of the wear coefficient of reverse total shoulder prostheses. J Mech Behav Biomed Mater 2016;55:53–66. https://doi.org/10.1016/j.jmbbm.2015.10.007.

[24]   Smith SL, Li BL, Buniya A, Ho Lin S, Scholes SC, Johnson G, et al. In vitro wear testing of a contemporary design of reverse shoulder prosthesis. J Biomech 2015;48:3072–9. https://doi.org/10.1016/j.jbiomech.2015.07.022.

[25]   Smith SL, Li L, Joyce TJ. Engineering of a multi-station shoulder simulator. Proc Inst Mech Eng Part H J Eng Med 2016;230:470–80. https://doi.org/10.1177/0954411915611161.

[26]   Griffiths MW, Athwal GS, Medley JB, Johnson JA, Langohr GDG. Wear of humeral polyethylene cups in reverse total shoulder arthroplasty with simulated rim damage from scapular notching. Biotribology 2020;22:1–8. https://doi.org/10.1016/j.biotri.2020.100123.

[27]   Langohr GDG, Athwal GS, Johnson JA, Medley JB. Wear simulation strategies for reverse shoulder arthroplasty implants. Proc Inst Mech Eng Part H J Eng Med 2016;230:458–69. https://doi.org/10.1177/0954411916642801.

[28]   Abdulla I, Langohr DG, Giles JW, Johnson JA, Athwal GS. The effect of humeral polyethylene insert constraint on reverse shoulder arthroplasty biomechanics. Shoulder Elb 2018;10:25–31. https://doi.org/10.1177/1758573217701065.

[29]   Oh JH, Shin SJ, McGarry MH, Scott JH, Heckmann N, Lee TQ. Biomechanical effects of humeral neck-shaft angle and subscapularis integrity in reverse total shoulder arthroplasty. J Shoulder Elb Surg 2014;23:1091–8. https://doi.org/10.1016/j.jse.2013.11.003.

[30]   Langohr GDG, Willing R, Medley JB, Athwal GS, Johnson JA. Contact mechanics

of reverse total shoulder arthroplasty during abduction: The effect of neck-shaft angle, humeral cup depth, and glenosphere diameter. J Shoulder Elb Surg 2016;25:589–97. https://doi.org/10.1016/j.jse.2015.09.024.

[31] Haverstock JP, King GJW, Athwal GS, Johnson JA, Langohr GDG. Elbow motion patterns during daily activity. J Shoulder Elb Surg 2020;29:2007–14. https://doi.org/10.1016/j.jse.2020.03.015.

[32] Langohr GDG, Haverstock JP, Johnson JA, Athwal GS. Comparing daily shoulder motion and frequency after anatomic and reverse shoulder arthroplasty. J Shoulder Elb Surg 2018;27:325–32. https://doi.org/10.1016/j.jse.2017.09.023.

[33] Van de Kleut ML, Bloomfield RA, Teeter MG, Athwal GS. Monitoring daily shoulder activity before and after reverse total shoulder arthroplasty using inertial measurement units. J Shoulder Elb Surg 2021;30:1078–87. https://doi.org/10.1016/j.jse.2020.07.034.

[34] Chapman RM, Torchia MT, Bell JE, Van Citters DW. Assessing Shoulder Biomechanics of Healthy Elderly Individuals during Activities of Daily Living Using Inertial Measurement Units: High Maximum Elevation Is Achievable but Rarely Used. J Biomech Eng 2019;141:1–7. https://doi.org/10.1115/1.4042433.

[35] Hagen MS, Allahabadi S, Zhang AL, Feeley BT, Grace T, Ma CB. A randomized single-blinded trial of early rehabilitation versus immobilization after reverse total shoulder arthroplasty. J Shoulder Elb Surg 2020;29:442–50. https://doi.org/10.1016/j.jse.2019.10.005.

[36] Matsuki K, Sugaya H, Hoshika S, Takahashi N, Kenmoku T, Banks SA. Scaption kinematics of reverse shoulder arthroplasty do not change after the sixth postoperative month. Clin Biomech 2018;58:1–6. https://doi.org/10.1016/j.clinbiomech.2018.07.005.

[37] Van de Kleut ML, Athwal GS, Faber KJ, Teeter MG. In vivo volumetric and linear wear measurement of reverse shoulder arthroplasty at minimum 5-year follow-up.

J Shoulder Elb Surg 2020;29:1695–702. https://doi.org/10.1016/j.jse.2019.11.031.

[38]   Mollon B, Mahure SA, Roche CP, Zuckerman JD. Impact of scapular notching on clinical outcomes after reverse total shoulder arthroplasty: an analysis of 476 shoulders. J Shoulder Elb Surg 2017;26:1253–61. https://doi.org/10.1016/j.jse.2016.11.043.

[39]   Terrier A, Merlini F, Pioletti DP, Farron A. Comparison of polyethylene wear in anatomical and reversed shoulder prostheses. J Bone Jt Surg - Ser B 2009;91:977–82. https://doi.org/10.1302/0301-620X.91B7.21999.

[40]   Wu G, Van Der Helm FCT, Veeger HEJ, Makhsous M, Van Roy P, Anglin C, et al. ISB recommendation on definitions of joint coordinate systems of various joints for the reporting of human joint motion - Part II: Shoulder, elbow, wrist and hand. J Biomech 2005;38:981–92. https://doi.org/10.1016/j.jbiomech.2004.05.042.

Chapter 4

In Vitro Crosslinked Polyethylene Wear for Reverse Total Shoulder Arthroplasty

OVERVIEW: Reverse total shoulder arthroplasty (RTSA) has become a popular treatment for many shoulder degenerations including rotator cuff arthropathy. There have been reported incidences of wear-related and damage-related implant failure in these designs, warranting investigation into the materials used. Crosslinked polyethylene (XLPE) is thought to be a suitable, more wear-resistant substitution for the currently used non-crosslinked polyethylene (non-XLPE) in RTSAs. The purpose of this study was to investigate the in vitro wear of a moderately crosslinked polyethylene in reverse total shoulder arthroplasty to provide a direct comparison to the wear of non-XLPE in identical conditions and to help predict clinical wear in designs that utilize the newer crosslinked polyethylene.

4.1 Introduction

Reverse total shoulder arthroplasty has been a popular treatment for a multitude of shoulder pathologies [1]; however, this particular implant has shown patterns of wear-related and damage-related complications in the early phases of implementation [2–5]. Similar wear-related failures have been observed in other joint replacements (i.e., hip and knee), but were reduced by the substitution of crosslinked polyethylene (XLPE) for the now obsolete non-crosslinked polyethylene (non-XLPE) [6]. This substitution has not yet fully become the standard practice in the RTSA design, which could be a result of the focus on loosening and scapular notching damage as clinical problems.

In vitro joint simulator wear testing has been regarded as a strategy for predicting clinical joint wear [7]. This process includes installing the joint replacement implants into a wear simulator, subjecting the implants to clinically relevant loads and motions, and then calculating the total volume loss of the humeral cup due to wear using measured mass loss and density of the polyethylene material. Using this method, the comparison of wear amounts for various implant designs under clinically relevant conditions can be done.

In vitro RTSA wear studies have been conducted under a variety of conditions resulting in various wear rates (Table 4-1). A series of papers from the Beaumont Health System, Royal Oak, MI, USA [8–11] presented the largest volumetric wear rates (Figure 4-1). The simulator used in these papers alternated between flexion/extension and adduction/abduction motion, every 0.25 Mc. As noted by the authors [11], the alternating motion paths likely promoted higher polyethylene wear and may have been responsible for the extended 'run-in' phase of about 2 Mc. A series of publications out of Newcastle University, Newcastle upon Tyne, England, UK [12–14] used a simulator representing a repeated "mug to mouth" motion. Although very consistent, their wear rates are among the lowest reported, likely highlighting the effect of their low loading throughout the simulation. The (present) group from the Roth | McFarlane Hand and Upper Limb Centre (HULC), London, ON, Canada utilized a simulator with a circumduction motion and relatively high loading (described in further detail in Methods section). The previous

studies out of HULC [15,16] have shown wear rates in between the Beaumont and Newcastle series. Similarly, two individual papers out of Hopital Cantonal, Fribourg, Switzerland [17] and Munster University, Munster, Germany [18] have also reported wear rates within the bounds of the Newcastle and Beaumont publications, but they did not use load-soaked controls in their assessments, potentially underreporting the wear observed. The Hopital Cantonal study also used an inversed-bearing RTSA design (polyethylene head and cobalt chromium cup), and the Munster experiment tested a glenosphere configuration made with TiAlVa instead of CoCr.

Table 4-3: Summary of *in vivo* RTSA wear simulations

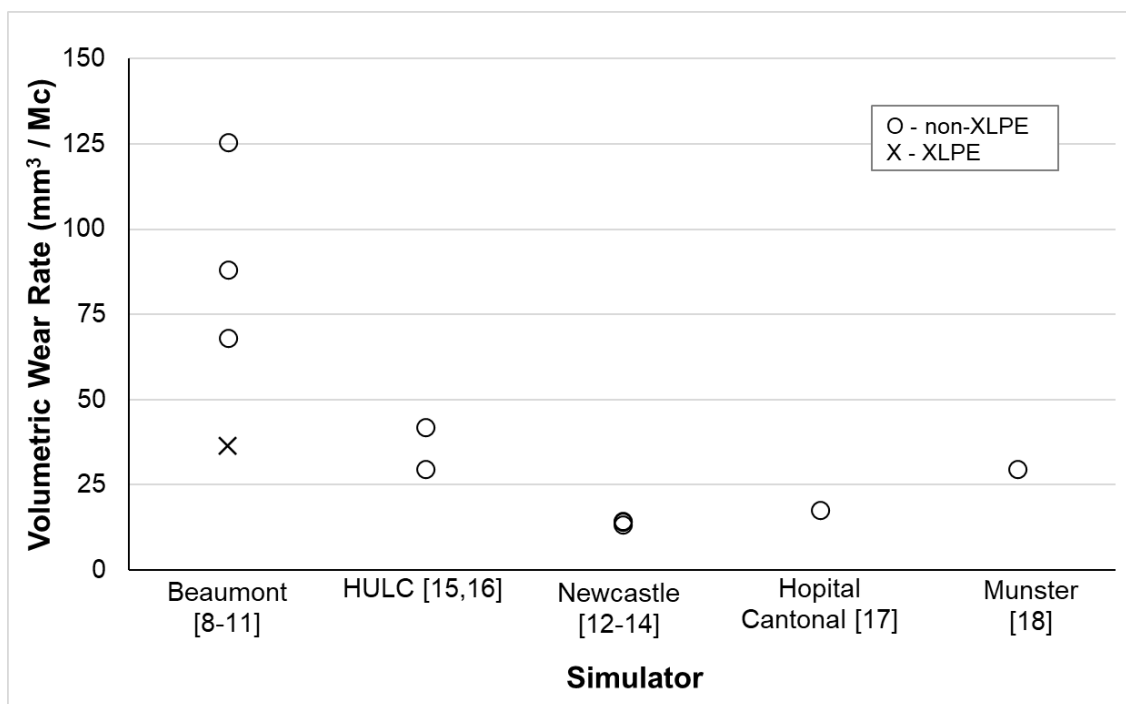|				RTSA Simulation Studies				
Authors	Group	Material	Lubricant	Load (N)	Range of Motion	Control	Wear Rate (mm³ / Mc)	Comments
Carpenter et al. [8]	Beaumont	non-XLPE	Bovine calf serum (21 g/L) + DI water	20 - 617.8 20 - 926.7	46° flex/ext 46° add/abd	Load Soaked	88.1	Tested pure abduction and then pure flexion afterwards.
Haggart et al. [9]	Beaumont	non-XLPE	Bovine calf serum (21 g/L) + DI water	20 - 617.8 20 - 926.7	46° flex/ext 46° add/abd	Load Soaked	68.0	Tested pure abduction and then pure flexion afterwards.
Peers et al. [10]	Beaumont	XLPE (5 Mrad)	Bovine calf serum (21 g/L) + DI water	20 - 617.8 20 - 926.7	46° flex/ext 46° add/abd	Load Soaked	36.5	Tested pure abduction and then pure flexion afterwards.
Vaupel et al. [11]	Beaumont	non-XLPE	Bovine calf serum (21 g/L) + DI water	20 - 617.8 20 - 926.7	46° flex/ext 46° add/abd	Load Soaked	125.5	Tested pure abduction and then pure flexion afterwards.
Mattei et al. [12]	Newcastle	non-XLPE	Newborn calf serum (26 g/L)	180 - 250	28° flex/ext 13° add/abd 59° IR/ER	Load Soaked	13.3	
Smith et al. [13]	Newcastle	non-XLPE	Newborn calf serum (26 g/L)	180 - 250	28° flex/ext 13° add/abd 25° IR/ER	Load Soaked	14.3	
Smith et al. [14]	Newcastle	non-XLPE	Newborn calf serum (26 g/L)	150 - 450	44° flex/ext 48° add/abd 43° IR/ER	Load Soaked	14.2	Pilot study (n=1)
Griffiths et al. [15]	HULC	non-XLPE	Alpla calf serum (30 g/L) + posphate buffered solution	813 - 914	45° flex/ext 45° add/abd	Load Soaked	29.7	
Langohr et al. [16]	HULC	non-XLPE	Alpla calf serum (30 g/L) + posphate buffered solution	813 - 914	45° flex/ext 45° add/abd	Load Soaked	42.0	Pilot study (n=1)
Kohut et al. [17]	Hopital Cantonal, Switzerland	non-XLPE	Bovine calf serum (30 g/L)	250 - 1000	43° flex/ext 11° add/abd 13° IR/ER	Soaked	17.4	Inversed Bearing
Dieckmann et al. [18]	Munster University, Germany	non-XLPE	Alpla calf serum (30 g/L) + phosphate buffered solution	100 - 500	20° flex/ext 70° add/abd	Soaked	29.7	Pilot study (n=1) Did not use CoCr glenosphere

Figure 4-1: Volumetric wear rates of *in vitro* RTSA simulations

Evidently, there exists large variations between the methods of each group's approach to RTSA wear simulation, which has yielded varying wear rate results. In order to properly compare the behaviour of two materials (i.e., non-XLPE and XLPE) under wear simulation, the simulations must be conducted under identical conditions with identical procedures. In 2016, Langohr et al. developed a simulation strategy [16] with load and motion profiles different to those used by Peers et al. [10]. This simulation strategy has been used to investigate the wear of non-XLPE humeral cups [15], but not yet with XLPE. Therefore, the purpose of this study was to investigate the *in vitro* wear of some XLPE humeral cups in RTSA using the simulation strategy from Langohr et al. [16] such that the results would be comparable to non-XLPE wear results. The implant geometries and protocols followed were identical to those of a previous study that investigated non-XLPE humeral cups [15], thus allowing a direct comparison of XLPE wear to non-XLPE wear in the same RTSA implant design.

4.2   Materials and Methods

4.2.1   Wear Simulation Strategy and Protocols

A modified orbital bearing hip simulator (Figure 4-2; MATCO, La Canada, CA, USA; model MMED EW08) was used following protocols established by Langohr et al. [16]. This protocol applied cyclic loading and circumduction motion at a frequency of 1.13 Hz. The clinical equivalent of this motion is circumduction with a $20 - 65°$ glenohumeral elevation combined with a $\pm 22.5°$ change in glenohumeral plane of elevation (Figure 4-3; Figure 4-4). The load profile included a peak load of 914 N (Figure 4-5). These conditions were considered to be representative of *in vivo* conditions with regard to producing wear rates in the simulator that were similar to those *in vivo* [16].
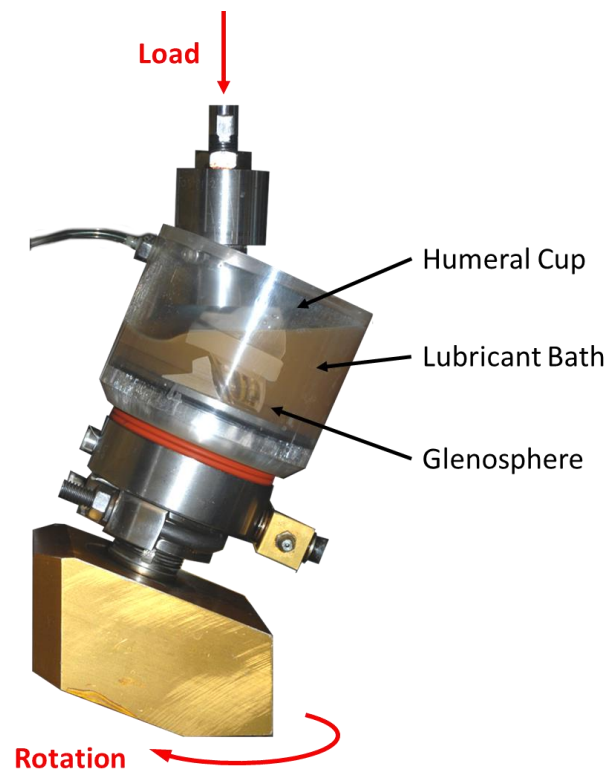
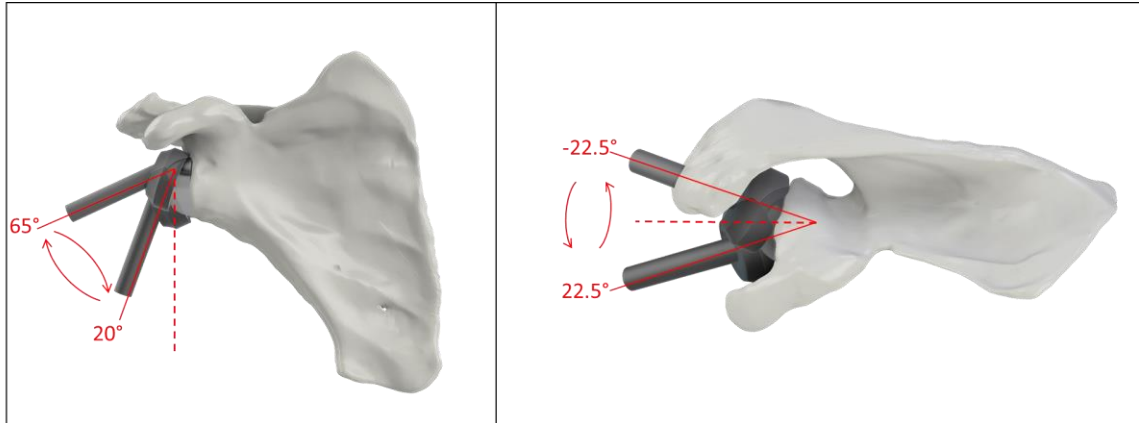

Figure 4-2: Shoulder wear simulator

Figure 4-3: Glenohumeral circumduction range of motion in simulator: frontal plane (left) and transverse plane (right)
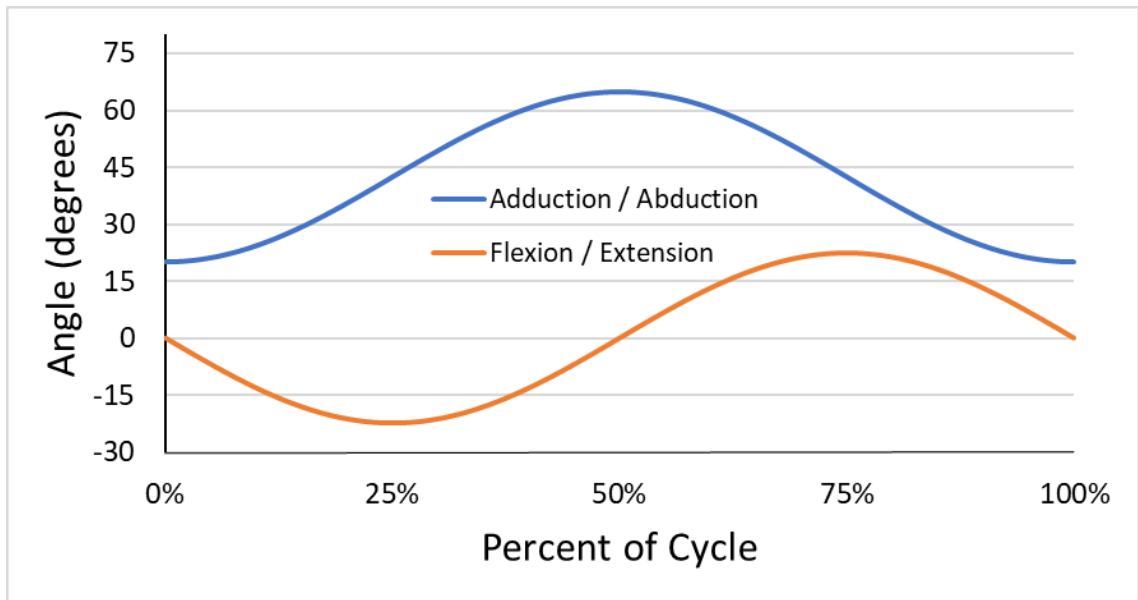

Figure 4-4: Motion profile of RTSA simulator
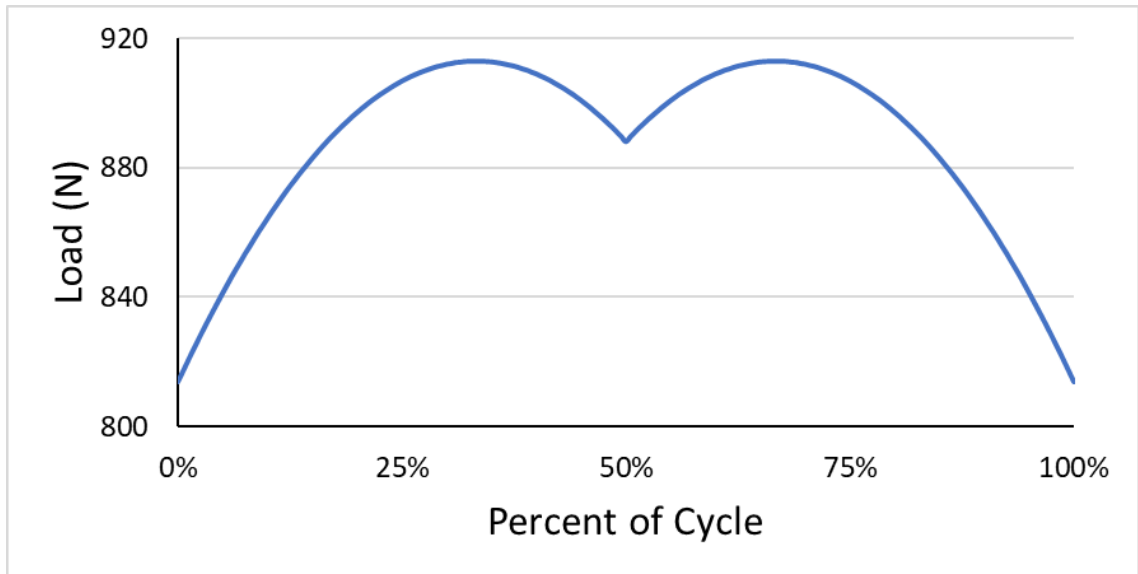
Figure 4-5: Load profile of RTSA simulator

Six RTSA implants (Figure 4-6; DePuy Delta XTEND, 38 mm, high mobility, 5 Mrad crosslinked, non-vitamin E cups) were tested, along with two load-soak controls of the same design subjected to identical conditions in deactivated simulator stations not having any relative motion applied between the articulating implant components. The implants had a 155° neck-shaft angle, a depth of 6.12 mm, and a diameter of 38 mm (Figure 4-7). The cups were sterilized by gamma radiation in nitrogen. This RTSA model was selected to allow for a direct comparison of results to a previous study applying the same protocol to non crosslinked cups [15].
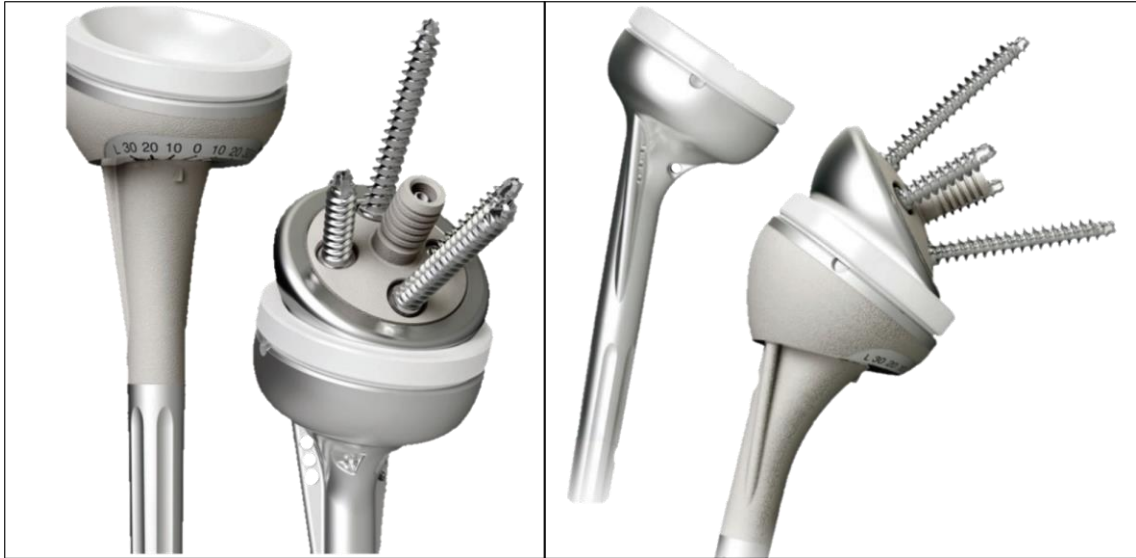
Figure 4-6: DELTA XTEND RTSA system from [19]
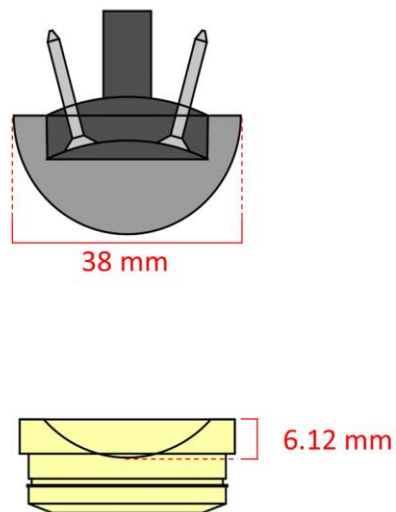
Figure 4-7: Implant dimensions

The lubricant used was comprised of non-iron alpha calf fraction serum (HyClone; GE Healthcare Life Sciences, South Logan, UT, USA) diluted to a total protein concentration of 30 g/L using phosphate buffered solution (VWR International, ON, Canada). Both sodium hyaluronate and antimycotic antibiotic were added to the lubricant at concentrations of 1.5 g/L and 10 mL/L, respectively. These lubricant constituents were

deemed to be the most clinically relevant substitute for synovial fluid in arthroplasty wear testing [20–23].

All specimens, including load soaks, were pre-soaked in de-ionized (DI) water prior to test initiation to minimize the amount of fluid absorbed during the simulation, which may lead to negative wear measurements [24–27]. Specimens were then handled using the protocol outlined in Table 4-2.

Table 4-2: Wear simulation protocol

Step	Description
1.	Specimens (cups and glenospheres) were cleaned in an ultrasonic cleaner in baths of 2% Liqui-NOX® solution (Alconox Inc., White Plains, NY, USA) for 10 minutes.
2.	Specimens were removed from the Liqui-NOX® solution and rinsed with DI water.
3.	Specimens were cleaned in an ultrasonic cleaner in baths of DI water for 5 minutes.
4.	Specimens were removed from the DI water and soaked in isopropyl alcohol for 5 minutes (to remove any residual surface water).
5.	Specimens were removed from the isopropyl alcohol and dried using a stream of nitrogen gas.
6.	Cups were set down and allowed to acclimatize next to the analytical balance for 10 minutes.
7.	The analytical balance was calibrated using the automatic calibration feature and tared.
8.	Two standard masses (20 g and 100 g) were weighed.
9.	The mass of each cup was obtained.
10.	Step 9 was repeated two times to obtain three measurements for each cup.
11.	The average of the three measurements was taken for each cup. If the average was not within 0.2 mg of each of the three readings, steps 8-11 were repeated.
12.	Step 8 was repeated to ensure the measurements were within 0.2 mg of the previous reading.
13.	Specimens were installed into the wear simulator and lubricant was added.
14.	Simulator was run for 0.25 Mc.
15.	Specimens were removed from the simulator.
16.	Specimens were scrubbed with a soft brush and rinsed with DI water to remove any adhered contaminants.
17.	Steps 1-12 were repeated.
18.	All lubricant was removed, and the simulator was thoroughly cleaned using DI water, a soft brush, and isopropyl alcohol.

Following this, a single specimen was re-installed and run for an additional 0.25 Mc (repeating steps 13-17 for n=1).

To obtain information regarding the sliding distances the simulator subjected to the humeral cup, the kinematic motion of the simulator was described using rotation matrices sampled at 100 Hz and input into a custom software program (Chapter 3, section 3.2.3.2). The program used the rotation matrices and implant geometry to determine the amount of relative motion subjected to five points on the cup's surface (i.e., centre, superior, inferior, anterior, and superior; Figure 4-8) during 0.25 Mc of simulation. These values will be important in establishing a link between number of cycles simulated and time spent *in vivo*.

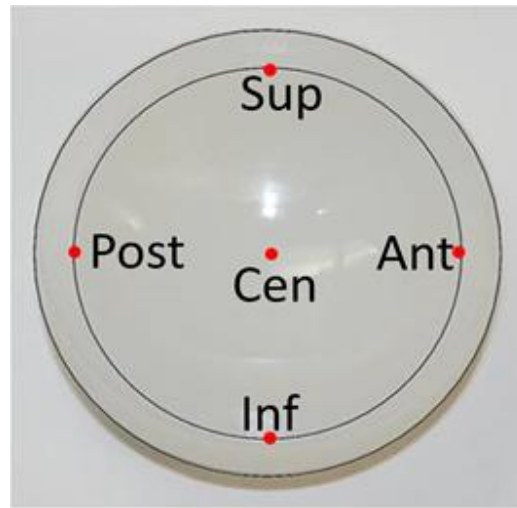**Figure 4-8: The five tracked points on the humeral cup**

4.2.2 Wear Assessment

A Mettler Toledo X205 Analytical Balance (Columbus, OH, USA) with a precision of 0.01 mg was used to measure volumetric wear. Real mass loss (Δm) was calculated by adding the average mass of fluid absorbed by the load soaks (Δm_s) to the apparent mass loss due to wear (Δm_w) as follows:

$$\Delta m = \Delta m_w + \Delta m_s \qquad\qquad (4\text{-}1)$$

where

$\Delta m_w = m_o - m_f$

m_o = mass at start of wear test

m_f = mass at end of wear test

The real mass loss was then divided by the density of XLPE (0.937 mg/mm^3 [28]) to produce total volumetric wear (w).

$$w = \frac{\Delta m}{0.937} \qquad\qquad (4\text{-}2)$$

4.2.3 Statistical Analysis

A two-tailed, equal-variance t-test was performed in Microsoft Excel to determine any significant differences between the wear of the XLPE and non-XLPE cups tested in each corresponding wear simulation at 0.25 Mc. The non-XLPE cups from Griffiths [15] were treated as a separate population from the XLPE cups used in the present study, thus the t-test was not paired and an equal variance was assumed. Alpha level was set to $\alpha = 0.05$.

4.3 Results

All XLPE cups exhibited wear of the polyethylene, ranging from 2.34 mm^3 to 3.83 mm^3 (Figure 4-9). At 0.25 Mc, the average wear ($\pm$ standard deviation) of the specimens tested was 2.90 $\pm$ 0.65 mm^3 for the XLPE cups, representing a 59.4% decrease (p<0.01) in wear compared to non-XLPE which had an average wear of 7.43 $\pm$ 0.53 mm^3 under identical conditions [15].
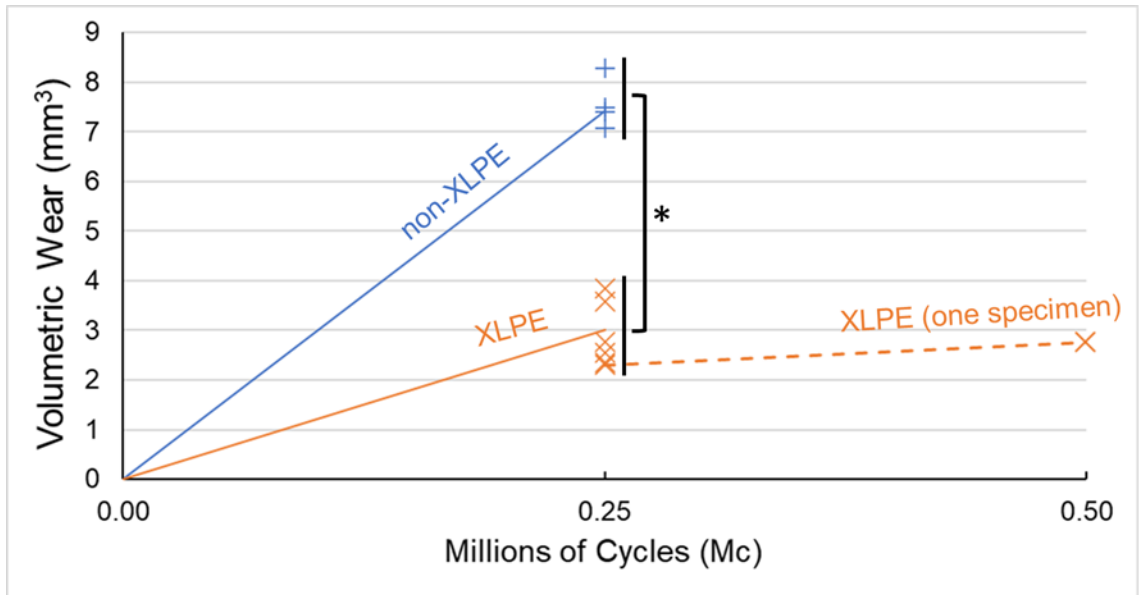
Figure 4-9: Polyethylene wear in both XLPE and non-XLPE

The specimen in one station was tested to 0.5 Mc in the simulator and experienced 2.30 mm^3 of wear at 0.25 Mc and 2.76 mm^3 of wear at 0.5 Mc (Figure 4-9). This represented a decrease in wear rate for this single specimen from 9.2 mm^3/Mc to 1.84 mm^3/Mc from the first 0.25 Mc to the second 0.25 Mc.

Visually, all cups (non-XLPE and XLPE) showed evidence of wear on their articulating surface, indicated by the polished section within the white dotted line (Figure 4-10). The surfaces of the superior aspect of the cups did not show any evidence of wear, with the original machining marks still present.
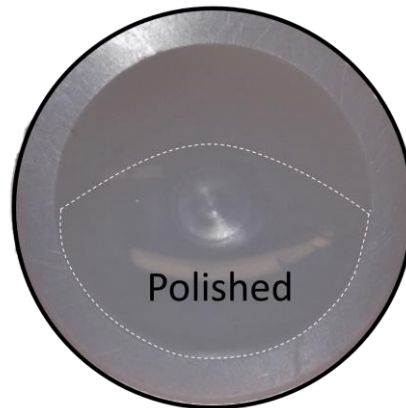
Figure 4-10: Visual examination of surface wear in XLPE cups

4.4 Discussion

The XLPE volumetric wear rate in the present study was less than the wear rates reported in all previous *in vitro* wear studies of non-XLPE humeral cups in RTSA [8,9,11–18] (Figure 4-11). More importantly, a 59% decrease in wear was found when switching from non-XLPE to XLPE in the present study, which is similar to the 57% decrease found by Peers et al. [10] when assessing the same change in their simulator. Although the volumetric wear values varied between the present work and Peers et al. [10], the differences can be attributed to differences in the testing protocols and are not so important when discussing the repeated trend of a significant wear decrease when utilizing XLPE instead of non-XLPE in RTSA. These findings suggest that humeral cups made using moderately crosslinked XLPE may produce less wear *in vivo* than those made using non-XLPE.

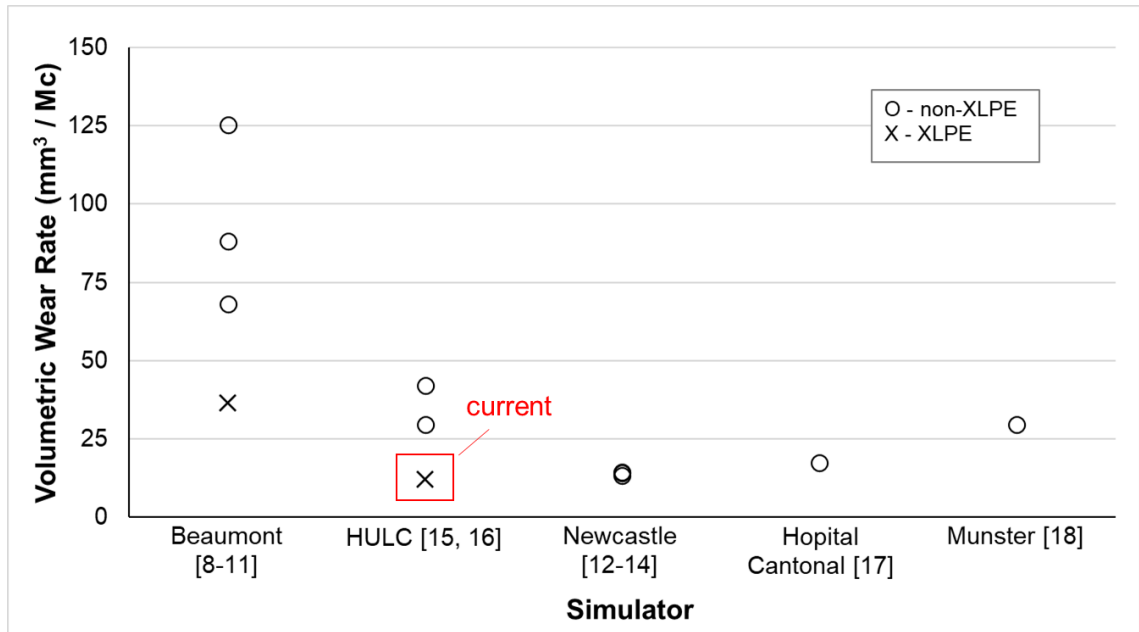**Figure 4-11: RTSA volumetric wear rate (mm³/Mc) of the current study compared to previous studies**

The reduction in wear rate observed in the single cup 0.5 Mc trial suggests that the rate of volumetric wear may decrease as the number of cycles increases, which may have been a result of run-in wear that occurred in the first 0.25 Mc. This trend, however, was not found in the simulator studies of Peers et al. [10], who saw a general increase in wear rate from 0 – 1.5 Mc, and then a plateau from 1.5 to 5 Mc. In the present simulator wear studies, more specimens must be tested for longer durations to draw any conclusions on the relationship between XLPE wear rate and number of cycles.

It is important to note that the humeral cup liners in the present study were only moderately crosslinked with 5 MRad of radiation and contained no added antioxidant. Wear rates are likely to decease further with larger radiation doses (those approaching 10 MRads) and the addition of an antioxidizing agent, such as vitamin E.

The visual presence of wear at the inferior aspect of the cup agreed with previous RTSA wear simulator studies (Figure 4-13) [15,16], and has been routinely observed in RTSA cups clinically [3–5,29], providing some reassurance that the simulator introduced clinically relevant loading and motions.
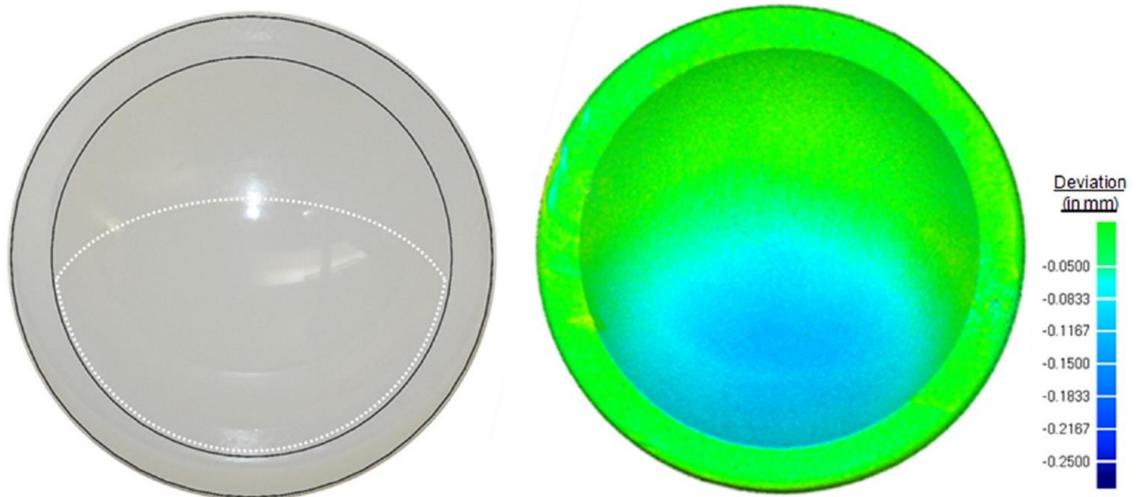
Figure 4-13: Humeral cup wear after 1 Mc in simulator [16]; outline of polished region in white (left) and micro-CT deviation map showing wear morphology (right)

The 2021 AOA NJRR [30] reported no difference in revision rates were detected between primary RTSAs using XLPE and those using non-XLPE. This similarity in revision rate between the two polymers may be the result of wear related problems accounting for a relatively small proportion of causes of revision within this population. The AOA NJRR had only presented cumulative revision percentages of primary RTSA by polyethylene type up to 10 years following instrumentation. It may have been the case that within this initial 10 years, although polyethylene wear was occurring, the effects of other failure mechanisms were overshadowing those wear related. Since roughly 15% of primary RTSA procedures were performed in patients 64 years and under in 2020 [1], a 10 year period does not represent a full RTSA lifecycle, so it will be interesting to see if any differences in wear rates arise between the two liner materials at 14 and 20 years post-op.

Retrieval studies have reported consistent humeral cup liner deterioration in failed RTSAs [2–5,31]. It is important to note a difference between polyethylene wear and polyethylene damage. Polyethylene wear is a slower process that occurs as a result of relative sliding motion, and sometimes subsurface fatigue, between two surfaces. Polyethylene damage is an impact-related deterioration involving high contact stresses that dislodge large chunks of polyethylene from the main body. Wear debris tends to be of smaller size and possesses a higher osteolytic potential than damage debris [32]. Damage can accelerate wear and

wear may also accelerate damage. Additionally, these two mechanisms can occur at the same time and produce some in-between deterioration mechanism that has features of both. Since the retrieval studies have shown evidence of both polyethylene wear and damage in humeral cup liners, the use of XLPE may reduce the overall polyethylene deterioration seen clinically.

A major strength of this study is the direct comparison it is able to make of XLPE to non-XLPE in RTSA humeral liners. The simulator used was also developed using clinical motion data and loading conditions.

This study was limited by its short duration and single motion profile, making it, at best, a pilot study rather than a full investigation. The simulations were only run to 0.25 Mc and then extrapolated linearly to compare to previously published wear rates per 1 Mc. Further tests employing greater simulation durations are needed in order to fully understand the wear behaviour of XLPE in RTSA. Although the motion profile was chosen with consideration for clinical data, it represents just the average sampled ROM, which may not be the best representation of a shoulder duty cycle. Furthermore, this study did not analyze the quantity and size of the wear particles. Since the body's reaction to the wear particles is dependent on particle diameter [32], no suggestions are able to be made regarding the dangers of XLPE wear in the RTSA. In the hip joint, however, XLPE wear debris was found to be lesser in both quantity and biological reactivity than the debris of non-XLPE [33].

4.5   Conclusion

Moderately crosslinked polyethylene produced less wear at 0.25 Mc than non-crosslinked polyethylene in RTSA joint wear simulations. A reduced volumetric wear *in vivo* may reduce particle-induced osteolysis, implant loosening, and subsequent arthroplasty revisions.

4.6 References

[1]   Australian Orthopaedic Association National Joint Replacement Registry.
        Australian Orthopaedic Association National Joint Replacement Registry
        (AOANJRR). Hip Knee & Shoulder Arthroplasty: 2021 Annual Report 2021.

[2]   Day JS, MacDonald DW, Olsen M, Getz C, Williams GR, Kurtz SM. Polyethylene
        wear in retrieved reverse total shoulder components. J Shoulder Elb Surg
        2012;21:667–74. https://doi.org/10.1016/j.jse.2011.03.012.

[3]   Kurdziel MD, Newton MD, Hartner S, Baker KC, Wiater JM. Quantitative
        evaluation of retrieved reverse total shoulder arthroplasty liner surface deviation
        and volumetric wear. J Orthop Res 2018;36:2007–14.
        https://doi.org/10.1002/jor.23849.

[4]   Wiater BP, Baker EA, Salisbury MR, Koueiter DM, Baker KC, Nolan BM, et al.
        Elucidating trends in revision reverse total shoulder arthroplasty procedures: A
        retrieval study evaluating clinical, radiographic, and functional outcomes data. J
        Shoulder Elb Surg 2015;24:1915–25. https://doi.org/10.1016/j.jse.2015.06.004.

[5]   Nam D, Kepler CK, Nho SJ, Craig E V., Warren RF, Wright TM. Observations on
        retrieved humeral polyethylene components from reverse total shoulder
        arthroplasty. J Shoulder Elb Surg 2010;19:1003–12.
        https://doi.org/10.1016/j.jse.2010.05.014.

[6]   Medley JB. Highly cross-linked polyethylene is the new 'gold standard' bearing
        material for total hip arthroplasty. Biosurface and Biotribology 2021:1–7.
        https://doi.org/10.1049/bsb2.12007.

[7]   Medley JB. Can physical joint simulators be used to anticipate clinical wear
        problems of new joint replacement implants prior to market release? Proc Inst
        Mech Eng Part H J Eng Med 2016;230:347–58.
        https://doi.org/10.1177/0954411916643902.

[8]   Carpenter S, Pinkas D, Newton MD, Kurdziel MD, Baker KC, Wiater JM. Wear

rates of retentive versus nonretentive reverse total shoulder arthroplasty liners in an in vitro wear simulation. J Shoulder Elb Surg 2015;24:1372–9. https://doi.org/10.1016/j.jse.2015.02.016.

[9] Haggart J, Newton MD, Hartner S, Ho A, Baker KC, Kurdziel MD, et al. Neer Award 2017: wear rates of 32-mm and 40-mm glenospheres in a reverse total shoulder arthroplasty wear simulation model. J Shoulder Elb Surg 2017;26:2029–37. https://doi.org/10.1016/j.jse.2017.06.036.

[10] Peers S, Moravek JE, Budge MD, Newton MD, Kurdziel MD, Baker KC, et al. Wear rates of highly cross-linked polyethylene humeral liners subjected to alternating cycles of glenohumeral flexion and abduction. J Shoulder Elb Surg 2015;24:143–9. https://doi.org/10.1016/j.jse.2014.05.001.

[11] Vaupel ZM, Baker KC, Kurdziel MD, Wiater JM. Wear simulation of reverse total shoulder arthroplasty systems: Effect of glenosphere design. J Shoulder Elb Surg 2012;21:1422–9. https://doi.org/10.1016/j.jse.2011.10.024.

[12] Mattei L, Di Puccio F, Joyce TJ, Ciulli E. Numerical and experimental investigations for the evaluation of the wear coefficient of reverse total shoulder prostheses. J Mech Behav Biomed Mater 2016;55:53–66. https://doi.org/10.1016/j.jmbbm.2015.10.007.

[13] Smith SL, Li BL, Buniya A, Ho Lin S, Scholes SC, Johnson G, et al. In vitro wear testing of a contemporary design of reverse shoulder prosthesis. J Biomech 2015;48:3072–9. https://doi.org/10.1016/j.jbiomech.2015.07.022.

[14] Smith SL, Li L, Joyce TJ. Engineering of a multi-station shoulder simulator. Proc Inst Mech Eng Part H J Eng Med 2016;230:470–80. https://doi.org/10.1177/0954411915611161.

[15] Griffiths MW, Athwal GS, Medley JB, Johnson JA, Langohr GDG. Wear of humeral polyethylene cups in reverse total shoulder arthroplasty with simulated rim damage from scapular notching. Biotribology 2020;22:1–8.

https://doi.org/10.1016/j.biotri.2020.100123.

[16]   Langohr GDG, Athwal GS, Johnson JA, Medley JB. Wear simulation strategies for reverse shoulder arthroplasty implants. Proc Inst Mech Eng Part H J Eng Med 2016;230:458–69. https://doi.org/10.1177/0954411916642801.

[17]   Kohut G, Dallmann F, Irlenbusch U. Wear-induced loss of mass in reversed total shoulder arthroplasty with conventional and inverted bearing materials. J Biomech 2012;45:469–73. https://doi.org/10.1016/j.jbiomech.2011.11.055.

[18]   Dieckmann R, Liem D, Gosheger G, Henrichs MP, Höll S, Hardes J, et al. Evaluation of a reconstruction reverse shoulder for tumour surgery and tribological comparision with an anatomical shoulder arthroplasty. Int Orthop 2013;37:451–6. https://doi.org/10.1007/s00264-012-1771-7.

[19]   DePuy International; DePuy Orthopedics. DELTA XTEND ™ Reverse Shoulder System Surgical Technique. Leeds, England: 2013.

[20]   Brandt JM, Brière LK, Marr J, MacDonald SJ, Bourne RB, Medley JB. Biochemical comparisons of osteoarthritic human synovial fluid with calf sera used in knee simulator wear testing. J Biomed Mater Res - Part A 2010;94:961–71. https://doi.org/10.1002/jbm.a.32728.

[21]   Brandt JM, Charron K, Zhao L, MacDonald SJ, Medley JB. Calf serum constituent fractions influence polyethylene wear and microbial growth in knee simulator testing. Proc Inst Mech Eng Part H J Eng Med 2012;226:427–40. https://doi.org/10.1177/0954411912444248.

[22]   Brandt JM, Mahmoud KK, Koval SF, MacDonald SJ, Medley JB. Antimicrobial agents and low-molecular weight polypeptides affect polyethylene wear in knee simulator testing. Tribol Int 2013;65:97–104. https://doi.org/10.1016/j.triboint.2013.02.019.

[23]   Brandt JM, Charron KD, Zhao L, MacDonald SJ, Medley JB. Lubricant Biochemistry Affects Polyethylene Wear in Knee Simulator Testing. Biotribology

2021;27:100185. https://doi.org/10.1016/j.biotri.2021.100185.

[24] Laraia K, Leone N, MacDolanald R, Blanchet TA. Effect of water and serum absorption on wear of unirradiated and crosslinked UHMWPE orthopedic bearing materials. Tribol Trans 2006;49:338–46. https://doi.org/10.1080/05698190600678663.

[25] Blanchet TA, Peterson SL, Rosenberg KD. Serum lubricant absorption by UHMWPE orthopaedic bearing implants. J Tribol 2002;124:1–4. https://doi.org/10.1115/1.1400996.

[26] Yao JQ, Blanchet TA, Murphy DJ, Laurent MP. Effect of fluid absorption on the wear resistance of UHMWPE orthopedic bearing surfaces. Wear 2003;255:1113–20. https://doi.org/10.1016/S0043-1648(03)00167-4.

[27] Brandt JM, Charron KDJ, MacDonald SJ, Medley JB. Mass gain behaviour of tibial polyethylene inserts during soak testing. Proc Inst Mech Eng Part H J Eng Med 2011;225:324–31. https://doi.org/10.1177/2041303310392629.

[28] Hunt BJ, Joyce TJ. A tribological assessment of Ultra High Molecular Weight Polyethylene types GUR 1020 and GUR 1050 for orthopedic applications. Lubricants 2016;4. https://doi.org/10.3390/lubricants4030025.

[29] Van de Kleut ML, Athwal GS, Faber KJ, Teeter MG. In vivo volumetric and linear wear measurement of reverse shoulder arthroplasty at minimum 5-year follow-up. J Shoulder Elb Surg 2020;29:1695–702. https://doi.org/10.1016/j.jse.2019.11.031.

[30] Australian Orthopaedic Association National Joint Replacement Registry. Australian Orthopaedic Association National Joint Replacement Registry (AOANJRR). Hip Knee & Shoulder Arthroplasty: 2021 Annual Report 2021:329–66.

[31] Nyffeler RW, Werner CML, Simmen BR, Gerber C. Analysis of a retrieved Delta III total shoulder prosthesis. J Bone Jt Surg - Ser B 2004;86:1187–91. https://doi.org/10.1302/0301-620X.86B8.15228.

[32]   Green TR, Fisher J, Bridget Matthews J, Stone MH, Ingham E. Effect of size and dose on bone resorption activity of macrophages by in vitro clinically relevant ultra high molecular weight polyethylene particles. J Biomed Mater Res 2000;53:490–7. https://doi.org/10.1002/1097-4636(200009)53:5<490::AID-JBM7>3.0.CO;2-7.

[33]   Baxter RM, MacDonald DW, Kurtz SM, Steinbeck MJ. Characteristics of highly cross-linked polyethylene wear debris in vivo. J Biomed Mater Res - Part B Appl Biomater 2013;101 B:467–75. https://doi.org/10.1002/jbm.b.32902.

Chapter 5

Thesis Closure

OVERVIEW: This final chapter reviews the research objectives detailed in Chapter 1 and continues on to summarize the findings of the studies performed to accomplish these objectives. The strengths and limitations of the present studies are discussed, and future directions are offered.

5.1   Summary and Conclusions

The main theme of this work was the investigation of XLPE as a suitable replacement for non-XLPE in the RTSA through the lens of tribology. Wear simulations were conducted to investigate XLPE wear under conditions similar to those found *in vivo*. Additionally, a computational model was created to better define the *in vivo* kinematics of the RTSA. Together, the findings of this project were intended to aid in the design and testing of future RTSA models.

Chapter 2 explored the wear of XLPE plates against CoCr pins under various contact loads (Objective 1). The findings provided evidence to suggest that XLPE wear may be load-dependent under the contact loads and pressures investigated in the present work. The negative wear volumes measured in this study indicated that XLPE wear against CoCr is markedly low – so much so that it was undetectable using our simulation protocol.

Chapter 3 provided a computer model that estimated *in vivo* glenohumeral sliding distance in individuals following RTSA (Objective 2). These estimations can be used to help guide future wear simulation protocols to make them more translatable; for example, one year of *in vivo* motion can be represented by roughly 1.25 Mc in our *in vitro* shoulder wear simulator. These results estimated a smaller annual number of cycles in the shoulder (1.25 Mc) than that of the lower limb (2 Mc), disagreeing with Hypothesis 2.

The model was run using each combination of implant size (38 mm and 42 mm) and NSA (135° and 155°), satisfying Objective 4. The results of this study agreed with hypothesis 4, suggesting that an increase in implant size may increase glenohumeral sliding distance, and a lesser NSA may decrease the risk of scapular notching. Hypothesis 3 held true for implants with a 155° NSA, but not for those with a 135° NSA.

Chapter 4 explored the wear of XLPE in the RTSA and compared it to that of non-XLPE in the same design using an *in vitro* wear simulator (Objective 5). These simulations

provided strong evidence to support the belief that XLPE wears less than non-XLPE in the RTSA, which could increase the implant's lifespan *in vivo*. These results agree with Hypothesis 5.

5.2 Strengths and limitations

The large sample size and long-duration data collections in Chapter 3 are significant strengths of the present work. This data collection method also had the benefit of tracking upper limb motion outside of the laboratory setting, capturing a more accurate representation of *in vivo* movement. The direct comparison of XLPE wear to non-XLPE wear in Chapter 4 was also a large strength. The shoulder simulator used was developed using *in vivo* motion data and loading characteristics, which enhanced the accuracy of the simulation.

The inability to account for implant deformation and subsequent contact area in Chapter 3 is a large limitation in the presented sliding distances. But as discussed, by looking at the load vector it can be assumed that the inferior and centre points of the cup were almost always in contact. The lack of published literature on scapular kinematics in RTSA limited the computational model's ability to account for glenohumeral positioning in all planes of elevation. The model also did not account for load-dependent changes to geometry within the glenohumeral joint. The inability of the MOCAP shirt to measure water-related activities resulted in the omission of daily bathing habits, which is a repeated task that most individuals with RTSA would perform. Having run for only 0.25 Mc, the shoulder wear simulation was considered to have a short duration. Running the simulation for at least 1 Mc would provide more information into the wear behaviour of XLPE in the RTSA.

5.3 Future Directions

An appropriate next step for the computational model would be to account for any geometric changes experienced by the RTSA due to joint loading and motion. Assuming more research will be published involving scapular kinematics in RTSA, the inclusion of

scapular rotation in multiple planes of elevation is needed. Modelling the effect of glenosphere inferior rotation, a common parameter altered in RTSA designs, would make the model more inclusive.

Determining the effects of simulated scapular contact on XLPE wear and damage in the RTSA would provide greater insight into RTSA failure mechanisms. As scapular contact is present in many individuals with RTSA, accounting for this would be a great addition to *in vitro* shoulder wear simulations.

5.4 Significance

The results of Chapter 4 provide strong evidence to expect reduced clinical wear in XLPE humeral liners vs non-XLPE humeral liners. This may help influence the transition from non-XLPE to XLPE in market approved RTSA designs. The annual glenohumeral sliding distance proposed in Chapter 3 provides a translation from *in vitro* simulation testing to projected *in vivo* clinical wear, which will not only help guide laboratory research protocols, but will also allow clinicians to better predict surgical outcomes and implant lifespans. The results from Chapter 3 further support the body of evidence suggesting a reduced NSA may decrease the incidence of humeral cup scapular contact.

5.5 Conclusions

Highly crosslinked polyethylene is likely a better suited material for use in the humeral cup liner than conventional polyethylene. Switching from non-XLPE to XLPE is expected to reduce the prevalence of wear-related complications in the RTSA. A reduced NSA may reduce the prevalence of scapular contact and scapular notching. With the growing popularity of this procedure, further research is warranted to better understand and prevent implant failure.

Curriculum Vitae

Christopher Millward

E D U C A T I O N

Sept 2019 – Present   **Master of Engineering Science**, Biomedical Engineering, Biomechanical
University of Western Ontario, London, Ontario

Sept 2014 – April 2019   **Bachelor of Arts**, Honors Specialization in Kinesiology
University of Western Ontario, London, Ontario

P R O F E S S I O N A L A F F I L I A T I O N S

Sept 2019 – April 2022   **Roth | McFarlane Hand and Upper Limb Centre**
St. Joseph's Health care, London, Ontario

Sept 2019 – April 2022   **Collaborative Program in MSK Health Research**
Bone and Joint Institute, University of Western Ontario, London, Ontario

R E S E A R C H E X P E R I E N C E

October 2020   **Research Consultant**
USports, Canada

Sept 2019 – April 2022   **Graduate Research Assistant**
Hand and Upper Limb Centre, London, Ontario

Sept 2016 – Apr 2019   **Undergraduate Researcher**
University of Western Ontario School of Kinesiology, London Ontario

June 2016 – Aug 2016   **Research Assistant**
Neurotrauma Impact Science Laboratory, University of Ottawa, Ottawa, Ontario

T E A C H I N G E X P E R I E N C E

Sept 2021 – Dec 2021   **Teaching Assistant** — Data Management and Applications (ECE 9014)
Faculty of Engineering, University of Western Ontario

Jan 2021 – **April 2021**	**Teaching Assistant** — Foundations of Engineering Practice (ES 1050) *Faculty of Engineering, University of Western Ontario*

Sept 2020 – **Dec 2020**	**Teaching Assistant** — Kinematics and Dynamics of Machines (MME/ MSE 3381) *Faculty of Engineering, University of Western Ontario*

Sept 2020 – **Present**	**Tutor** — Introduction to Human Biomechanics *Multiple universities across Canada*

LEADERSHIP ROLES

Sept 2020 – **April 2021**	**Seminar Coordinator** *School of Biomedical Engineering, University of Western Ontario*

CONFERENCE POSTERS

Millward, C., Langohr, G.D.G., Medley, J.B. (2022) Initial Simulator Wear of Crosslinked Polyethylene in Reverse Total Shoulder Arthroplasty. *Canadian Orthopaedic Association Annual Meeting,* June 9-10, Quebec City, Quebec

Millward, C., Athwal, G.S., Johnson, J.A., Medley, J.B., Langohr, G.D.G. (2022) *In-Vivo* Sliding distances for Points on the Humeral Cup in Reverse Total Shoulder Arthroplasty. *Canadian Orthopaedic Association Annual Meeting,* June 9-10, Quebec City, Quebec

Millward, C., Langohr, G.D.G., Medley, J.B. (2022) In-Vitro Cross-Linked Polyethylene Wear for Reverse Total Shoulder Arthroplasty. *Orthopaedic Research Society Annual Meeting,* February 4-7, Tampa Bay, Florida

Millward, C., Athwal, G.S., Johnson, J.A., Medley, J.B., Langohr, G.D.G. (2022) Reverse Total Shoulder Arthroplasty Glenohumeral Sliding Distances During Daily Living. *Orthopaedic Research Society Annual Meeting,* February 4-7, Tampa Bay, Florida